Summer 2010

Regulator of G protein signaling 3 modulates Wnt5b calcium dynamics and somite patterning

Christina M. Freisinger
University of Iowa

REGULATOR OF G PROTEIN SIGNALING 3 MODULATES WNT5B CALCIUM DYNAMICS AND SOMITE PATTERNING

by

Christina M Freisinger

An Abstract

Of a thesis submitted in partial fulfillment
of the requirements for the Doctor of
Philosophy degree in Biology
in the Graduate College of
The University of Iowa

July 2010

Thesis Supervisor: Associate Professor Diane Slusarski

ABSTRACT

The process of vertebrate development requires communication among many cells of the embryo in order to define the body axis (front/back, head/tail or left/right). The Wnt signaling network plays a key role in a vast array of cellular processes including body axis patterning and cell polarity. One arm of the Wnt signaling network, the non-canonical Wnt pathway, mediates intracellular Ca^{2+} release via activation of heterotrimeric G proteins. Regulator of G protein Signaling (RGS) proteins can accelerate inactivation of G proteins by acting as G protein GAPs and are uniquely situated to control the amplitude of a Wnt signal. I hypothesize that individual RGS proteins are critical in modulating the frequency and amplitude of Wnt/Ca^{2+} signaling in different tissues and at different developmental stages and this modulation is essential for developmental patterning events. To this end, this thesis is focused on the effects G protein regulation has on intracellular Ca^{2+} release dynamics and developmental patterning events.

I combine cellular, molecular and genetic analyses with high resolution Ca^{2+} imaging to provide new understanding of the role of RGS proteins on Wnt mediated Ca^{2+} release dynamics and developmental patterning events. In chapter 2, I describe endogenous Ca^{2+} dynamics from the very first cell divisions through early somitogenesis in zebrafish embryos. I find that each phase of zebrafish development has a distinct pattern of Ca^{2+} release, highlighting the complexity of Ca^{2+} ion and cellular physiology.

In Chapter 3, I identify *rgs3* as potential modulator of Ca^{2+} dynamics and Chapter 4 expands upon these observations by providing data supporting that Rgs3 function is necessary for appropriate frequency and amplitude of Ca^{2+} release during somitogenesis and that Rgs3 functions downstream of Wnt5 activity. My results provide new evidence that a member of the RGS protein family is essential for modulating the non-canonical Wnt network to assure normal tissue patterning during development.

In Chapter 5, I report the identification and characterization of Rgs3b, a paralogue to Rgs3, in zebrafish. I describe results indicating that Rgs3b is poised to interact with Wnt11 indicating that individual RGS genes may have unique roles in modulating Wnt/Ca^{2+} signaling in different tissues or different stages. In conclusion, this thesis provides data supporting that individual RGS proteins are critical in modulating the frequency and amplitude of Wnt/Ca^{2+} signaling in different tissues and at different developmental stages and this is a substantial breakthrough in understanding how RGS proteins function to fine-tune known signaling pathways.

Abstract Approved: _____
Thesis Supervisor

_____
Title and Department

_____
Date

REGULATOR OF G PROTEIN SIGNALING 3 MODULATES WNT5B CALCIUM DYNAMICS AND SOMITE PATTERNING

by

Christina M Freisinger

A thesis submitted in partial fulfillment
of the requirements for the Doctor of
Philosophy degree in Biology
in the Graduate College of
The University of Iowa

July 2010

Thesis Supervisor: Associate Professor Diane Slusarski

Graduate College
The University of Iowa
Iowa City, Iowa

CERTIFICATE OF APPROVAL

_____

PH.D. THESIS

_____

This is to certify that the Ph.D. thesis of

Christina M Freisinger

has been approved by the Examining Committee
for the thesis requirement for the Doctor of Philosophy
degree in Biology at the July 2010 graduation.

Thesis Committee: _____
Diane Slusarski, Thesis Supervisor

_____
Douglas Houston

_____
Robert Cornell

_____
Jim Lin

_____
Joseph Frankel

To My Mother: Sue Harkness
To My Grandmother: Gladys Noack

ACKNOWLEDGMENTS

I would like fist thank my advisor Dr. Slusarski. Diane has played a significant role in helping me to develop my thesis. In addition to providing guidance she has always listened to my opinions, encouraged me to present my ideas and genuinely cares about my personal and professional growth. Thanks to all my committee members Drs. Cornell, Houston, Frankel and Lin for their time and effort in guiding to complete this thesis project. In addition to my committee members the Biology program and especially Phil Ecklund have been instrumental in guiding me through graduate school. For the past seven years Phil has always been there to answer all of my questions.

Additionally, I would like to thank all the members of the Slusarski lab including Trudi Westfall, Hilary Griesbach, Patricia Schneider, Igor Schneider, Xue Mei, Sarah Derry, Shengda Lin, Lisa Baye, Pam Pretorius and Svetha Swaminathan for all of their help, ideas and fruitful discussions. I have grown to think of all the lab members as family and they will be dearly missed.

Special thanks to my boyfriend KC and to all the friends I have made during my graduate carrier including Sara Sheeley, Shannin Zevian, Erin Bailey, Paulina Mena, Madhu Roy, Derek Peters and Steve Butcher. Without the support from my great friends and our weekly Friday discussions at Joe's my scientific career thus far would be far less enjoyable and exciting.

I would like to end by thanking my family including my mother, grandmother and brothers. I would like to especially thank my mother who always been there for me. She has always encouraged me to do my best and most important of all she taught me to be happy and love what I do. I know that without her love and support, I would never have had the courage and wisdom to succeed personally and professionally.

ABSTRACT

The process of vertebrate development requires communication among many cells of the embryo in order to define the body axis (front/back, head/tail or left/right). The Wnt signaling network plays a key role in a vast array of cellular processes including body axis patterning and cell polarity. One arm of the Wnt signaling network, the non-canonical Wnt pathway, mediates intracellular Ca^{2+} release via activation of heterotrimeric G proteins. Regulator of G protein Signaling (RGS) proteins can accelerate inactivation of G proteins by acting as G protein GAPs and are uniquely situated to control the amplitude of a Wnt signal. I hypothesize that individual RGS proteins are critical in modulating the frequency and amplitude of Wnt/Ca^{2+} signaling in different tissues and at different developmental stages and this modulation is essential for developmental patterning events. To this end, this thesis is focused on the effects G protein regulation has on intracellular Ca^{2+} release dynamics and developmental patterning events.

I combine cellular, molecular and genetic analyses with high resolution Ca^{2+} imaging to provide new understanding of the role of RGS proteins on Wnt mediated Ca^{2+} release dynamics and developmental patterning events. In chapter 2, I describe endogenous Ca^{2+} dynamics from the very first cell divisions through early somitogenesis in zebrafish embryos. I find that each phase of zebrafish development has a distinct pattern of Ca^{2+} release, highlighting the complexity of Ca^{2+} ion and cellular physiology.

In Chapter 3, I identify *rgs3* as potential modulator of Ca^{2+} dynamics and Chapter 4 expands upon these observations by providing data supporting that Rgs3 function is necessary for appropriate frequency and amplitude of Ca^{2+} release during somitogenesis and that Rgs3 functions downstream of Wnt5 activity. My results provide new evidence that a member of the RGS protein family is essential for modulating the non-canonical Wnt network to assure normal tissue patterning during development.

In Chapter 5, I report the identification and characterization of Rgs3b, a paralogue to Rgs3, in zebrafish. I describe results indicating that Rgs3b is poised to interact with Wnt11 indicating that individual RGS genes may have unique roles in modulating Wnt/Ca^{2+} signaling in different tissues or different stages. In conclusion, this thesis provides data supporting that individual RGS proteins are critical in modulating the frequency and amplitude of Wnt/Ca^{2+} signaling in different tissues and at different developmental stages and this is a substantial breakthrough in understanding how RGS proteins function to fine-tune known signaling pathways.

TABLE OF CONTENTS

LIST OF TABLES viii

LIST OF FIGURES ix

LIST OF ABBREVIATIONS xi

CHAPTER 1 INTRODUCTION TO THE WNT SIGNALING NETWORK 1

Introduction 1
The Wnt signaling Network 1
Frizzled Proteins are G protein Coupled Receptors 4
G Protein Signaling 5
Regulators of G Protein Signaling 5
Goals 6
Zebrafish model system 6

CHAPTER 2 CALCIUM ACTIVITY IN ZEBRAFISH EMBRYOS 13

Introduction 13
Ca^{2+} Sources 13
Ca^{2+} Imaging 14
Cleavage period Ca^{2+} dynamics 15
Blastula period Ca^{2+} dynamics 17
Gastrula period Ca^{2+} dynamics 18
Segmentation period Ca^{2+} dynamics 23
Discussion 25
Materials and Methods 26
Zebrafish 26
Preparation and calibration of injection micropipette 26
Micro-Injections 27
Intracellular Ca^{2+} Imaging 27

CHAPTER 3 IDENTIFICATION OF A NOVEL REGULATER OF INTRACELLULAR CALCIUM RELEASE 40

Introduction 40
Regulators of G protein Signaling 41
Cloning and Characterization of R4 subfamily members 42
Endogenous requirement of RGS proteins 43
Discussion 47
Materials and Methods 48
Zebrafish 48
Micro-Injections 48
Zebrafish rgs2, 3, 4, 5, 16 and 12 cloning 48
Morpholino Micro-Injections 49
In situ hybridization 49

CHAPTER 4 REGULATOR OF G PROTEIN SIGNALING 3 MODULATES WNT5B CA^{2+} DYNAMICS AND SOMITE PATTERNING 57

Introduction 57

Rgs3 expression overlaps with Wnt5b 58
Rgs3 inhibits Wnt5b induced Ca^{2+} dynamics 59
Endogenous requirement of Rgs3 during embryogenesis 61
Rgs3 function is necessary for endogenous Ca^{2+} dynamics in somites 64
Rgs3 and Wnt5b interaction 66
Rgs3 and the Wnt signaling network 67
Discussion and Future directions 70
Materials and Methods 72
Zebrafish 72
Zebrafish *rgs3* point mutant 72
Micro-Injections 73
Cell Transplantation 73
TopFlash luciferase assay 74
Whole mount in situ hybridization 74
Western Analysis 75
Immunohistochemistry 75
Intracellular Calcium Imaging 76
Statistical analysis 77

CHAPTER 5 IDENTIFICATION OF RGS3B IN ZEBRAFISH 92

Introduction 92
EF hand Motif 92
Identification of Rgs3 splice variants 93
Gene duplicates 94
Identification of Rgs3b 96
Endogenous requirement of Rgs3b-2 97
Endogenous requirement of Rgs3b 99
Discussion 101
Materials and Methods 102
Zebrafish 102
5' rapid amplification of cDNA ends (RACE) 102
Zebrafish rgs3 point mutant 102
Micro-Injections 103
Whole mount in situ hybridization 103
Immunohistochemistry 104
Statistical analysis 104

CHAPTER 6 CONCLUSIONS AND FUTURE DIRECTIONS 112

Introduction 112
Summary 112
Conclusions 113
Future directions 115

REFERENCES 117

LIST OF TABLES

Table 1: Zebrafish RGS Percent Identities to Corresponding Human RGS Proteins.....50

Table 2: Morphological (48hpf) and Molecular (15hpf) Analysis of *rgs3* Knockdown and Rescue 83

LIST OF FIGURES

Figure 1: A Simplified Schematic of Wnt/β-catenin Signaling....8
Figure 2: A Simplified Schematic of Wnt/calcium Signaling. 9
Figure 3: A Simplified Schematic of the Wnt signaling Network....10
Figure 4: A Simplified Schematic of G protein Signaling....11
Figure 5: Zebrafish Developmental Stages....12
Figure 6: Analyzing Intracellular Calcium Dynamics. 29
Figure 7: Cleavage Stage Calcium Dynamics 30
Figure 8: Blastula Period Calcium Dynamics. 31
Figure 9: Epiboly Stage Calcium Dynamics. 32
Figure 10: Ubiquitous and YSL Targeted Injections. 33
Figure 11: YSL Targeted GFP-Monomeric-Actin Injections. 34
Figure 12: Calcium Dynamics in *betty boop* 35
Figure 13: DN-p38 Induces Ectopic Calcium Release 36
Figure 14: Calcium Dynamics During Zebrafish Somitogenesis. 37
Figure 15: Calcium Dynamics During Zebrafish Neurulation 38
Figure 16: Calcium Dynamics During Zebrafish Neural Rod Formation. 39
Figure 17: RGS Proteins have Unique and Overlapping Expression Patterns. 51
Figure 18: Heart Defects in RGS Morphants. 52
Figure 19: Cardiovascular Defects in RGS Morphants. 53
Figure 20: RGS Morphant Phenotypes. 54
Figure 21: Analysis of Rgs3, 4 and 5 Knockdown 55
Figure 22: Analysis of Rgs3 Morphants Convergent-Extension Defect. 55
Figure 23: Analysis of *rgs3* Knockdown. 56
Figure 24: Temporal and Spatial Expression of *rgs3* Throughout Zebrafish Development. 78
Figure 25: *rgs3* Expression is Adjacent and Overlapping with *wnt5*. 79

Figure 26: Rgs3 Inhibits *wnt5b* Induced Ca^{2+} Dynamics. 80

Figure 27: Rgs3 Knockdown is Reminiscent of Altered Wnt Signaling. 81

Figure 28: *rgs3* Morphant Phenotypes and Functional Rescue. 82

Figure 29: Calcium Dynamics During Zebrafish Somitogenesis. 84

Figure 30: rgs3 Impacts Segmentation Stage Calcium Dynamics. 85

Figure 31: *rgs3* Functions Downstream of *wnt5* to Impact Segmentation Stage Calcium Dynamics. 86

Figure 32: *rgs3* and wnt5 Expression in Morphant Embryos 87

Figure 33: *rgs3* Interacts with the Wnt Signaling Network. 88

Figure 34: Flag-*rgs3* Results in Decreased Dvl2-Myc Expression. 90

Figure 35: *rgs3* Does Not Directly Bind to Dvl2-Myc. 89

Figure 36: rgs3 Knockdown Influences Wnt/β-catenin Signaling. 91

Figure 37: Alignment of Human and Zebrafish Rgs3 105

Figure 38: Temporal and Spatial Expression of Rgs3b Throughout Zebrafish Development. 106

Figure 39: *rgs3b-2* Morphant Phenotypes and Functional Rescue. 107

Figure 40: Statistically Significant Suppression of rgs3b-2 Knockdown Requires a Functional RGS Domain 108

Figure 41: *rgs3b* Gene Knockdown. 109

Figure 42: Characterization of the Aberrant Transcript Produced by *rgs3b 772*sa MO Injection. 1102

Figure 43: *rgs3b* Morphant Phenotypes. 111

LIST OF ABBREVIATIONS

AP	Anterior-Posterior
APC	Adenomatous Polyposis tumor suppressor protein
Ca^{2+}	Calcium
CE	Convergent extension
DAG	Diacylglycerol
DDC	Duplication/Degeneration/Complementation
DEP	Dishevelled, EGL-10 and Pleckstrin
Dig	Digoxigenen
DIX	Dishevelled and axin
DN	Dominate Negative
DNP	Dinitrophenyl
Dvl	Dishevelled
Eng1	Engrailed 1
ER	Endoplasmic reticulum
EST	Expressed Sequence Tagged
EVL	enveloping layer
FZ	Frizzled
GAP	GTPase-activating protein
GPCR	G Protein Coupled Receptor
GSK	Serine Threonine Kinase
hpf	Hours post fertilization
IP_3	Inositol 1,4,5-trisphosphate
IP_3R	Inositol 1,4,5-trisphosphate Receptor
LEF/TCF	Lymphoid Enhancer Factor/T-Cell Factor
MAPK	Mitogen Activated Protein Kinase
MAPKAPK2	Mitogen Activated Protein Kinase Activated Protein Kinase 2
Met	Methionine
MO	Morpholino
PBS	Phosphate-Buffered Saline
PCP	Planar cell polarity
PDZ	PSD-95, Discs-large and ZO-1
PI	phosphatidylinositol
PIP_2	phosphatidylinositol (4,5)-bisphosphate
PLC	phospholipase C
pL	picoliters
ppt	Pipetail
RACE	Rapid Amplification of cDNA Ends
RGS	Regulators of G protein Signaling
RLU	Relative Luciferase activity Units
RT-PCR	Reverse Transcriptase Polymerase Chain Reaction
TxR	Texas Red
WMISH	Whole-mount *in situ* hybridization
Wt	Wildtype
YSL	Yolk syncytial layer

CHAPTER 1

INTRODUCTION TO THE WNT SIGNALING NETWORK

Introduction

All animals originate from an egg. Upon fertilization, a single cell gives rise to the many cells which rearrange to form the adult tissues and organs. During embryogenesis, growth factors such as the Wnts and their associated receptors can modulate calcium (Ca^{2+}) release leading to activation of Ca^{2+} binding proteins. Although it's been shown that Ca^{2+} release within a cell is tightly controlled, how the release dynamics result in a specific biological output in embryonic development is less clear. This thesis is focused on the effects G protein regulation has on intracellular Ca^{2+} release dynamics and developmental patterning events. In this introduction, I will describe the Wnt signaling network, key players such as G proteins and the importance of precisely regulating the amplitude as well as duration of Wnt/Ca^{2+} signaling.

The Wnt signaling Network

Wnts are a large family of cysteine-rich secreted glycoproteins that interact with receptors of the Frizzled (Fz) family to signal across the plasma membrane (Wodarz and Nusse 1998). The Wnt signaling network has been classified into β-catenin-dependent and β-catenin-independent pathways (Cadigan and Nusse 1997; Slusarski, Corces et al. 1997; Willert and Nusse 1998; Kohn and Moon 2005).

β-catenin-dependent Wnt signaling acts through the stabilization of β-catenin and subsequent transcriptional activation of β-catenin targets (Willert and Nusse 1998) (Figure 1). In the absence of Wnt/β-catenin signaling, β-catenin is rapidly sequestered in a cytoplasmic degradation complex containing axin, the adenomatous polyposis tumor suppressor protein (APC) and the serine threonine kinase GSK-3β. GSK-3 phosphorylation of β-catenin targets the latter for proteasomal degradation. Vertebrate Wnt1, Wnt3a and Wnt8 have been shown to activate β-catenin-dependent Wnt signaling

and have therefore been classified as canonical Wnts (Dale 1998). Binding of canonical Wnts to their co-receptors Fz and LRP5/6 (low-density lipoprotein receptor-related protein) activates a cytoplasmic phosphoprotein (Dishevelled, Dvl) which downregulates GSK-3 and inhibits the degradation of β-catenin. Stabilized β-catenin protein enters the nucleus, where it then interacts with the members of the LEF/TCF (lymphoid enhancer factor/T-cell factor, DNA binding proteins) transcription factor family to promote the activation of downstream target genes.

Core components such as Fz and Dvl are utilized in both β-catenin-dependent and β-catenin-independent signaling and it has predicated that Dvl is a branch point between Wnt/β-catenin and Wnt/Ca^{2+}. Dishevelled is characterized by having an amino terminal DIX (Dishevelled and axin) domain, a central PDZ (PSD-95, Discs-large and ZO-1) domain and a C-terminal DEP (Dishevelled, EGL-10 and Pleckstrin) domain (Klingensmith, Nusse et al. 1994; Axelrod, Miller et al. 1998). The DIX domain of Dvl2 is important for localization to axin and the β-catenin destruction complex (Kishida, Yamamoto et al. 1999), the PDZ domain has been shown to interact with the intracellular domains of Fz receptors (Wharton 2003) while the DEP domain is required for membrane localization (Park, Gray et al. 2005). Mutants lacking the DIX domain have been shown to activate Wnt/Ca^{2+} (Sheldahl, Slusarski et al. 2003) and planer cell polarity signaling independent of Wnt/Fz activation (Boutros, Paricio et al. 1998; Tada and Smith 2000), while mutants lacking either the PDZ or DEP domain of Dvl2 suppress β-catenin-independent signaling.

In vertebrate development, changes in β-catenin-independent Wnt signaling are manifested by altered cell movement during gastrulation often resulting in convergence extension defects. Unlike the β-catenin-dependent Wnt signaling, which acts through the stabilization of β-catenin, activation of β-catenin-independent Wnt signaling has been shown to lead to Ca^{2+} release as well as activation of Rac, Rho and other cytoskeletal components in vertebrates (Kohn and Moon 2005; Cadigan and Liu 2006). In the

zebrafish embryo, *wnt5* overexpression results in an increase in the frequency of intracellular Ca^{2+} release in a manner that is dependent on G-protein activity and the phosphatidylinositol (PI) cycle (Slusarski, Corces et al. 1997; Slusarski, Yang-Snyder et al. 1997), thus linking Wnt activity to inositol 1,4,5-trisphosphate (IP_3)-dependent Ca^{2+} release and defining the Wnt/Ca^{2+} signaling pathway (Figure 2).

In non-excitable (non-neuronal) cells, a majority of intracellular Ca^{2+} release occurs through IP_3-sensitive Ca^{2+} channels present in the endoplasmic reticulum (ER) membrane (reviewed in (Berridge, Bootman et al. 2003). The PI cycle is activated in response to many hormones and growth factors that bind to cell surface receptors. Two predominant receptor classes are the G-protein coupled receptor class and the receptor tyrosine kinase class. Extracellular ligand stimulation of these receptors activates a PI-specific phospholipase C (PLC). Activated PLC converts membrane-bound phosphatidylinositol (4,5)-bisphosphate (PIP_2) into IP_3 and lipophilic diacylglycerol (DAG). IP_3 subsequently binds to receptors (IP_3R) located principally on the ER triggering the rapid release of Ca^{2+} into the cytosol of the cell (Figure 2). At the same time, DAG produced by PIP_2 hydrolysis can act as an additional second messenger to further activate downstream targets such as protein kinase C (PKC).

Emerging evidence suggests that the ability of Wnt ligands to activate different signaling pathways, Wnt/β-catenin and Wnt/Ca^{2+}, appears to be controlled by the timing of expression and receptor context, not to mention the correct combination of intracellular effectors. Although Wnt signaling has been classified as β-catenin-dependent and β-catenin-independent, the hypothesis that Wnt/Ca^{2+} signaling influences the Wnt/β-catenin pathway resulting in a complex Wnt signaling network has been proposed (Freisinger, Schneider et al. 2008). The concept of a Wnt signaling network was originally suggested by the apparent antagonism of certain pairs of Wnt ligands when expressed in *Xenopus* and zebrafish embryos (Moon, Christian et al. 1993; Slusarski, Yang-Snyder et al. 1997). Expression of ligands that activate Wnt/β-catenin

signaling in these embryos, such as Wnt-8, results in ectopic axis induction. However, when *wnt5* is co-expressed with *wnt8*, the Wnt8 axis induction phenotype is suppressed. Stimulating Ca^{2+} release, via activated serotonin receptor, also antagonizes Wnt8-induced expansion of dorsal domains (Slusarski, Yang-Snyder et al. 1997), supporting that the identified Wnt5 antagonism of Wnt/β-catenin is mediated by Ca^{2+} release. On the other hand, pharmacological or genetic reduction of the Wnt/Ca^{2+} pathway in zebrafish embryos or mouse limb buds generates ectopic accumulation of nuclear β-catenin and activation of β-catenin transcriptional targets (Topol, Jiang et al. 2003; Westfall, Brimeyer et al. 2003; Westfall, Hjertos et al. 2003). Additionally, inhibition of G-protein function dorsalizes Xenopus embryos (Kume, Saneyoshi et al. 2000). These observations are consistent with a model in which IP_3-dependent Ca^{2+} release, promoted by Wnt/Ca^{2+} signaling activity; negatively regulates the Wnt/β-catenin signaling pathway (Figure 3).

Frizzled Proteins are G protein Coupled Receptors

Wnts interact with receptors of the Fz family (Wodarz and Nusse 1998) and due to structural similarities Fz receptors have been classified as members of the G protein coupled receptor (GPCR) superfamily. GPCRs function to transfer extracellular signals across the cell membrane to intracellular effectors. To date, over 800 GPCRs have been identified in the human genome and their functions are essential to regulate multiple biological processes (Fredriksson, Lagerstrom et al. 2003).

Structurally Fz receptors share key features with GPCRs, such as an extracellular ligand binding domain, seven trans-membrane-spanning sequences and an intracellular C-terminal tail. Over the past decade evidence supports that Fz receptors couple to G proteins. In fact, the Slusarski lab has shown that Wnt proteins work though specific Fz homologues to activate G proteins and to modulate Ca^{2+} release in zebrafish embryos (Slusarski, Corces et al. 1997; Slusarski, Yang-Snyder et al. 1997; Ahumada, Slusarski et al. 2002; Westfall, Hjertos et al. 2003). Moreover, in *Drosophila*, Wnt target genes have

been shown to be upregulated when Gαo is over-expressed and constitutively active Gαo is sufficient to restore Wnt signaling in the absence of Fz activity (Katanaev, Ponzielli et al. 2005). In addition, epistasis experiments indicate that G proteins function downstream of Fz and upstream of Dishevelled (Katanaev, Ponzielli et al. 2005).

G Protein Signaling

G proteins are heterotrimeric cell membrane associated proteins which consist of alpha (α), beta (β) and gamma (γ) subunits. As depicted in Figure 4A, ligand binding induces a conformational change which catalyzes a guanine nucleotide exchange inducing the Gα subunit to release GDP and bind GTP. When Gα binds GTP, it dissociates from Gβγ leading to active Gα and βγ subunits which are free to stimulate their downstream effectors and second messengers. The Gα subunit has intrinsic GTP hydrolysis which resets the cycle (Premont, Inglese et al. 1995; Hollinger and Hepler 2002) (Figure 4B).

Due to their extensive ability to modulate diverse signaling pathways GPCR function is tightly controlled. One of the best-understood mechanisms of signal desensitization involves phosphorylation of stimulated GPCRs by specific kinases followed by receptor interaction with arrestins (Premont, Inglese et al. 1995). However because active Gα and Gβγ subunits act as signal transducers, the key reaction in termination of GPCR signaling is the hydrolysis of Gα-GTP to Gα-GDP, via the intrinsic GTPase activity of Gα, resulting in formation of the inactive heterotrimeric G protein.

Regulators of G Protein Signaling

One level of G protein signaling is regulated by ligand stimulation. However, another level of regulation resides in the duration of signaling via active Gα-GTPand Gβγ subunits. A class of proteins, Regulators of G protein Signaling (RGS proteins) have been shown to influence the duration of G protein signaling (De Vries, Zheng et al. 2000; Ross and Wilkie 2000; Hollinger and Hepler 2002; Siderovski and Willard 2005).

RGS proteins are classified based on the presence of a highly conserved 130 amino acid RGS domain. The RGS domain allows protein binding to activated Gα subunits and subsequently accelerates the rate of GTP hydrolysis by up to 1000-fold (Watson, Linder et al. 1996; Hepler, Berman et al. 1997; Kozasa 1998) (Figure 4C). By functioning as GTPase-activating proteins (GAPs) for G proteins, RGS proteins are uniquely situated to modulate the intensity and duration of Wnt signaling. However, no studies have ascertained the possible importance of RGS proteins in Wnt/Ca^{2+} signaling or whether changes in frequency and or amplitude of signaling result in biological defects.

Goals

Previous work in our lab and others had identified that G protein signaling is required for embryonic Ca^{2+} release activity (Slusarski, Yang-Snyder et al. 1997; Ahumada, Slusarski et al. 2002). The primary goal of my thesis was to determine how the amplitude and duration of Ca^{2+} release activity translates into a distinct biological output. To accomplish this goal I had to first characterize endogenous Ca^{2+} activity in zebrafish (Chapter 2), identify a specific regulator of Ca^{2+} activity (Chapter 3 and 5) and determine if altering Ca^{2+} dynamics translates into a specific developmental output (Chapter 4).

Zebrafish model system

The zebrafish (*Danio rerio)* are tropical freshwater fish which originated in the Ganges region in Eastern India. Zebrafish have a generation time of 3-4 months and mature breading pairs can lay hundreds of eggs in a single day. Fertilized zebrafish embryos develop rapidly and by just 30 hours post fertilization it is possible to directly visualize their internal organs (Figure 5).

Their small size (4-6 cm), external egg lay, fecundity and rapid development make zebrafish an ideal model system for understanding development. The transparency

of the embryo allows for direct visualization of the internal organs during development in the live embryo, use of transgenic lines expressing fluorescent proteins under the control of tissue specific promoters (such as a vascular specific line) and the ability to do *in vivo* Ca^{2+} release imaging. Additionally, zebrafish are known to have 25 chromosome pairs and are diploid allowing for predictable analysis of genetic mutants.

The amenable traits of the zebrafish allow me to verify the direct physiological responses *in vivo* in mutant or mis-expressed backgrounds and evaluate impact in the whole animal, especially if specific tissues have different responses. The ease of manipulation of zebrafish embryos allows for easy introduction of reagents while their rapid development allows for fast evaluation of embryonic defects.

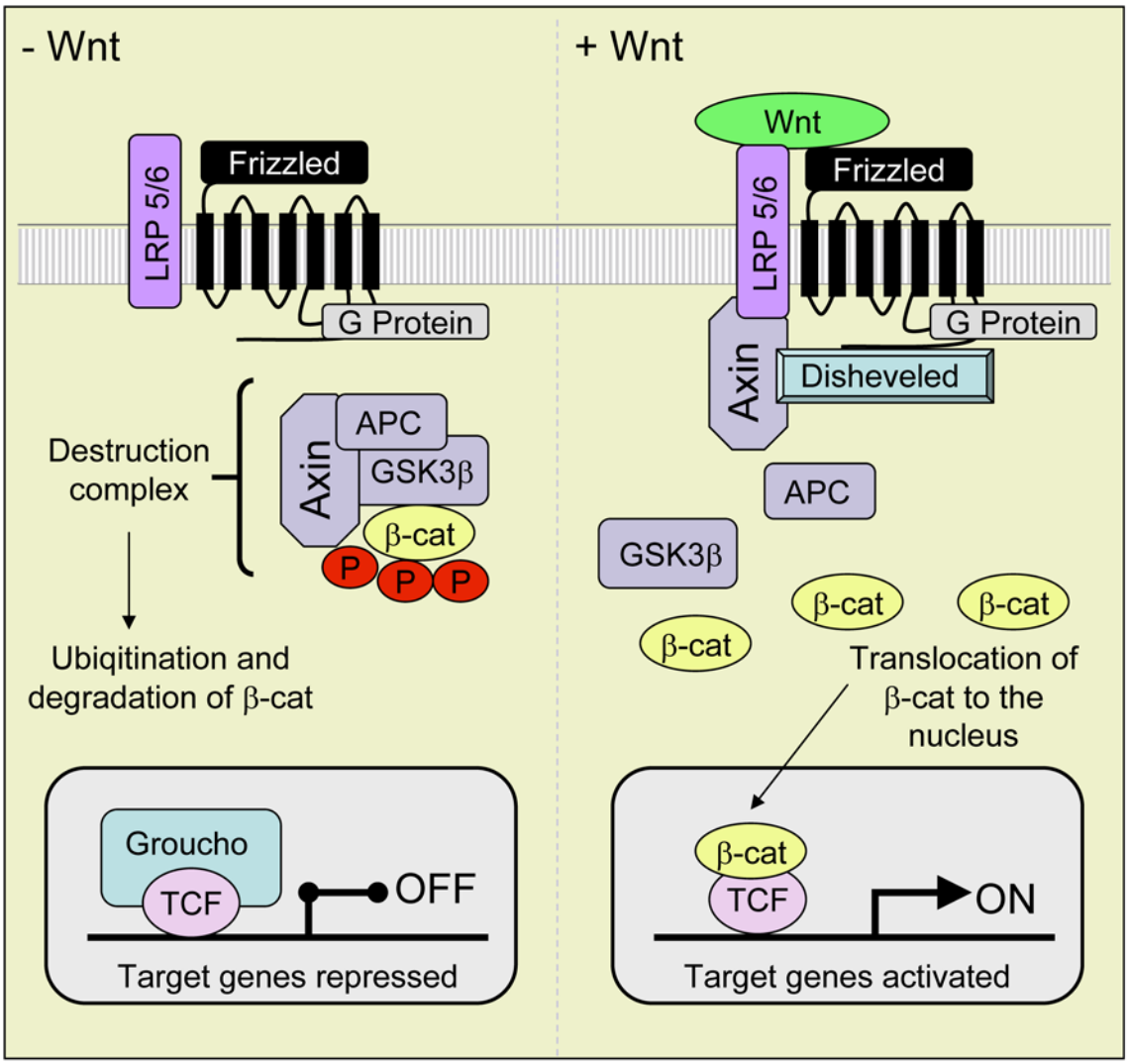

Figure 1: A Simplified Schematic of Wnt/β-catenin Signaling. Wnt/β -catenin signaling dependent components in the absence of a Wnt ligand on the left side and in the presence of a Wnt ligand on the right side of the dotted line. Binding of a Wnt ligand to a Frizzled/LRP-5/6 receptor complex leads to stabilization of β-catenin and activation of target genes. APC= adenomatous polyposis tumour suppressor protein, GSK-3β= serine threonine kinase and β-cat= β-catenin.

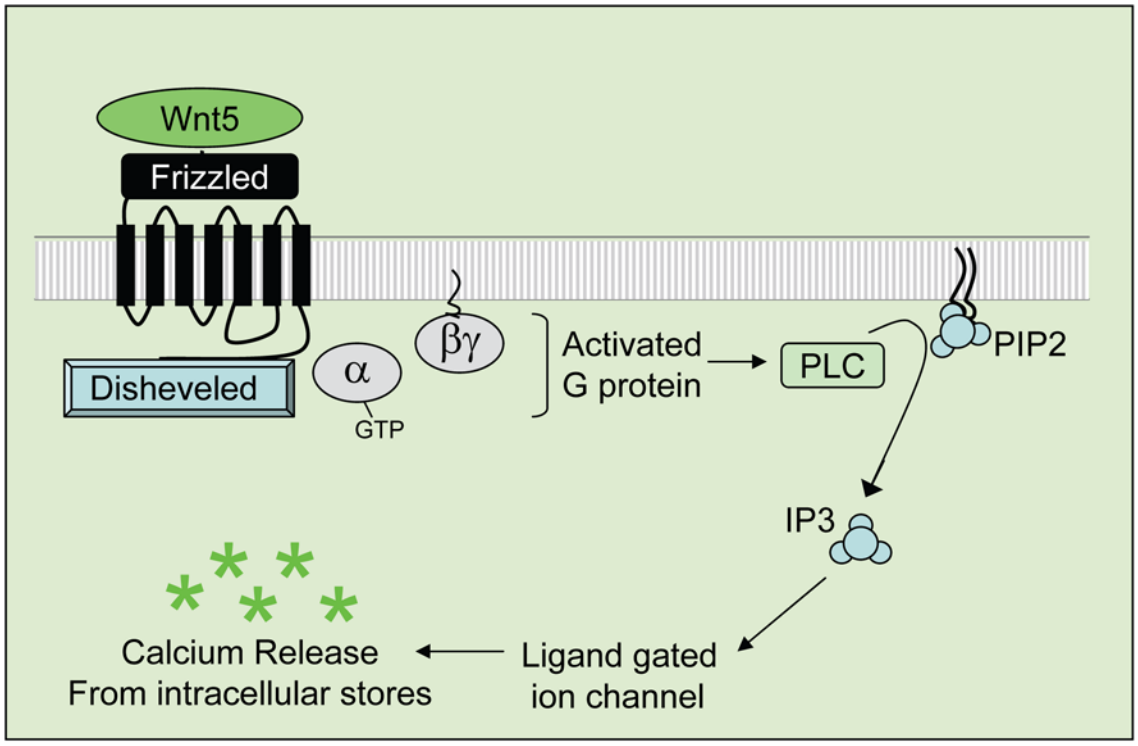

Figure 2: A Simplified Schematic of Wnt/calcium Signaling. Activation of the Wnt/calcium pathway results in intracellular calcium release in a manner that is dependent on G protein activity and the PI cycle.

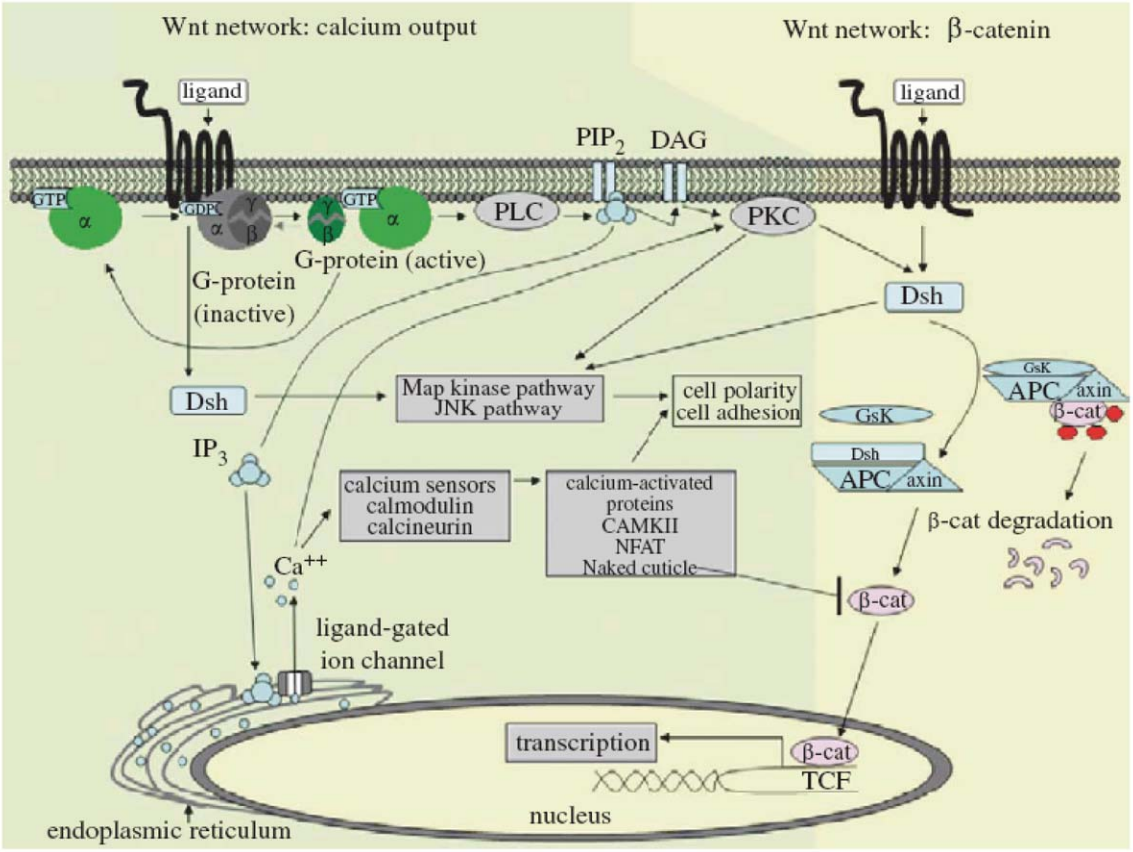

Figure 3: A Simplified Schematic of the Wnt Signaling Network. β-catenin-independent pathways are encased in green region and β-catenin-dependent components are in the yellow region. β-cat = β-catenin (modified from Freisinger, Schneider et al. 2008).

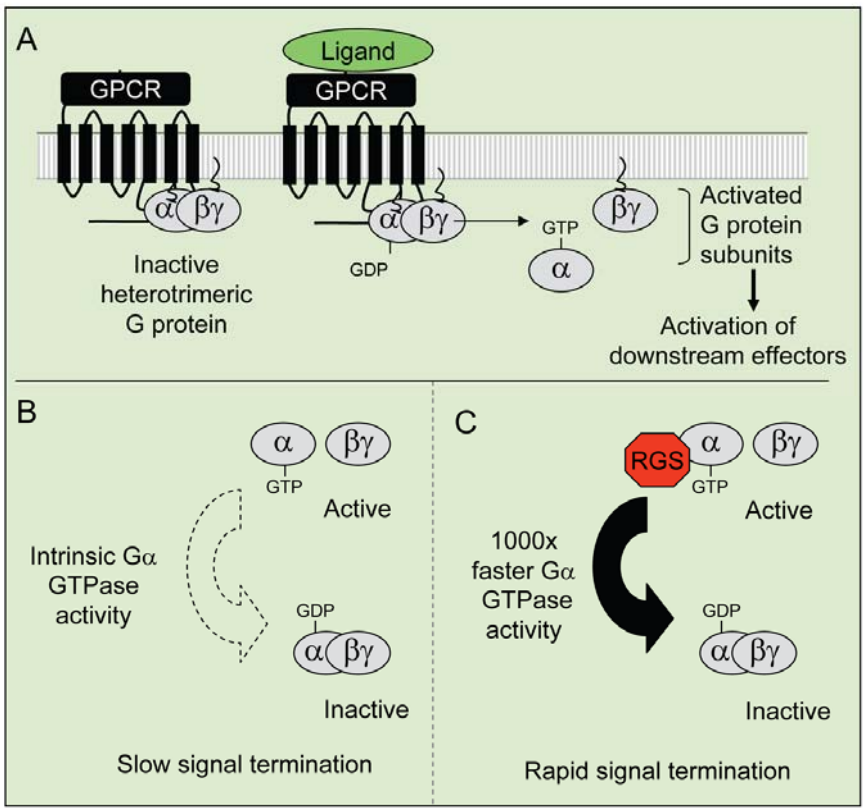

Figure 4: A Simplified Schematic of G protein Signaling. Extracellular ligand binds a seven-transmembrane receptor catalyzing exchange of GDP to GTP on Gα. (A) Gα-GTP dissociates from Gβγ and the subunits transmit intracellular signals. (B) The Gα subunit has intrinsic GTPase activity converting Gα-GTP back to Gα-GDP. (C) Gα-GDP binds Gβγ and reforms the inactive heterotrimer (Gαβγ). (C) RGS binding to Gα-GTP stimulates signal termination by acting as a GAP.

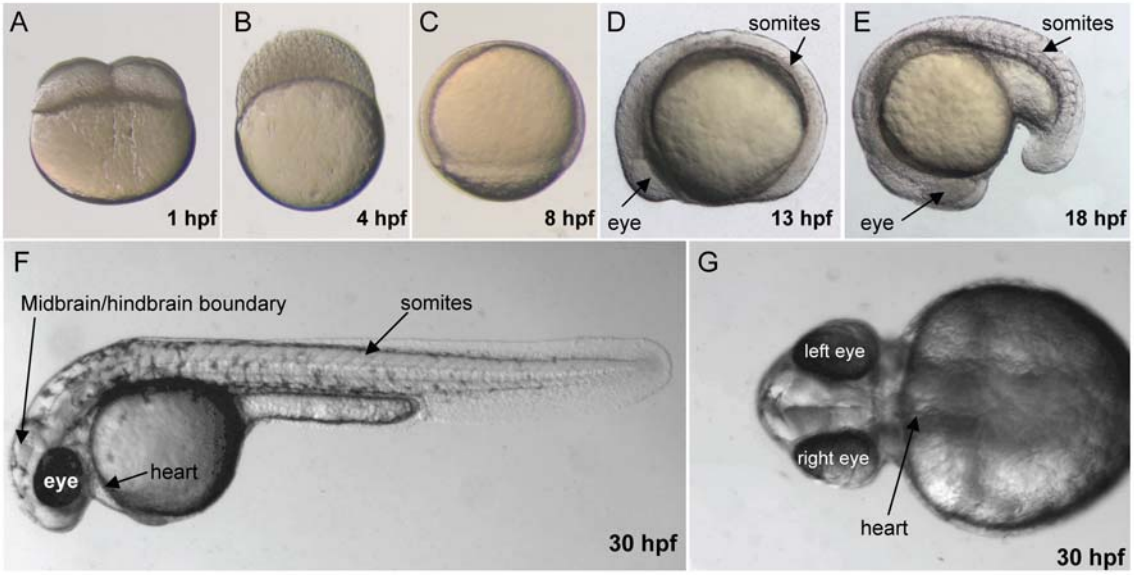

Figure 5: Zebrafish Developmental Stages. Images of live zebrafish embryos from 1 hpf to 30 hpf. (A-F) Lateral and (G) Dorsal view, oriented with (A-C) the animal pole to the top or (D-G) the anterior to the left. hpf= hours post fertilization.

CHAPTER 2

CALCIUM ACTIVITY IN ZEBRAFISH EMBRYOS

Introduction

Ca^{2+} release is a key signal for many cellular processes including neuronal synapse, muscle contraction, cell division and fertilization. As an essential second messenger molecule, the dynamics of Ca^{2+} release inside a cell are tightly regulated. Ca^{2+} levels are predominantly controlled by a gradient of Ca^{2+} concentration either across the plasma membrane or across the membrane of intracellular Ca^{2+} stores. The opening of specialized ion channels and the release from intracellular organelles generates bursts of Ca^{2+} into the cytosol. The location, extent and duration of the ion channel opening can result in a local or global signaling event.

In zebrafish embryos, Ca^{2+} release dynamics have been described during epiboly, gastrulation and organogenesis (Reinhard, Yokoe et al. 1995; Slusarski, Yang-Snyder et al. 1997; Gilland, Miller et al. 1999; Slusarski and Corces 2000; Webb and Miller 2000; Webb and Miller 2003; Lyman Gingerich, Westfall et al. 2005; Slusarski and Pelegri 2007; Freisinger, Schneider et al. 2008; Schneider, Houston et al. 2008). Each phase of zebrafish development has a distinct pattern of Ca^{2+} release, highlighting the complexity of Ca^{2+} ion and cellular physiology. In this chapter, I characterize endogenous Ca^{2+} release during the cleavage, blastula, epiboly and early somite stages.

Ca^{2+} Sources

Although critical for many processes, Ca^{2+} ions are not metabolized by the cell. Instead, Ca^{2+} enters the cell across either the plasma membrane or the membrane of intracellular organelles. Depending on the location of the ion channels and the extent and duration of the channel opening, local or global changes in Ca^{2+} levels in the cytosol of the cell can result. Intricate crosstalk and feedback between release circuits can stimulate Ca^{2+}- induced Ca^{2+} release, influencing neighboring receptors and potentially triggering a

regenerative wave (Berridge 1997; Berridge, Bootman et al. 2003; Roderick, Berridge et al. 2003). In addition, continued stimulation and/or depletion of ER stores activate a store operated Ca^{2+} entry influx pathway located at the plasma membrane (Parekh and Putney 2005).

Ca^{2+} Imaging

Ca^{2+} indicators have proven to be useful tools in the investigation of the role of Ca^{2+} in the Wnt signal transduction network. Intracellular Ca^{2+} dynamics can be directly visualized in the live transparent zebrafish embryo using either bioluminescent (aequorin) or fluorescent Ca^{2+} reporters (Ca^{2+} green-1 and Fura-2). While bioluminescent Ca^{2+} reporters can be used over a long time-course they only provide a low-resolution map of Ca^{2+} activity, fluorescent Ca^{2+} reporters however provide higher resolution readout and can identify individual cells with high intracellular Ca^{2+} levels (Freisinger, Houston et al. 2008).

For my investigation, I choose to use a fluorescent Ca^{2+} reporter and microscope-based applications to highlight Ca^{2+} activity in intact zebrafish embryos. The basic technical approach is to detect endogenous Ca^{2+} release activity with a light source to excite a Ca^{2+} indicator in a sample, coupled with a detector that monitors indicator emission (Freisinger, Houston et al. 2008). This approach has the advantage of being able to provide a high enough resolution image allowing us to identify individual cells with high intracellular Ca^{2+} levels.

I choose to use the Ca^{2+} reporter Fura-2 instead of other fluorescent Ca^{2+} reporters such as Ca^{2+} green because Fura-2 is a ratiometric dye and Ca^{2+} green is a single wavelength reporter. One problem with Ca^{2+} reporters which utilize a single wavelength is that they can interpret differences in cell thickness and uneven distribution of the fluorescent indicator as a Ca^{2+} dependent change. Fura-2 utilizes two wavelengths and therefore has reduced sensitivity to signal artifacts.

Fura-2, is a fluorescent derivative of the Ca^{2+} chelator EGTA developed by Tsien and colleagues (Grynkiewicz, Poenie et al. 1985), to detect changes in Ca^{2+}. The excitation spectra are different between the Ca^{2+} bound (340 nm) and Ca^{2+} free (380 nm) forms. By taking the ratio of the fluorescence intensity at these two wavelengths, an estimate of intracellular free Ca^{2+} can be derived. The ratio image, a pixel by pixel match of both excitation wavelengths, is calculated by computer software (RatioTool, Inovision). The pseudocolored ratio image provides a spatial and temporal measurement of Ca^{2+} dynamics with low Ca^{2+} represented by blue and high Ca^{2+} represented by yellow/red. (Figure 6A). The sequence of ratio images is processed and the Ca^{2+} fluxes (transients) are then determined by a subtractive analog patterned after (Lechleiter, Girard et al. 1991; Chang and Meng 1995) and described in (Slusarski and Corces 2000; Freisinger, Houston et al. 2008) (Figure 6B). Subtractive images are then superimposed to create a compiled subtractive image which is then converted into a topographical representation in which the color and peak height indicate the total number of Ca^{2+} transients present in that region of the embryo (Figure 6C).

Cleavage period Ca^{2+} dynamics

After fertilization, cytoplasm streams toward the animal pole of the embryo resulting in the separation of the blastodisc from the yolk (Figure 7A). Next the zygote enters the cleavage stage. In the cleavage stage (2-64 cell), the zygote undergoes rapid (15 minute), synchronous cell divisions with no growth phase (Kimmel, Ballard et al. 1995). Due to the large size of the yolk, the cytoplasmic divisions are meroblasic and the blastomeres remain interconnected until the 16 cell stage when some of the cells become completely cleaved from the rest. This rapid synchronous cell division results in an increased number of smaller cells while maintaining the overall mass of the zygote.

Ca^{2+} dynamics during the cleavage stage have been characterized using both fluorescent and luminescent Ca^{2+} reporters. In sea urchin, increases in Ca^{2+} concentration

have been observed in the cleavage furrows, and cleavage formation is inhibited by lithium treatment. Lithium is proposed to block the PI cycle by inhibiting inositol turnover (Berridge, Downes et al. 1989). This inhibition can be rescued by the addition of myo-inositol (Stricker 1995; Wilding, Torok et al. 1995; Becchetti and Whitaker 1997), supporting the conclusion that Ca^{2+} has a key role in the progression of cleavage stage development. In the frog embryo, IP_3 dependent Ca^{2+} signals have been observed in the forming cleavage furrows (Muto, Kume et al. 1996). While in zebrafish, increases in intracellular Ca^{2+} concentration have been associated with positioning the cleavage plane, and several distinct Ca^{2+} signals have been identified which accompany the stages of cytokinesis (Chang and Meng 1995; Webb, Lee et al. 1997; Creton, Speksnijder et al. 1998; Lee, Webb et al. 2003). Further studies have indicated that the localized rise in Ca^{2+} during the cleavage period is required for furrow deepening and positioning (Lee, Webb et al. 2003; Lee, Webb et al. 2006) and is IP_3 dependent (Chang and Meng 1995); (Webb, Lee et al. 1997).

Using Fura-2, I am able to accurately image Ca^{2+} dynamics during zebrafish development. I find that intracellular Ca^{2+} release is dramatically increased in the forming cleavage furrows of 2, 4 and 8 cell zebrafish embryos (Figure 7B'-D'). Ca^{2+} activity during the first rounds of cell division is very dynamic in the forming furrows and propagates as the furrows deepen during cytokinesis. I observe a furrow positioning signal, a furrow propagation signal or wave, and a central positioning signal. These signals are similar to those described using a luminescent Ca^{2+} reporter (Webb, Lee et al. 1997; Lee, Webb et al. 2003). Antagonists of the IP_3 receptor have been shown to block furrow deepening and transient Ca^{2+} release supporting the conclusion that cleavage stage Ca^{2+} dynamics are IP_3 dependent (Lee, Webb et al. 2003). After cytokinesis, the Ca^{2+} signal disappears and intracellular Ca^{2+} levels return to resting levels. These data verify that during the cleavage period of zebrafish development, Ca^{2+} dynamics are an essential feature of cell cleavage.

Blastula period Ca^{2+} dynamics

After the cleavage stage the zygote starts the blastula period. During this time the embryo enters the midblastula transition, cell cycles lengthen, cell divisions become asynchronous and zygotic transcription begins. Additionally, it is during the blastula period that the yolk syncytial layer (YSL) forms and epiboly begins (Kimmel, Ballard et al. 1995).

Ca^{2+} activity in the zebrafish blastula has been observed in the enveloping layer (EVL) and YSL (Reinhard, Yokoe et al. 1995; Slusarski, Yang-Snyder et al. 1997; Slusarski and Corces 2000). Cells in the EVL have unique characteristics; they are tightly sealed and form an epithelial–like monolayer over the deep cells. During the blastula period, I observe that EVL-specific Ca^{2+} fluxes are present in a cell or small cluster of cells lasting for short intervals (<15 seconds) (Figure 8A'-C' arrows) as well as YSL-specific Ca^{2+} which displays sustained elevation in a population of cells (Figure 8 A'-C' arrow head). These results are consistent with two distinct types of Ca^{2+} release events that have been characterized, including aperiodic transient fluxes found mainly in the enveloping layer and dorsal forerunner cells (Reinhard, Yokoe et al. 1995; Slusarski, Corces et al. 1997; Lyman Gingerich, Westfall et al. 2005; Schneider, Houston et al. 2008)and sustained increases in Ca^{2+} levels in the deep cell layer and yolk syncytial layer (Westfall, Brimeyer et al. 2003; Holloway, Gomez de la Torre Canny et al. 2009). *In vivo* imaging in zebrafish indicates that the rapid aperiodic Ca^{2+} release persists until the midblastula transition stage (Reinhard, Yokoe et al. 1995; Slusarski, Yang-Snyder et al. 1997; Slusarski and Corces 2000).

It has been suggested that PI-cycle dependent Ca^{2+} activity is connected to body plan formation and the establishment of the primary axes, in which regions of the embryo receive signals to determine the cells that will contribute to the dorsal (back) or ventral (belly) tissue as well as anterior (head/top) and posterior (tail/bottom) regions. The idea that increased IP_3 levels may trigger Ca^{2+} release during the blastula period has been

corroborated by drug inhibition studies (Slusarski, Corces et al. 1997). Classical work using lithium, an inhibitor of inositol turnover (Berridge, Downes et al. 1989), induced expansion of dorsal structures in Xenopus (Kao, Masui et al. 1986; Kao and Elinson 1988; Kao and Elinson 1989; Kao and Elinson 1998), and similar effects were obtained in zebrafish (Stachel, Grunwald et al. 1993; Aanstad and Whitaker 1999). Zebrafish mutants with increased Ca^{2+} activity in the EVL during blastula stages, such as *hecate*, have defects in the formation of dorso-anterior structures (Lyman Gingerich, Westfall et al. 2005) while zebrafish mutants with decreased Ca^{2+} activity during blastula stages, such as *pipetail* (Wnt5b mutant), exhibit hyperdorsalization (Westfall, Brimeyer et al. 2003). Additionally, by blocking the PI cycle and depleting intracellular Ca^{2+} stores we observe distinct hyperdorsalization phenotypes in zebrafish embryos (Westfall, Hjertos et al. 2003) and inhibiting Ca^{2+} activity in *hecate* mutant embryos results in expansion of dorsal genes, such as *chordin* (Lyman Gingerich, Westfall et al. 2005), further supporting that blastula period Ca^{2+} dynamics may directly have a role in dorso-ventral axis formation. These observations are consistent with a model in which IP_3-dependent Ca^{2+} release, promoted by Wnt/Ca^{2+} signaling activity; negatively regulates the Wnt/β-catenin signaling pathway and therefore axis induction (Figure 3).

Gastrula period Ca^{2+} dynamics

As epiboly continues the zygote enters the gastrula period and the EVL cells form a protective layer over the blastoderm. During gastrulation, cell movements result in the formation of three germ layers: ectoderm, mesoderm and endoderm. Additionally, cells undergo a variety of morphogenetic movements to thicken (dorsal convergence) and elongate (axis extension) the embryo, also called convergent extension (CE; (Keller 2002).

In intact zebrafish embryos, localized increases in intracellular Ca^{2+} (Lee, Webb et al. 2003) as well as intercellular Ca^{2+} waves have been observed during gastrulation

(Gilland, Miller et al. 1999; Webb and Miller 2003). The function of Ca^{2+} waves may be to synchronize and coordinate cellular responses (Meyer 1991). Indeed, pan-embryonic Ca^{2+} waves are proposed to coordinate CE movements and cell migration to the future dorsal side (Wallingford, Ewald et al. 2001). The relationship between Ca^{2+} waves and cell movement is supported by the finding that, in *Xenopus* embryos, pharmacological inhibition of such waves results in CE defects without altering cell fate (Wallingford, Ewald et al. 2001; Wallingford, Vogeli et al. 2001). Wnt genes that result in the activation of Ca^{2+} release in the blastula embryo, such as Wnt5 (Slusarski, Yang-Snyder et al. 1997; Westfall, Hjertos et al. 2003), can also alter morphogenetic movements later during gastrulation when misexpressed (Moon, Campbell et al. 1993; Ungar, Kelly et al. 1995). Additionally, zebrafish homozygous zygotic Wnt5/*ppt* mutants have reduced Ca^{2+} release frequency and display CE defects (Westfall, Brimeyer et al. 2003) further suggesting that Ca^{2+} release activity funtions to coordinate CE movements and cell migration.

In zebrafish, endogenous Ca^{2+} release activity, as well as a requirement for Ca^{2+} during epiboly, supports its playing an important role in epiboly progression (Cheng, Miller et al. 2004). I imaged live zebrafish embryos during gastrulation (Figure 9). Here, I report that Ca^{2+} levels are low during early to 60% epiboly (Figure 9). This is consistent with previous reports which refer to this period as the "quiet" period for Ca^{2+} (Creton, Speksnijder et al. 1998; Gilland, Miller et al. 1999; Webb and Miller 2003; Lee, Webb et al. 2006).

Webb and Miller have identified the appearance of Ca^{2+} waves in zebrafish embryos after 50% epiboly (Webb and Miller 2003), suggesting a role for Ca^{2+} signaling in the final progression of epiboly. It has been proposed that when zebrafish embryos reach 50% epiboly an actin mediated contraction occurs and functions to aid the progression of the blastoderm over the yolk cell (Cheng, Miller et al. 2004). Alterations in the precise control of this contraction result in premature closing of the blastopore

which ruptures the yolk cell (Holloway, Gomez de la Torre Canny et al. 2009). Indeed the maternal-effect mutant, *betty boop*, displays a defect in epiboly characterized by increased contraction of the actin band at the yolk margin and dramatic constriction resulting in the yolk cell being ruptured (Holloway, Gomez de la Torre Canny et al. 2009). *Betty boop* mutant embryos have a null mutation in the serine-threonine kinase Mitogen Activated Protein Kinase Activated Protein Kinase 2 (MAPKAPK2). MAPKAPK2 is MAP kinase regulated, and has been shown to function in the gradual closing of the blastopore over a 3-hour period from 50% epiboly through to its completion (Holloway, Gomez de la Torre Canny et al. 2009).

Whole blastoderm transplants as well as YSL *MAPKAPK2* RNA injections demonstrate that *Betty boop* functions in the yolk cell to regulate epiboly (Holloway, Gomez de la Torre Canny et al. 2009). YSL targeted injections, take advantage of the fact that in zebrafish, during the tenth cell division (512 cell stage) the marginal cells collapse and release their nuclei and cytoplasm into the yolk forming the YSL (Kimmel, Ballard et al. 1995). After the YSL is formed the blastomeres are closed off from the yolk cell. Injection of reagents into the one-four cell zebrafish embryo when all of the blastomeres are interconnected results in uniform expression (Figure 10A-D), while injection of reagents into the yolk after the YSL has formed results in expression being contained within the yolk cell and YSL (Figure 10E-H).

Fluorescence images of YSL targeted GFP-monomeric actin support the conclusion that an actin band is starting to be assembled at 30% epiboly in *betty boop* mutant embryos (Figure 11D) and wild-type (Figure 11A) embryos. As epiboly progresses the formation of the actin band in *betty boop* mutants appears disorganized (Figure 11E) compared to wild-type embryos (Figure 11C) and at 50% epiboly when the actin band is fully formed it constricts in *betty boop* mutant embryos rupturing the yolk cell (Figure 11F).

Considering the known role for Ca^{2+} in positively regulating actin contraction (Means 2000), I investigated whether Ca^{2+} dynamics are altered in *betty boop* mutant embryos in which the blastopore closes prematurely, rupturing the yolk cell (Holloway, Gomez de la Torre Canny et al. 2009). I examined Ca^{2+} dynamics from late blastoderm stages through early epiboly by ratiometric imaging with the fluorescent Ca^{2+} indicator, Fura-2. Time-lapse microscopy and transient composite analysis of Ca^{2+} activity showed a dramatic increase in Ca^{2+} release in *betty boop* mutant embryos compared to wild-type embryos (Figure 12D-F). During epiboly, Ca^{2+} activity in the YSL is maintained at a sustained level in wild-type embryos (Figure 12A-C). In age-matched *betty boop* mutant embryos, ectopic Ca^{2+} release activity is observed in deep regions of the embryo, most likely the YSL (Figure 12D-F). This ectopic release increases in frequency and intensity as epiboly progresses until eventual bursting (Figure 12F'). Analysis of Ca^{2+} fluxes throughout early epiboly in a composite pseudo-colored image shows low Ca^{2+} activity at the margin in wild-type (Figure 12A-C), which is clearly increased in *betty boop* mutant embryos (Figure 12D-F) (Holloway, Gomez de la Torre Canny et al. 2009). Thus the increased Ca^{2+} release may lead to increased contraction of the actin band at the yolk margin and the dramatic constriction observed in *betty boop* (MAPKAPK2) mutant embryos.

In collaboration with Daniel Wagner (Rice University), I next investigated the impact of p38 Mitogen Activated Protein Kinase (MAPK). p38 MAPK is hypothesized to phosphorylate *betty boop*/MAPKAPK2 and therefore function upstream of MAPKAPK2 in regulating epiboly in the zebrafish embryo. Indeed, it has been shown that during the cleavage period, p38 is asymmetrically activated and that overexpression of a dominant negative (DN) form of p38 results in the inhibition of cytokinesis of the blastomeres on the future dorsal side in a cell-autonomous manner (Fujii, Yamashita et al. 2000). Although a strong correlation between p38 activation and the formation of the dorsal side was found, overexpression of DN-p38 was unable to alter the expression of

dorsal genes. This caused the authors to conclude that dorsal determinants may inhibit cytokinesis, and that p38 is required to alleviate this inhibition, thus allowing cytokinesis to occur on the dorsal side (Fujii, Yamashita et al. 2000). The fact that Ca^{2+} release is required for cytokinesis and *betty boop*/MAPKAPK2 zebrafish mutants display ectopic Ca^{2+} release led me to investigate if there is a link between p38 activation and Ca^{2+} fluxes.

In order to investigate the role of p38, I monitored Ca^{2+} release dynamics in control Texas red, p38 and DN-p38 injected embryos. I find that embryos unilaterally injected with p38 had a wt-like Ca^{2+} profile (Figure 13B') while embryos unilaterally injected with DN-p38 had increased Ca^{2+} activity in the injected side as well as a *betty boop* like phenotype (Figure 13C' and C'', respectively). Interestingly, one embryo injected unilaterally with the DN-p38 had wt-like Ca^{2+} profile (Figure 13D') and did not display a *betty boop* like phenotype (Figure 13D''), indicating that I may have injected the RNA into the future ventral side where there is no endogenous p38 to inhibit. My preliminary results suggest that p38 is required to modulate endogenous Ca^{2+} release dynamics and loss of p38 results in ectopic Ca^{2+} activity impacting cytokinesis as well as causing a premature contraction of the actin band at 50% epiboly and subsequent lysis of the yolk cell (*betty boop*-like phenotype). As this was only a preliminary study, additional epitasis experiments as well as Ca^{2+} imaging of embryos uniformly injected with DN-p38 as well as YSL targeted RNA injections are needed to confirm the relationship between p38, MAPKAPK2 and Ca^{2+} release.

The ectopic Ca^{2+} release in MAPKAPK2 mutants and DN-p38 overexpressing embryos are consistent with increased actin contraction causing the abnormal morphogenesis movements observed. During early epiboly when Ca^{2+} release is normally infrequent, I observed striking Ca^{2+} dynamics in DN-p38 overexpressing embryos and MAPKAPK2 mutants, coincident with the abnormal shimmying movements observed prior to 50% epiboly, suggesting abnormal F-actin contractile movements prior

to 50% epiboly. Furthermore, I observed increased and sustained levels of Ca^{2+} at the margin at the time morphological constriction is apparent in *betty boop* mutants. The constriction phenotype in *betty boop* mutant embryos, is remarkable in its precise timing at specifically the 50% epiboly point in all mutant embryos, reflecting the precise timing of the F-actin band formation. It has been postulated that only when the actin band fully forms at 50% epiboly does the abnormal Ca^{2+} dynamics cause lethality through the unregulated constrictive force of the actin band (Holloway, Gomez de la Torre Canny et al. 2009).

Experimental data support the model that during the gastrula period of zebrafish development there are localized increases in intracellular Ca^{2+} as well as intercellular Ca^{2+} waves. Altering Ca^{2+} dynamics during epiboly has many detrimental effects such as altering cell fate and cell migration. Together these data support that gastrula period Ca^{2+} dynamics function to coordinate the spatial and temporal regulation of developmental processes during epiboly. This regulation is essential for the formation of the germ layers as well as for proper convergent-extension movements.

Segmentation period Ca^{2+} dynamics

After epiboly is complete, the embryo enters the segmentation period. During this period, organ rudiments become visible, somites form anterior to posterior and the tail elongates (Kimmel, Ballard et al. 1995). In a global overview, using the bioluminescent Ca^{2+} reporter R-aequorin, Creton et al. (Creton, Speksnijder et al. 1998) identified the presence of Ca^{2+} waves, gradients and spikes in zebrafish embryos during somitogenesis. Increases in intracellular Ca^{2+} have been identified in the brain rudiment, the forming somites as well as the elongating tail (Webb and Miller 2000; Webb and Miller 2006). The location and timing of increases in intracellular Ca^{2+} indicates that Ca^{2+} signals may influence neurulation, patterning of the paraxial mesoderm as well as the formation of somite boundaries.

In order to expand the understanding of endogenous Ca^{2+} activity during somitogenesis, I monitored Ca^{2+} activity in developing somites and tail during zebrafish somitogenesis. I find that Ca^{2+} release activity during somitogenesis is dynamic with sustained Ca^{2+} levels in the presomitic mesoderm, lateral to the somite forming region and flanking the midline/notochord (Figure 14C''-E''). Representative pseudocolored ratio images from a time-lapse series of Ca^{2+} measurements, spanning the 3-13 somite stages are shown (Figure 14). The notochord and forming somites can be identified in the grayscale fluorescence images (Figure 14B'-E'). Overlay of grayscale and ratio images illustrate the regions of increased Ca^{2+} levels relative to morphology (Figure 14B''-E''). As somitogenesis proceeds, sustained Ca^{2+} levels appear between in distinct regions between the somites (Figure 14C''-E'', arrowheads). In addition, I observe localized short-lived (<15 seconds) increases in Ca^{2+} release (referred to as transients). I report that from the 3 to 14 somite stage, Wt embryos average 5.6 Ca^{2+} transients per hour (±1.3 n=3). My reported frequency of Ca^{2+} transients as well as the observation of sustained Ca^{2+} activity in the trunk and tail region are consistent with previous reports of Ca^{2+} activity during zebrafish somitogenesis (Creton, Speksnijder et al. 1998) (Webb and Miller 2000) (Webb and Miller 2006; Webb and Miller 2007). Interestingly, while somites form at a regular rate, the frequency of Ca^{2+} transients in the trunk is sporadic indicating that the transients may function to maintain boundaries rather than influence the somite clock (Webb and Miller 2007).

In zebrafish, neurulation and segmentation periods overlap (Kimmel, Ballard et al. 1995); therefore I also performed pilot experiments imaging Ca^{2+} dynamics during neural tube formation. I find that Ca^{2+} release activity during neurulation is dynamic. Concentrating on the forebrain region, I observe sustained Ca^{2+} levels anterior to the telencephalon and lateral to the forming diencephalon. Representative pseudocolored ratio images from a time-lapse series of Ca^{2+} measurements, spanning the 1-12 somite stages are shown (Figure 15B-E). The neural keel and forming optic primordia can be

identified in the grayscale fluorescence images (Figure 15B'-E'). Overlay of grayscale and ratio images illustrate the regions of increased Ca^{2+} levels relative to morphology (Figure 15B''-E'').

Concentrating on the hindbrain region, I observe sustained Ca^{2+} levels lateral to the neural plate in the forming neural keel and lateral to the neural rod ((Figure 16B"-D''). Representative pseudocolored ratio images from a time-lapse series of Ca^{2+} measurements, spanning the 3-12 somite stages are shown (Figure 16B-D). The neural plate, neural keel and the neural rod can be identified in the grayscale fluorescence images (Figure 16B'-D'). Overlay of grayscale and ratio images illustrate the regions of increased Ca^{2+} levels relative to morphology (Figure 16B''-D''). The sustained Ca^{2+} activity in the neural keel and adjacent to the forming neural tube and optic primordia suggests that Ca^{2+} influences key patterning events during neurulation

Discussion

In conclusion, progression from egg to embryo requires a dynamic interaction of signal transduction networks. I have shown that each phase of zebrafish development has a distinct pattern of Ca^{2+} release, highlighting the complexity of Ca^{2+} ion and cellular physiology. *In vivo* imaging studies are a critical step in the comprehensive analysis of Ca^{2+} signaling in development. Coupling *in vivo* imaging with molecular, genetic or pharmacological tools will determine the mechanism by which Ca^{2+} signaling is modulated and interpreted in the embryo.

In this chapter I have described endogenous Ca^{2+} dynamics from the very first cell divisions through early somitogenesis in zebrafish embryos. This characterization provides a baseline for incorporating Ca^{2+} dynamics into known signaling pathways, thus providing the capacity to discern the true nature of the cellular basis of pattern formation. Relevant to this discussion is the fact that Ca^{2+} release is heterogeneous. I hypothesize that specific cellular responses can be triggered by differences in the amplitude,

frequency and duration of intracellular Ca^{2+} oscillations. Such oscillations can be derived from changes in upstream steps within the PI cycle, such as G-protein activity, PLC activity and IP_3 levels (Hirose, Kadowaki et al. 1999) (Liu, DeCostanzo et al. 2001; McCarron, MacMillan et al. 2004; Rey, Young et al. 2005).

In the following chapters I investigate the effect G protein regulation has on the amplitude and duration of Ca^{2+} release activity and how this translates into a distinct biological output. To accomplish this, I focus on a class of proteins hypothesized to negatively regulate G protein signaling (Chapter 3). From this characterization, I identify a novel regulator of Ca^{2+} dynamics. I go on to characterize the spatial and temporal dynamics of Ca^{2+} release in morphant embryos (Chapter 4). I end by identifying a closely related family member that contains a predicted Ca^{2+} binding domain (Chapter 5). This work expands our knowledge about how intricate Ca^{2+} signals are integrated into developmental pathways and discrete morphological events.

Materials and Methods

Zebrafish

Zebrafish were maintained in a 14-hour light / 10-hour dark cycle at 28^{o}C. Embryos were collected from natural pairwise matings and staged by both hours post fertilization (hpf) at 28.5ºC and by using morphological criteria described in Kimmel et al. (Kimmel, Ballard et al. 1995). Collection of embryos was carried out as described by Westerfield (Westerfield 1995). Animal welfare assurance number: A3021-01

Preparation and calibration of injection micropipette

A tapered needle was pulled from a micropipette (Drummond, 25 lambda microcap) on a standard needle puller. The needle was then backfilled with 0.5 – 1 μL of Fura-2 and mounted onto the micromanipulator or some other support. Next the needle tip was broke back with fine forceps under a light microscope and lowered into a petri

dish with oil. A drop of Fura-2 was injected into the oil the diameter was measured with a calibrated eyepiece reticule. Next the injection pressure/time was adjusted to yield an injection volume of ~3 nanoliter volume.

Micro-Injections

Zebrafish embryos were microinjected with a pressure injector (Harvard apparatus) with approximately 3 nanoliter volumes at the 1-cell stage. Embryos were placed into an injection dish (petri dish with 1.5% agarose that has small depressions formed by 1 mm capillaries and covered with egg water) and the needle was positioned to penetrate the chorion. Next, the needle was gently inserted through the yolk into the blastodisc and the ratiometric Ca^{2+}-sensing dye Fura-2-Dextran or Bis-Fura-2-Dextran (Molecular Probes) was injected. The needle was then slowly withdrawn using forceps to support the embryo.

Intracellular Ca^{2+} Imaging

The excitation spectra are different between the Ca^{2+} bound (340 nm) and Ca^{2+} free (380 nm) forms. By taking the ratio of the fluorescence intensity at these two wavelengths, an estimate of intracellular free Ca^{2+} can be derived, to some degree, independent of cell thickness and distribution of the fluorescent indicator (which can vary in living cells). For cellular blastoderm stage imaging, embryos were oriented in a lateral position in a glass-bottomed dish on a Zeiss axiovert epifluorescence microscope. Image pairs at 340 and 380-nm excitation wavelengths (510-nm emission) were collected at 15-second intervals. Each imaging session collected 300 image pairs. The ratio image, a pixel by pixel match of both excitation wavelengths, is calculated by computer software (RatioTool, Inovision). The sequence of ratio images was processed and the Ca^{2+} fluxes (transients) were determined by a subtractive analog patterned after (Lechleiter, Girard et al. 1991; Chang and Meng 1995) and described in (Slusarski and Corces 2000; Freisinger, Houston et al. 2008). The ratio image (340nm, Ca^{2+}-saturated and 380nm,

Ca^{2+}-free) imported for publication is encoded in 8 bits and converted to pseudocolor with low ratio (low Ca^{2+}) represented by blue and high ratio (high Ca^{2+}) represented by yellow/red.

For somite imaging, 2-6 somite stage embryos were oriented in low melt agarose (.38%) in a dorsal or lateral orientation. Time courses collected images pairs until 12-15 somite stage at 15-second intervals (Approximately 1000 images pairs). Image pairs were converted to ratio images as described above. Sequential ratio images were manually analyzed for changes in Ca^{2+} transients. Somite stage Ca^{2+} transients were defined as a localized increase in Ca^{2+} which persists no longer than thirty seconds.

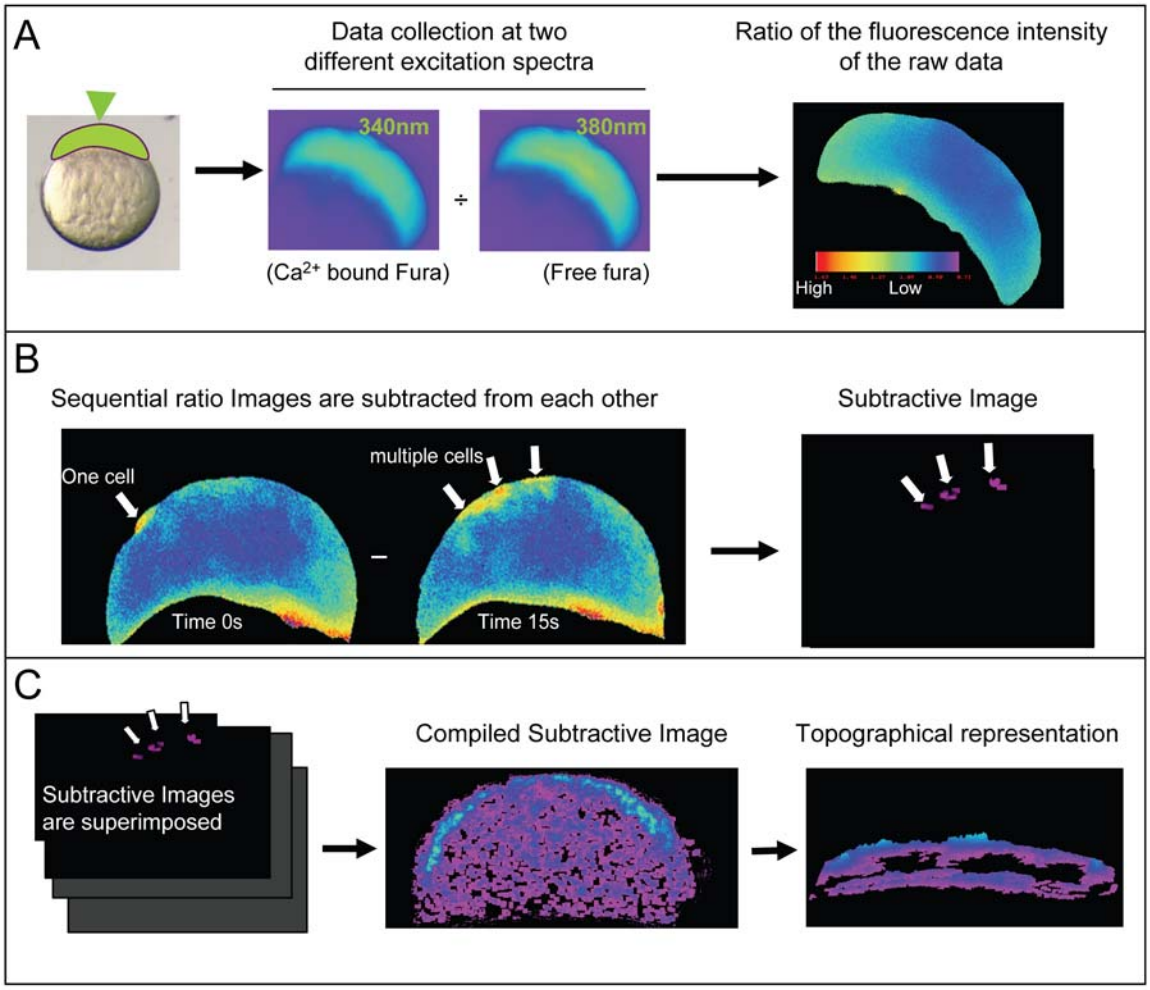

Figure 6: Analyzing Intracellular Calcium Dynamics. One cell stage embryos are injected with Fura-2 and ratio images are created by taking the ratio of the fluorescence intensity at 340 nm and 380 nm. (A) The pseudocolored ratio image provides a spatial and temporal measurement of calcium dynamics with low calcium represented by blue and high calcium represented by yellow/red. (B) The sequence of ratio images is processed and calcium fluxes (transients) are identified in a subtractive image. (C) In order to determine calcium activity over a time-course, subtractive images are superimposed to create a compiled subtractive image which is then converted into a topographical representation in which the color and peak height indicate the total number of calcium transients present in that region of the embryo.

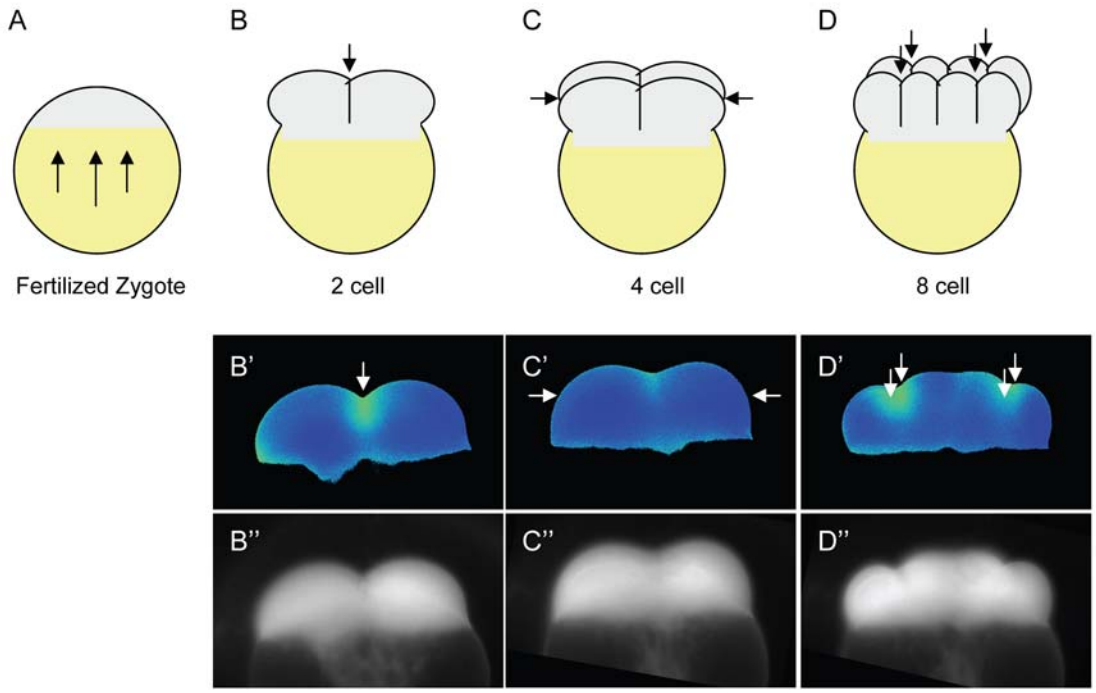

Figure 7: Cleavage Stage Calcium Dynamics. (A-D) Schematic of the first three rounds of cell division during the cleavage stage. (A) Fertilized zygote (0 hpf) with arrows representing yolk streaming. (B) 2 cell (3/4 hpf), (C) 4 cell (1hpf), and (D) 8cell (1 ¼ hpf) embryos with arrows representing the cleavage plane. Animal pole to the top (gray) and vegetal pole to the bottom (yellow). (B'-D') Representative ratio images, pseudocolored with low ratio (low calcium) represented by blue and high ratio (high calcium) represented by yellow/red. (B''-D'') Grayscale fluorescence images illustrating embryo morphology.

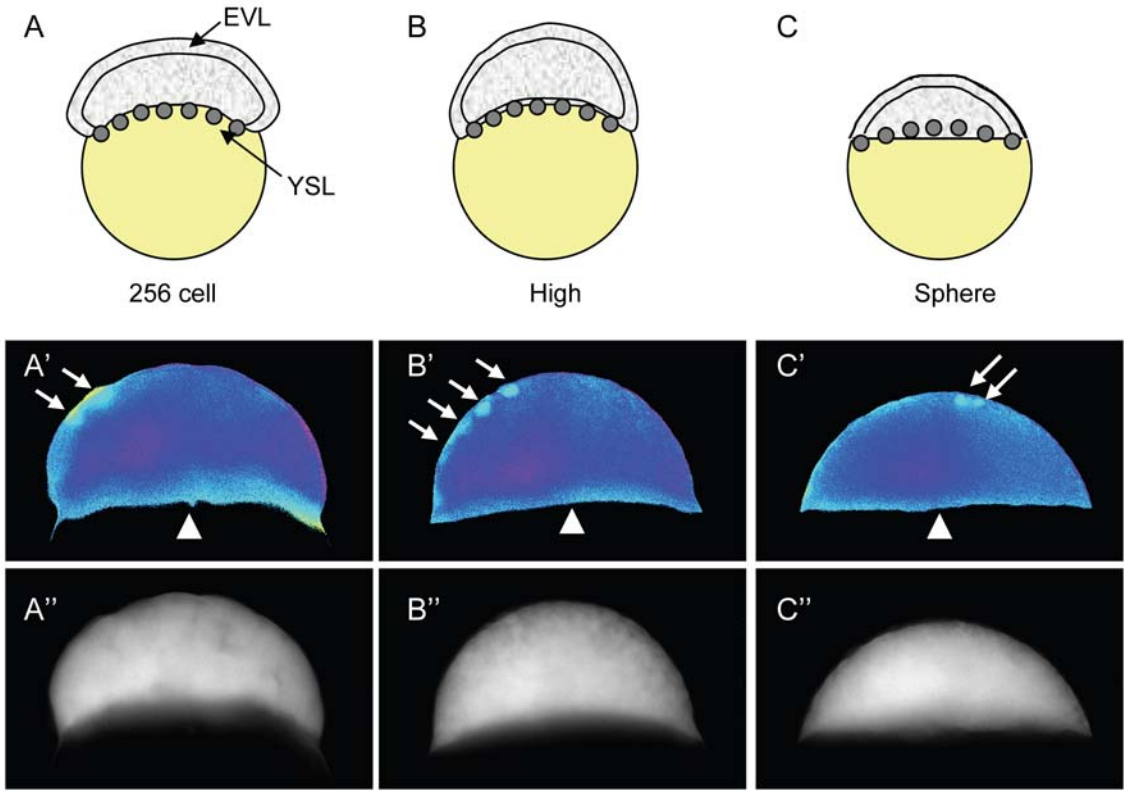

Figure 8: Blastula Period Calcium Dynamics. Schematic of Zebrafish embryos at (A) 256 cell (2.5 hpf), (B) High stage (3 hpf), and (C) Sphere stage (4hpf). Animal pole to the top (gray) and vegetal pole to the bottom (yellow). (A'-C') Representative ratio images, pseudocolored with low ratio (low calcium) represented by blue and high ratio (high calcium) represented by yellow/red. Arrows indicate calcium transients and arrow heads indicate areas with sustained calcium activity. (A''-C'') Grayscale fluorescence images indicating embryo morphology. EVL= enveloping layer, YSL = yolk syncytial layer.

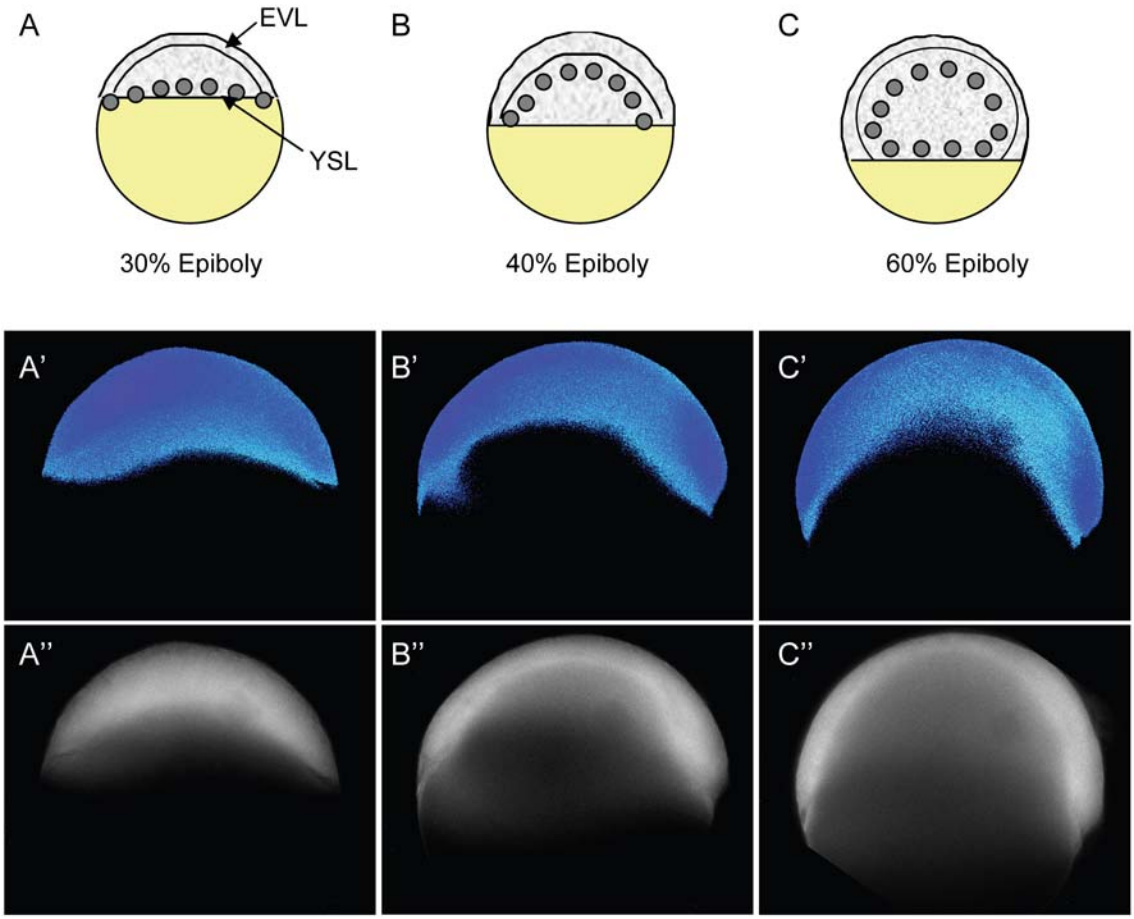

Figure 9: Epiboly Stage Calcium Dynamics. Schematic of Zebrafish embryos at (A) 30% epiboly (4.5 hpf), (B) 40% epiboly (5 hpf), and (C) 60% epiboly (6 hpf). Animal pole to the top (gray) and vegetal pole to the bottom (yellow). (A'-C') Representative ratio images, pseudocolored with low ratio (low calcium) represented by blue and high ratio (high calcium) represented by yellow/red. (A''-C'') Grayscale fluorescence images. EVL= enveloping layer, YSL = yolk syncytial layer.

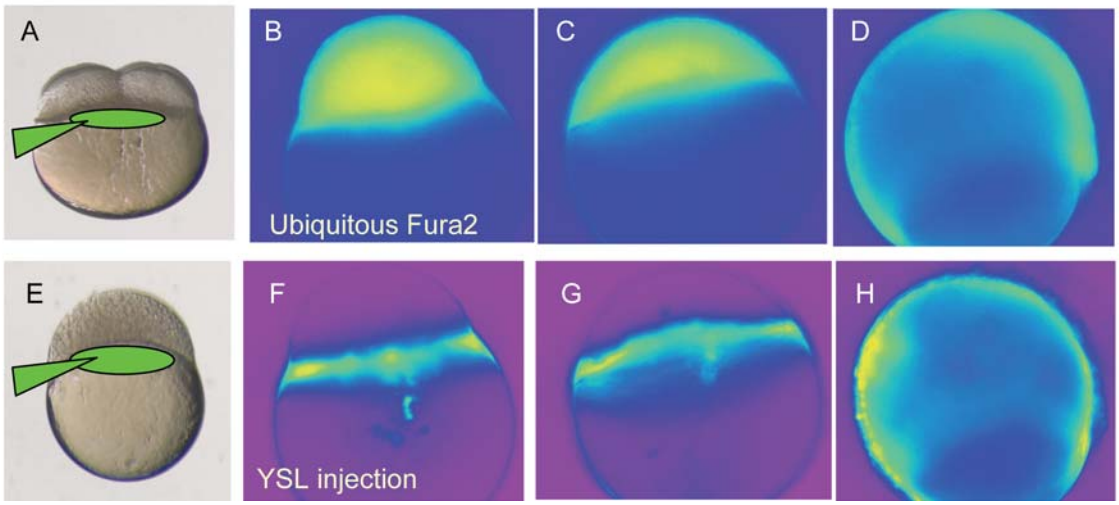

Figure 10: Ubiquitous and YSL Targeted Injections. Image illustrating injection into a (A) 4cell and (E) 512 cell zebrafish embryo. Lateral fluorescent images of (B and F) 512 cell, (C and G) 30% epiboly, and (D and H) 80% epiboly embryos after (B-D) 4cell or (F-H) 512 cell injection.

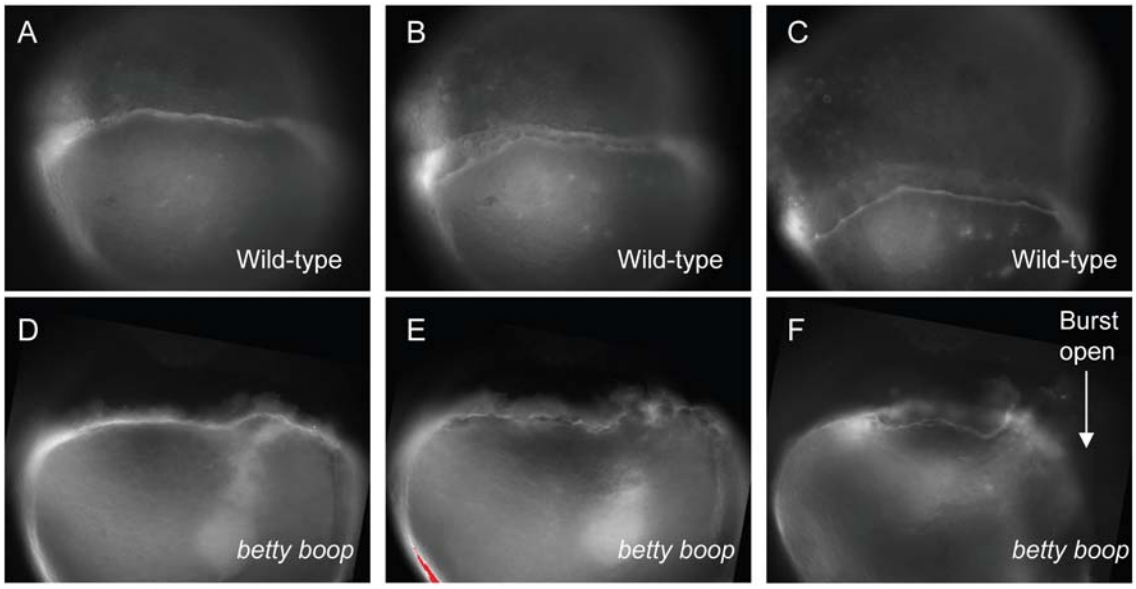

Figure 11: YSL targeted GFP-Monomeric-Actin Injections. Lateral fluorescent images of (A and D) 30% epiboly, (B and E) 40% epiboly, and (C and F) 50% epiboly (A-C) wild-type and (D-F) *betty boop* zebrafish embryos. Animal pole to the top and vegetal pole to the bottom.

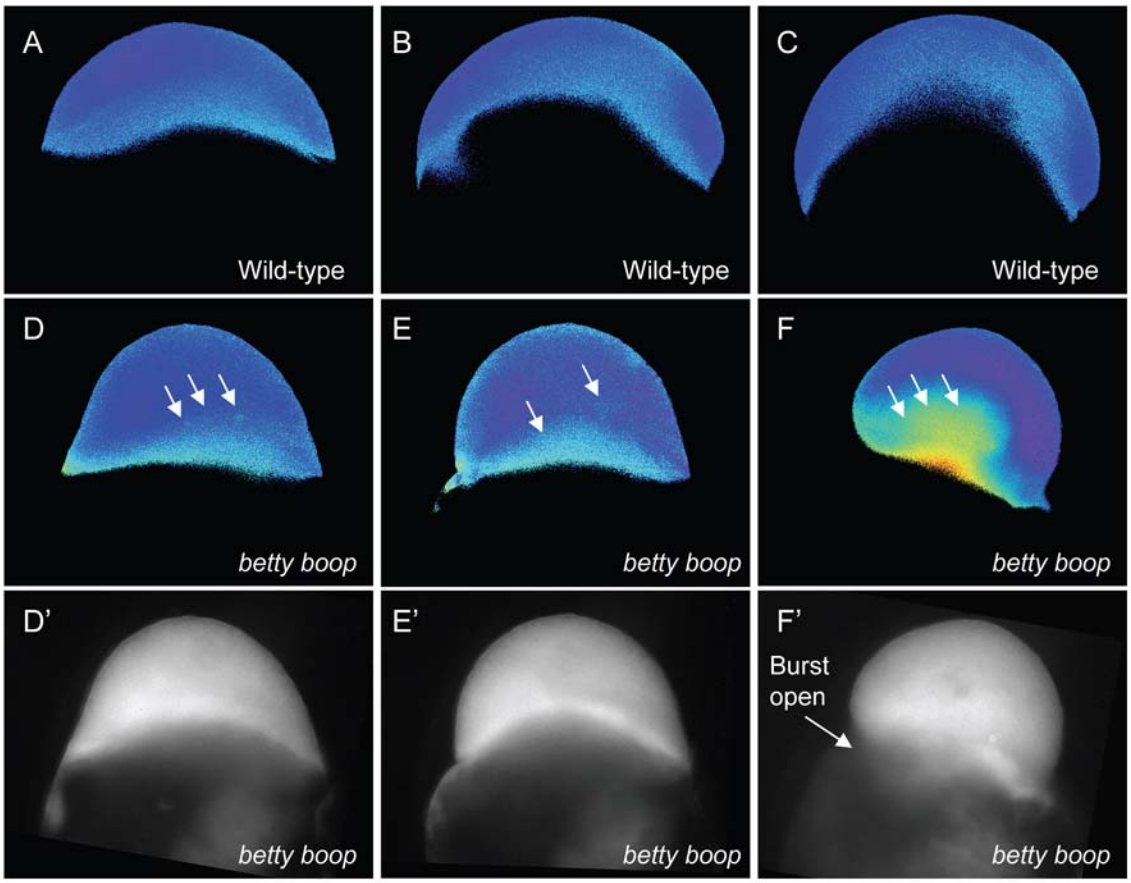

Figure 12: Calcium Dynamics in *betty boop*. (A-F) Representative ratio images, pseudocolored with low ratio (low calcium) represented by blue and high ratio (high calcium) represented by yellow/red of (A-C) wild-type and (D-F) *betty boop* mutant zebrafish embryos at (A and D) 30% epiboly, (B and E) 40% epiboly, and (C and F) 50% epiboly. (D-F) Arrows indicate ectopic calcium flashes in the *betty boop* embryo. (D'-F') Grayscale fluorescence images indicate morphology.

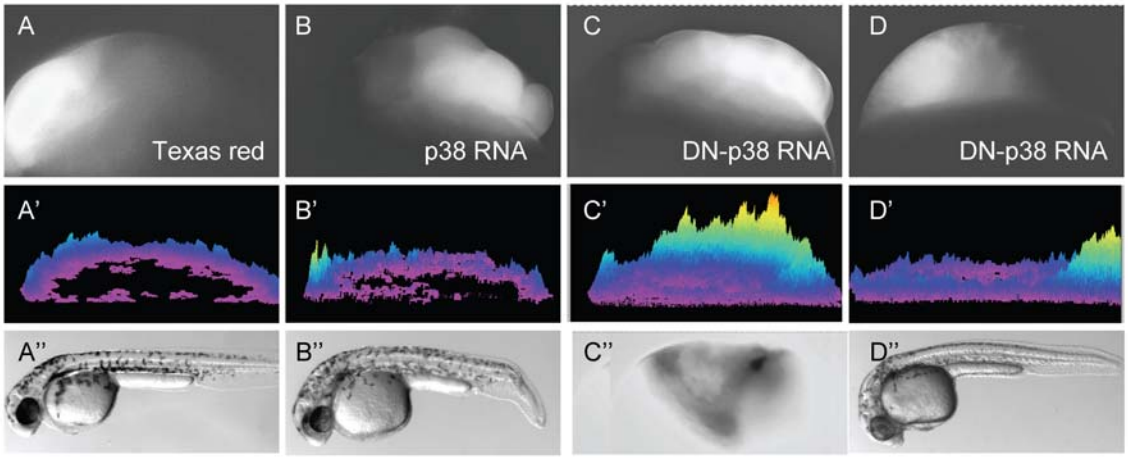

Figure 13: DN-p38 Induces Ectopic Calcium Release. Lateral fluorescence images of embryos with (A) unilaterally localized TxR, (B) TxR/p38, and (C-D) TxR/DN-p38 over-expression. (A'-D') Corresponding Ca^{2+} release composites of Fura-2 ratiometric imaging time course showing total calcium release activity as peaks and colors mapped topographically and (A''-D'') resulting morphological phenotypes of (A", B" and D'') 48 hpf and bursting (C'') 50% epiboly embryos.

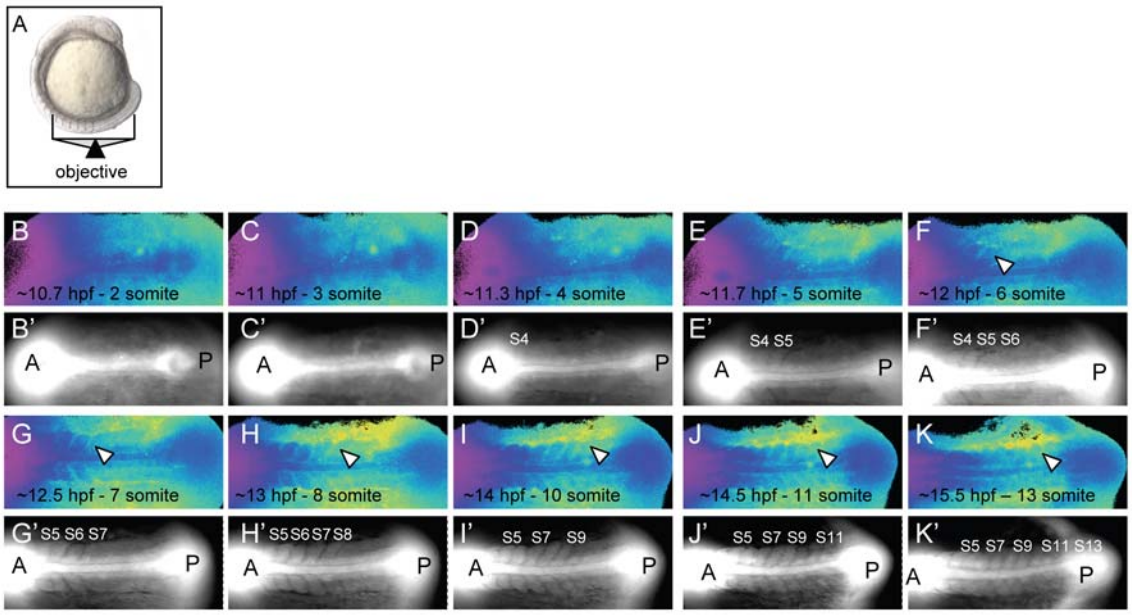

Figure 14: Calcium Dynamics During Zebrafish Somitogenesis. (A) Illustration of the position of a 10 somite stage (14 hpf) zebrafish embryo relative to the objective during calcium imaging. (B-K) Representative ratio images, pseudocolored with low ratio (low calcium) represented by blue and high ratio (high calcium) represented by yellow/red, of 2-13 somite stage embryos. The forming somites and notochord can be identified by the (B'-K') grayscale fluorescence images. Arrowheads indicate areas of sustained Calcium activity between forming somites. Ant. is Anterior, Pos. is Posterior and S is somite number.

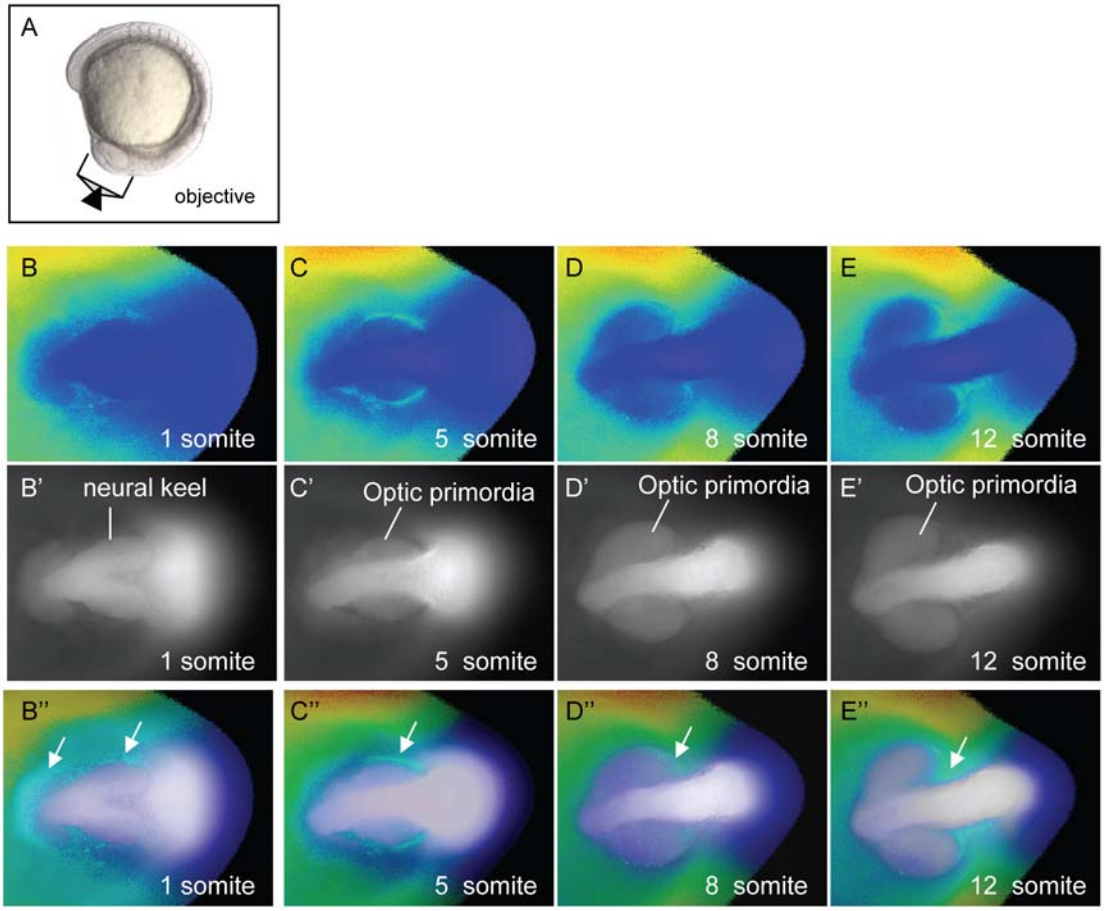

Figure 15: Calcium Dynamics During Zebrafish Neurulation. Illustration of the position of a 10 somite stage (14 hpf) zebrafish embryo relative to the objective during calcium imaging (A). All images are dorsal views with the anterior to the left. Representative ratio images, pseudocolored with low ratio (low calcium) represented by blue and high ratio (high calcium) represented by yellow/red, of 1, 5, 8 and 12 somite stage embryos (B-E respectively). The forming diencephalon and optic primordia can be identified by the grayscale fluorescence images (B'-E'). Overlay of grayscale and ratio images illustrate the regions of calcium release activity relative to morphology (B''-E''). Arrowheads indicate areas of sustained calcium anterior to the telencephalon and lateral to the forming diencephalon.

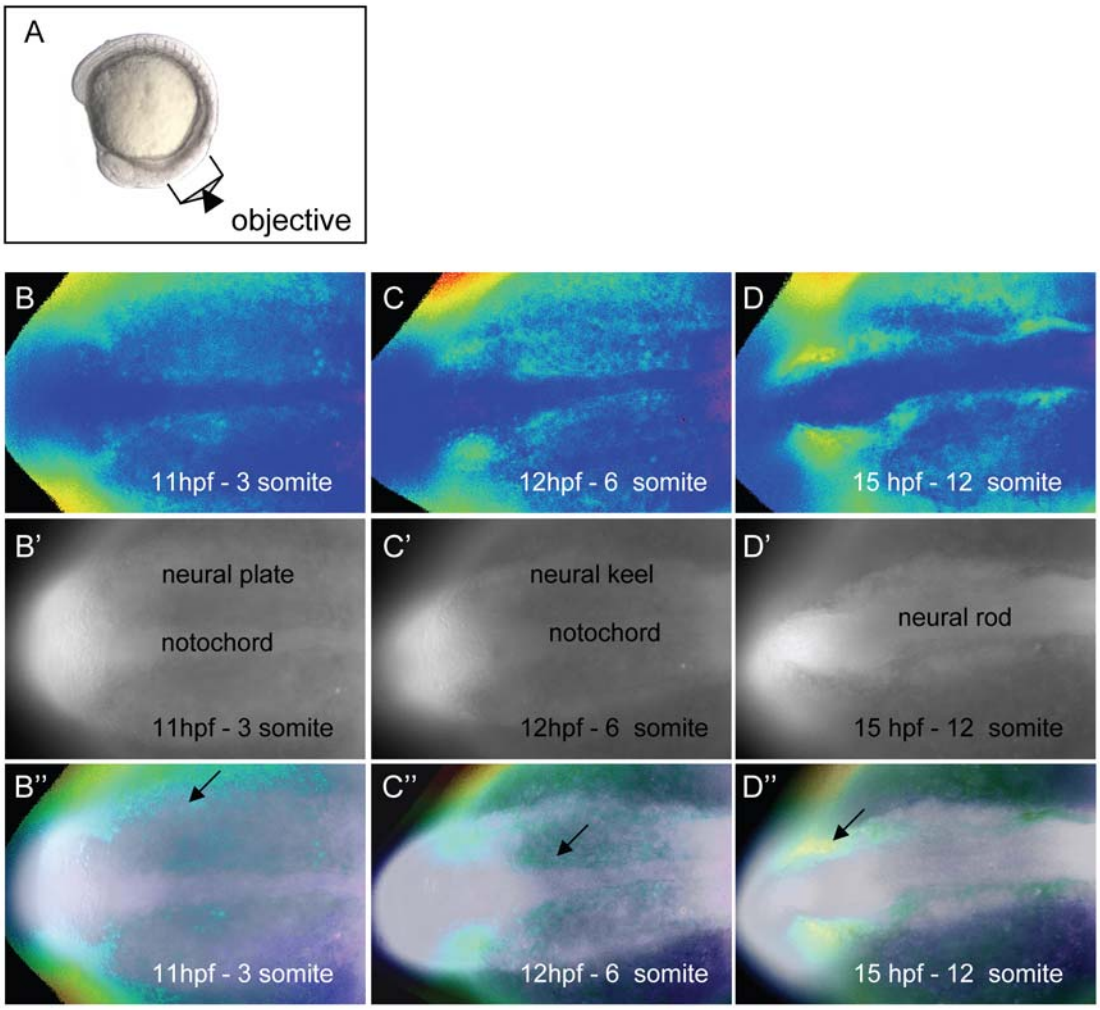

Figure 16: Calcium Dynamics During Zebrafish Neural Rod Formation. (A) Illustration of the position of a 10 somite stage (14 hpf) zebrafish embryo relative to the objective during calcium imaging. All images are dorsal views with the anterior to the left. (B-D) Representative ratio images, pseudocolored with low ratio (low calcium) represented by blue and high ratio (high calcium) represented by yellow/red, of (B) 3, (C) 6 and (D) 12 somite stage embryos. (B'-D') Grayscale fluorescence images indicating the notochord, neural plate, neural keel and neural rod. (B''-D'') Overlay of grayscale and ratio images illustrate the regions of calcium release activity relative to morphology. Arrowheads indicate areas of sustained calcium (B') lateral to the neural plate, (C'') in the forming neural keel and (D'') lateral to the neural rod.

CHAPTER 3
IDENTIFICATION OF A NOVEL REGULATOR OF INTRACELLULAR CALCIUM RELEASE

Introduction

During early vertebrate development Ca^{2+} signaling is required for epiboly, gastrulation, convergent extension as well as the generation of various organs (Webb and Miller 2000; Slusarski and Pelegri 2007). In zebrafish, intracellular Ca^{2+} transients have been observed in the outermost embryonic cell layer at the beginning of the blastula period (Reinhard, Yokoe et al. 1995; Slusarski and Pelegri 2007). As the blastula phase progresses these Ca^{2+} transients appear at short intervals resulting in appearance of Ca^{2+} waves in the EVL (Reinhard, Yokoe et al. 1995; Slusarski, Yang-Snyder et al. 1997). Later, during the gastrula phase, transient localized Ca^{2+} domains as well as pan-embryonic rhythmic Ca^{2+} waves have been identified in the forming anterior/posterior axis of the embryo (Gilland, Miller et al. 1999; Webb and Miller 2003; Freisinger, Schneider et al. 2008).

Ca^{2+} release is heterogeneous. Specific cellular responses can be triggered by differences in the amplitude, frequency and duration of intracellular Ca^{2+} oscillations. Such oscillations can be derived from changes in upstream steps within the PI cycle, such as G-protein activity, PLC activity and IP_3 levels (Hirose, Kadowaki et al. 1999; Luo, Popov et al. 2001; McCarron, MacMillan et al. 2004; Thore, Dyachok et al. 2004; Nomikos, Blayney et al. 2005; Rey, Young et al. 2005). We have shown that early Ca^{2+} transients are, in part, modulated by Wnt5 (Slusarski, Yang-Snyder et al. 1997; Westfall, Hjertos et al. 2003) The zebrafish *wnt5b* genetic mutant (*pipetail*) shows reduced Ca^{2+} release (Westfall, Brimeyer et al. 2003) and the ventralized maternal effect mutant *hecate* shows ectopic Ca^{2+} release (Lyman Gingerich, Westfall et al. 2005). Moreover, inhibition of Ca^{2+} release results in alteration of dorsal ventral patterning, cell movement

and left-right patterning (Westfall, Hjertos et al. 2003; Schneider, Houston et al. 2008). These observations suggest that the kinetics of Ca^{2+} release, both transient and sustained, translate into distinct developmental outputs (Freisinger, Schneider et al. 2008).

In this chapter, I focus on identifying an endogenous regulator of Ca^{2+} release. We have previously shown that Wnt proteins work through specific Fz homologues to activate G proteins and stimulate PI signaling pathways (Slusarski, Corces et al. 1997). Data, from multiple model systems, support the conclusion that Wnt/Fz signaling is mediated via G protein activation. I use zebrafish to investigate the developmental functions of G Protein Coupled Receptor signaling in development. This is accomplished through manipulation of the functions of RGS. To date, a detailed expression analysis of zebrafish RGS genes has not been reported.

I have isolated zebrafish RGS2, 3, 4, 5, and 16 genes and determined their expression patterns in the embryo. The developmental requirements for Rgs3, 4, and 5 were determined by gene knockdown. I find that zebrafish RGS genes have both unique and overlapping temporal and spatial expression patterns, and are required for normal somite formation and vascular outgrowth. In addition, I identify Rgs3 as a logical candidate in modulating the Wnt/Ca^{2+} pathway.

Regulators of G protein Signaling

The existence of RGS proteins was first shown by genetic studies in yeast (Dohlman, Apaniesk et al. 1995) and Caenorhabditis elegans (Koelle and Horvitz 1996) where the yeast pheromone desensitization factor Sst2p and the Caenorhabditis elegans Sst2p homolog Egl-10 were found to negatively regulate Gpa1 and GOA-1, respectively, both homologs of the mammalian G protein Gαo. The presence of a conserved domain of approximately 130 amino acids in Sst2p and Egl-10 (i.e., the RGS domain) enabled Koelle and Horvitz to demonstrate the existence of a family of mammalian proteins with this domain. More than 20 mammalian genes encode proteins with this hallmark RGS

domain. Subsequent studies demonstrated that RGS proteins or isolated RGS domains display GTPase-activating protein activity towards Gi and Gq proteins (De Vries, Zheng et al. 2000; Ross and Wilkie 2000), providing insight into how RGS proteins could function to turn off G proteins following their GTP-dependent activation by receptors.

Based on size, amino acid identity and structural domains the RGS protein family is subdivided into six distinct subfamilies (RZ, R4, R7, R12, RA and RL) (See review(Siderovski and Willard 2005). To determine if RGS proteins function as endogenous regulators of Ca^{2+} release, I selected the simplest RGS subfamily (R4) for initial characterization, this subfamily will be referred to as the R4 subfamily. R4 subfamily members are small (20-30 kDa) proteins, consisting mainly of the conserved RGS domain (except isoforms of RGS3 and RGS1) and have been shown to serve almost exclusively as negative regulators of G protein signaling (Tesmer, Berman et al. 1997; Hollinger and Hepler 2002).

Members of the R4 subfamily include RGS 1, 2, 3, 4, 5, 8, 13, 16 and 18. This group of RGS proteins is of interest because we have previously shown that Wnt5 induced Ca^{2+} release requires G protein activation (Slusarski, Corces et al. 1997; Slusarski, Yang-Snyder et al. 1997). Thus, by functioning as GTPase-activating proteins (GAPs) for G proteins, RGS proteins are uniquely situated to modulate the intensity and duration of Wnt/Ca^{2+} signaling.

Cloning and Characterization of R4 subfamily members

It must be acknowledged that, despite the evidence that RGS proteins can accelerate the GTPase activity of G proteins in vitro, the functional role of this activity in vertebrates has largely been shown in phototransduction (Chen, Burns et al. 2000), where RGS9 functions to rapidly inactivate transducin following its activation by rhodopsin.

As a first step in determining the function of R4 family members I used BLAST analysis of expressed sequence tagged databases to identify transcripts encoding

zebrafish R4 RGS homologues. Sequence information (Sanger Institute) was used to design gene specific primers and clone zebrafish RGS genes. I cloned zebrafish cDNAs of Rgs2, Rgs3, Rgs4 and Rgs16 and Shengda Lin cloned Rgs5. Primers were targeted to the stop codon and the initiator methionine based on published EST data. RT-PCR was used to identify gene products, I find that *rgs2*, *rgs3, rgs4*, *rgs5* and *rgs16* are expressed from maternal to larval stages and have identities to human RGS homologues which range from 35% to 71% (Table 1).

To compare the spatial and temporal distribution of these proteins, Whole Mount *In Situ* Hybridization (WMISH) was performed with gene specific antisense probes in a developmental profile (0 to 48 hours post fertilization, hpf) (Figure 17). During the segmentation period (10-24 hpf) *rgs2* is expressed in the hatching gland (Figure17A), *rgs*3 is expressed in the developing somites, posterior tail and in the anterior brain (Figure17C), *rgs4* is expressed in the pronephric ducts (Figure17E), *rgs5* is expressed along the trunk, midbrain and posterior tail (Figure17G) and *rgs16* is expressed ubiquitously (Figure17I). During the pharyngula period (24-48 hpf) *rgs2* is expressed in the hatching gland and migrating neural crest (Figure17B), *rgs3* is expressed in the posterior somites, tail and in the midbrain/hindbrain boundary (Figure17D), *rgs4* is expressed in the pronephric ducts (Figure17F) and *rgs5* is expressed in the somites, midbrain, mucous cells and posterior tail (Figure17H). The variety of RGS expression patterns suggests that members of the R4 subfamily could have overlapping yet distinct roles in development.

Endogenous requirement of RGS proteins

A large wealth of what we know about RGS function to date has been derived from tissue culture studies (Makino, Handy et al. 1999; Mukhopadhyay and Ross 1999; Ross 2002; Mao, Zhao et al. 2004; Willars 2006). Although informative, these studies do not provide information on specific organs and tissue in the context of the whole animal.

In addition, many analyses were via over-expression (Heo, Ha et al. 2006; Sambi, Hains et al. 2006; Schoeber, Topala et al. 2006) and don't demonstrate the endogenous roles of RGS proteins. To test the functional requirement of RGS genes, I utilized an antisense oligonucleotide-based gene knock down approach (Morcos 2000). Morpholino oligos (MO) were designed to block translation or splicing of *rgs*3, 4, and 5.

Morphological analysis revealed dramatic changes in heart tube morphology in *rgs3* MO and *rgs5* MO injected embryos (morphants) (Figure 18B and D). Heart tube morphology was unaffected in *rgs4* morphants (Figure 18C). To further characterize the cardiovascular defects, I analyzed vessel outgrowth. The Tg(Fli1:EGFP) line, which drives green fluorescent protein expression in the developing vasculature (Weinstein 2002), was used to visualize the forming vasculature system. At 20 hpf, intersegmental vessels sprout from the aorta, one vessel runs between each pair of somites, and by 35 hpf the intersegmental vessels have fully extended dorsally between somites to form the dorsal longitudinal anastomotic vessel (Figure 19A) (Torres-Vazquez, Gitler et al. 2004). The intersegmental vessels are the only vessels functioning in the trunk until approximately 87 hpf. Vessel formation was evaluated *in vivo* by fluorescence microscopy of Tg(Fli1:EGFP) embryos. In control MO injected embryos; intersegmental vessels sprout from the dorsal aorta and extend dorsally to the dorsal longitudinal anastomotic vessel (Figure 19B). Rgs3 and Rgs5 morphants display disrupted intersegmental vessel formation (Figure 19C) whereas Rgs4 morphant vessel formation is the same as control (Figure 19E).

The somites function as signaling centers for the developing blood vessels. By acting as a repulsive cue, semaphorins, expressed in the central portion of the somites, restrict the growth of intersegmental vessel to the intersegmental boarders (Gitler, Lu et al. 2004; Torres-Vazquez, Gitler et al. 2004). Zebrafish mutants characterized by defects in somite boundary patterning, such as *fused-somites*, undergo initial vasculogenesis but display severe defects in the patterning and migration of intersegmental vessels (van

Eeden, Granato et al. 1996; Shaw, Castranova et al. 2006). Because Rgs3 and Rgs5 morphants display disrupted intersegmental vessel formation it was of interest to investigate somite formation.

The somites are transient structures, derived from mesoderm, which give rise to cartilage and muscle. The transparency of zebrafish embryos allows direct visualization of the somites as they form sequentially in an anterior to posterior fashion. Morphologically, somites can be seen as discrete epithelial blocks flanking the midline which take on a chevron shape (Figure 20A-B). I find that Rgs3 morphants lose the chevron shape of their somites and display tighter packed somites but maintain discrete somite boundaries (Figure 20C) while, Rgs4 and 5 morphants did not have any morphological somite defects (Figure 20D and E).

Somite formation in segmentation is important in patterning the anterior to posterior axis. Alterations in axis formation result in decreased body length and can often be attributed to abnormal convergent-extension movements, which genetic evidence supports is dependent on Wnt signaling (Rauch, Hammerschmidt et al. 1997; Heisenberg, Tada et al. 2000; Carreira-Barbosa, Concha et al. 2003). In fact, Wnt5/*piptail* (Rauch, Hammerschmidt et al. 1997) and Wnt11/*silverblick* (Heisenberg, Tada et al. 2000) zebrafish mutants display convergence extension defects.

Convergent-extension occurs during the gastrula period of zebrafish development. During convergent-extension there is a coordinated movement of mesodermal cells to the midline where they converge and medio-laterally intercalate resulting in an extension of the anterior-posterior axis. Alterations in convergent-extension movements result in morphological changes such as shorter anterior-posterior length and increased somite width. Interestingly, while Rgs4 and Rgs5 morphants had normal body length (Figure 21C-D) when compared to control injected embryos (Figure 21A), Rgs3 morphant embryos had tighter packed somites resulting in a decrease in anterior to posterior length (Figure 21B).

In order to determine if Rgs3 morphants had an earlier convergence extension defect, I used the muscle and somite marker MyoD to determine if the developing somites were laterally expanded. MyoD is a transcription factor involved in regulating muscle differentiation and is strongly expressed in the adaxial cells and developing somites. Whole mount in situ hybridization of wild-type embryos reveals blocks of MyoD positive cells flanking the midline (Figure 22A). Unlike cells of wild-type embryos, the cells of Rgs3 morphants fail to converge on the midline, resulting in a lateral expansion of the somites (Figure 22B). Additionally, Rgs3 morphant cells fail to extend along the anterior-posterior axis, leading to a shorter embryo. To further characterize the convergent-extension defect Pax2 was used to highlight forebrain and hindbrain structures. Pax2 is expressed in the anterior retina, midbrain/hindbrain, and otic vesicle (Figure 22C). Rgs3 morphants show a reduced distance between these structures, when compared to wild-type embryos (Figure 22D). This is consistent with the MyoD expression pattern indicating altered anterior posterior axis extension.

The distinct phenotype associated with Rgs3 knockdown, in particular the lack of convergence to the midline and shortened anterior to posterior extension, is reminiscent of defects associated with the Wnt signaling network which is necessary for polarized cell movements. In fact, *rgs*3 knockdown results in reduced anterior-posterior extension similar to that seen with loss of *wnt5* (Figure 23B-C). To determine if Rgs3 is a logical candidate to modulate zebrafish Ca^{2+} dynamics, I investigated if Rgs3 was expressed in the right tissues and at the right developmental period to influence Wnt signaling. Whole mount in situ hybridization reveals that *rgs3* and *wnt5b* show both overlapping and adjacent expression domains in the somites and in the posterior tailbud (Figure 23D-G). As Wnt5b is a secreted ligand, the proximity of *rgs3* to *wnt5b* producing cells suggests that Rgs3 may function in modulating Wnt5b signaling.

Discussion

Our data support that zebrafish RGS proteins have dynamic expression patterns and unique developmental requirements. Culture studies in yeast support the conclusion that the levels of RGS protein exist in a rate-limiting amount (Dohlman, Song et al. 1996), suggesting that raising or decreasing RGS protein levels may have profound effects on G protein signaling. I find that knockdown of three individual RGS members produced remarkably different results, indicating that individual RGS proteins have unique developmental requirements.

*rgs*3 knockdown resulted in body patterning defects reminiscent of Wnt mutants, *rgs4* knockdown produced no gross morphological defect, and *rgs*5 knockdown resulted in an intersegmental migration defect. It has been shown that Rgs5 knockout mice demonstrate tumor angiogenesis defects (Hamzah, Jugold et al. 2008) which is consistent with the abnormal vessel migration that I observe in a zebrafish rgs5 knockdown.

Cell culture studies provide data indicating that RGS4 and RGS5 are short-lived *in vitro* due to degradation by the N-end rule pathway (Lee, Tasaki et al. 2005). Indeed, zebrafish Rgs4 and Rgs5 have a conserved Cys-2 residue consistent with N-end rule degradation (Lee, Tasaki et al. 2005). The fast turnover of Rgs4 and Rgs5 may account for the mild gene knockdown phenotypes which are consistent with mouse RGS4 and RGS5 knockouts in which mutant mice appear normal and fertile (Grillet, Pattyn et al. 2005; Nisancioglu, Mahoney et al. 2008).

In conclusion, by investigating zebrafish RGS proteins I was able to identify *rgs3* as a potential modulator of Ca^{2+} dynamics. I identified r*gs*3 as having an overlapping expression pattern with *wnt5b* in zebrafish and found that individual knockdown of either *rgs3* or *wnt5b* gene function produces similar somite patterning defects. In Chapter 4, I expand on these observations by characterizing the spatial and temporal dynamics of Ca^{2+} release in Rgs3 morphant embryos.

Materials and Methods

Zebrafish

Zebrafish were maintained in a 14-hour light / 10-hour dark cycle at 28^{o}C. Embryos were collected from natural pairwise matings and staged by hpf at 28.5ºC and by using morphological criteria described in Kimmel et al. (Kimmel, Ballard et al. 1995). Collection of embryos was carried out as described by Westerfield (Westerfield 1995). Animal welfare assurance number: A3021-01

Micro-Injections

Zebrafish embryos were microinjected with a pressure injector (Harvard apparatus) with approximately 3 nanoliter volumes at the 1-cell stage. Embryos were placed into an injection dish (petri dish with 1.5% agarose that has small depressions formed by 1 mm capillaries and cover with egg water) and the needle was positioned to penetrate the chorion. Next, the needle was gently inserted through the yolk into the blastodisc and the appropriate MO mix was injected. The needle was then slowly withdrawn using forceps to support the embryo.

Zebrafish rgs2, 3, 4, 5, 16 and 12 cloning

I searched zebrafish homologues of known R4 subfamily genes in public databases of the zebrafish genome (the Sanger Institute) and expressed sequence tagged (EST) databases using the program TBLASTX (National Center for Biotechnology Information, NCBI). Next, forward and reverse primers encompassing the translational start and stop sites of *rgs2*, 3, 4, 5, and 16, were designed using Primer-3 primer prediction program (Rozen and Skaletsky 2000). Zebrafish *rgs* cDNAs were amplified by PCR from 0-48 hpf zebrafish cDNA libraries prepared and cloned into pCRII TOPO TA cloning vector (Invitrogen). Multiple clones were sequenced on a PE-Applied Biosystems Model 3700 sequencer using the ABI BigDye sequencing system.

MO-resistant *rgs*3 was directionally subcloned (5'-3') into the pCS^{2+} expression vector (Turner and Weintraub 1994).

Morpholino Micro-Injections

Morpholinos (Gene-Tools) for zebrafish RGS3 (Chromosome 5) (*rgs3* MO: 5'-AGTCGGTTCTTCATGTCTTTGGCCC-3', , the 5 bp mismatched (in lowercase letters) control missense *rgs3* MO (*rgs3* MOmm 5'-TCaCCcAGAAATCCtCCATtGTcTG-3'), *rgs4* (Chromosome 6) (*rgs4* MO 5'-AAGAGCAGCAAGCCCTTTACACATG-3') and *rgs5* (Chromosome 6) (*rgs5* MO 5'-GCTAATCCCTTACACATTTTCTGAG-3') were air-pressure-injected at concentrations of 300-600 μM into the one cell-stage at the yolk and cytoplasm interface. The control morpholino did not produce any phenotype when injected alone at 600 μM. For rescue experiments, *in vitro*-transcribed capped MO-resistant *rgs3* RNAs (75–100 ng/μl) were coinjected with *rgs3* MO. Injected embryos were then characterized by morphological and molecular analysis. Vasculature defects were characterized in a Tg(Fli1:GFP) background (Weinstein 2002).

In situ hybridization

Embryos were dechorionated and fixed overnight in 4% paraformaldehyde. Representative developmental stages include: 1-1000 cell stage, epiboly, tailbud, 12-20 hpf, 24 hpf, and 48 hpf. Whole-mount In Situ Hybridization was performed as previously described (Thisse, Thisse et al. 1993; Westfall, Brimeyer et al. 2003), using both digoxigenen-labeled antisense RNA probes and digoxigenen-labeled sense RNA probes (controls). Detection was carried out using BM purple (Roche Applied Science) and the reaction was stopped in phosphate-buffered saline (PBS). Embryos were mounted and photographed using a Zeiss Stemi M13 Stereoscope using Axiocam digital camera.

Zebrafish cDNA	Identity of Total protein	Identity of RGS domain
Rgs2	35%	57%
Rgs3	60%	82%
Rgs4	46%	45%
Rgs5	71%	71%
Rgs16	44%	59%

Table 1: Zebrafish RGS Percent Identities to Corresponding Human RGS Proteins

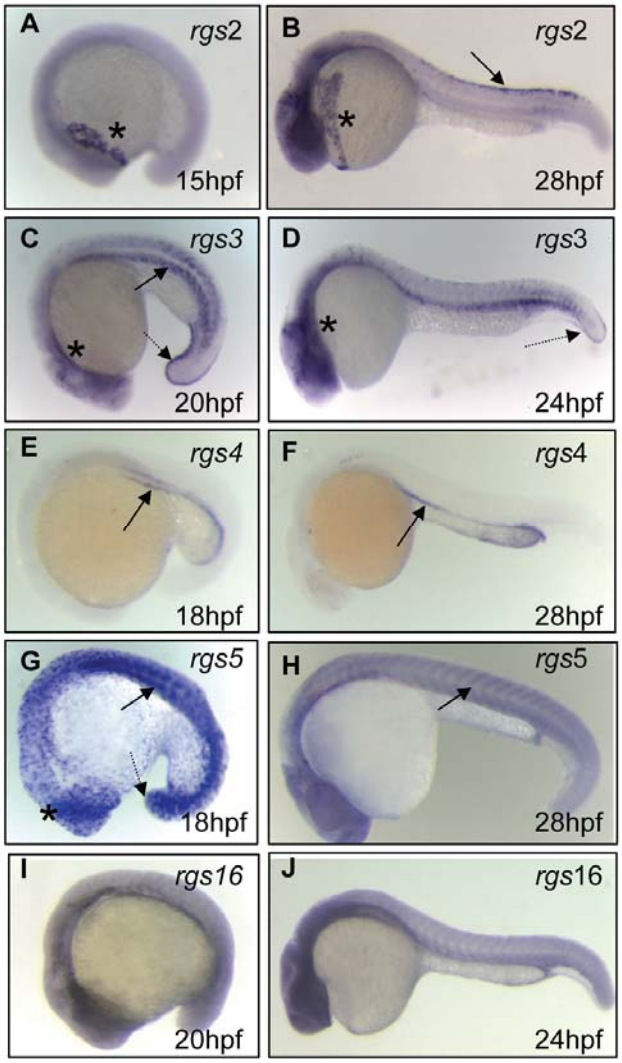

Figure 17: RGS Proteins have Unique and Overlapping Expression Patterns. WMISH of (A and I) 15 hpf, (E and G) 18 hpf, (C) 20 hpf, (D) 24 hpf and (B, F, H, and J) 28 hpf wildtype embryos with (A-B) *rgs*2, (C-D) *rgs*3 (C-D), (E-F) *rgs*4, (G-H) *rgs*5 and (I-J) *rgs*16. *rgs*2 is expressed in the hatching gland (*) and migrating neural crest (arrow). *rgs*3 is expressed in the developing somites (arrow), posterior tail (dashed arrow) and in the midbrain/hindbrain boundary (*). *rgs* 4 is expressed in the pronephros (arrow). *rgs*5 is expressed in the somites (arrow), midbrain (*), and posterior tail (dashed arrow). *rgs*16 is expressed ubiquitously. Sense probes (negative control) gave no specific hybridization signal.

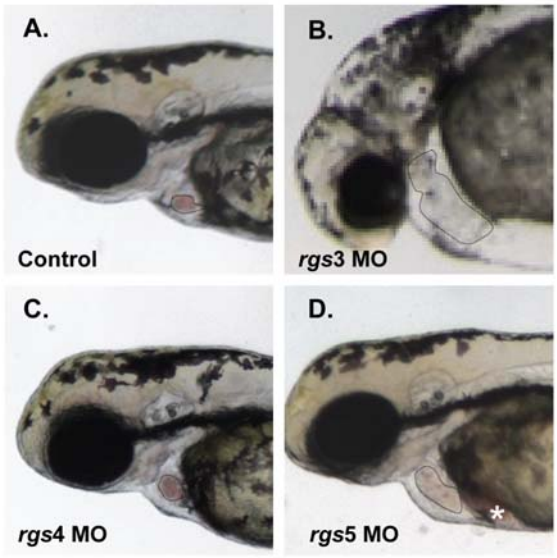

Figure 18: Heart Defects in RGS Morphants. Lateral image of 48 hpf (A) Control MO, (B) *rgs*3 MO, (C) *rgs*4 MO and (D) *rgs*5 MO injected embryos. (D) Asterisk indicates blood pooling.

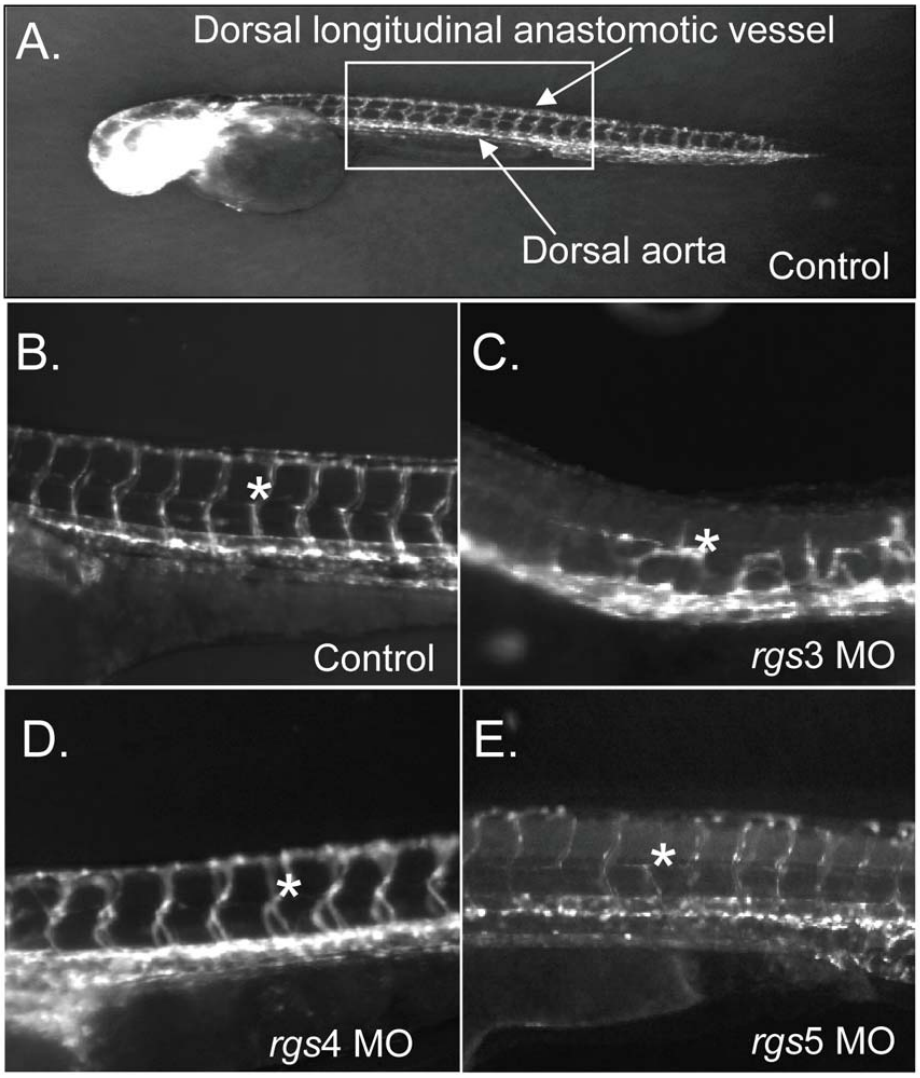

Figure 19: Cardiovascular Defects in RGS Morphants. (B-D) Fluorescence image of the trunk region (white box A) of 48 hpf transgenic fli1-GFP (B) Control MO, (C) *rgs3* morphant, (D) *rgs*4 morphant and (E) *rgs5* morphant embryos. Asterisks indicate intersegmental vessels.

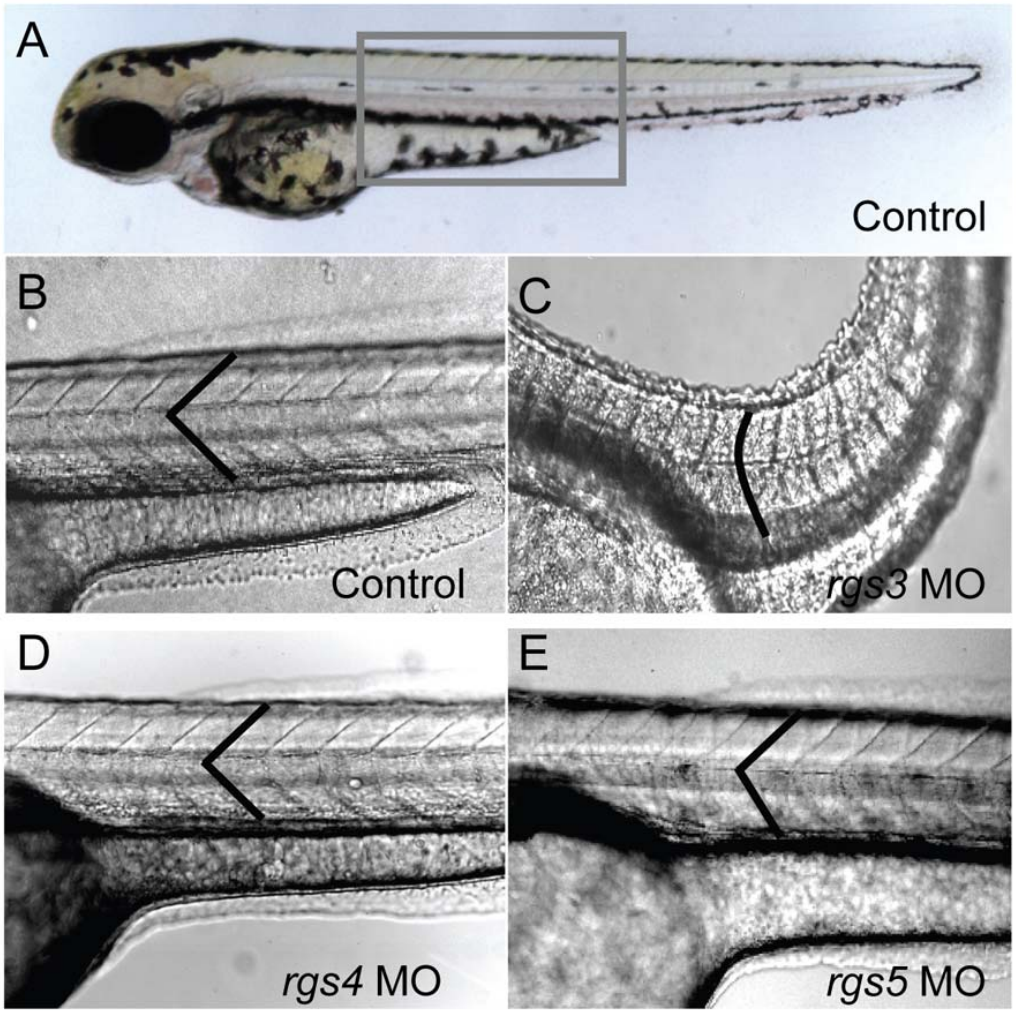

Figure 20: RGS Morphant Phenotypes. (A) Lateral view of 48 hpf embryo. (A) Grey box indicates trunk region shown in B-E. (B) Control MO, (C) *rgs*3 MO, (D) *rgs*4 MO, and (E) *rgs*5 MO embryos. Black line indicates the shape of one somite.

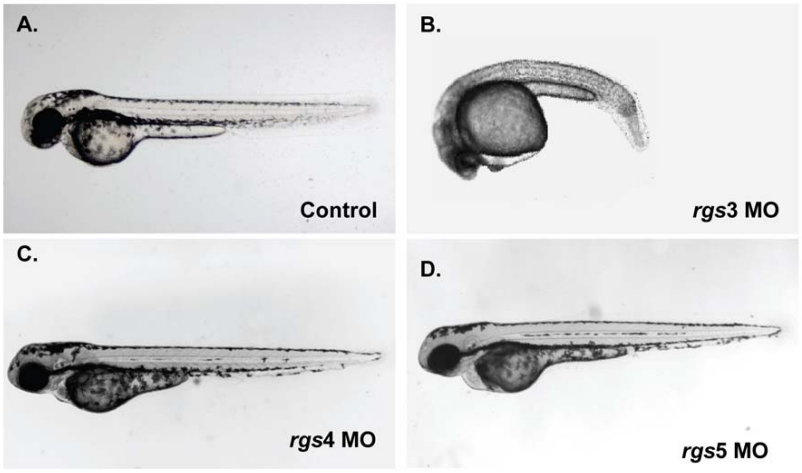

Figure 21: Analysis of Rgs3, 4 and 5 Knockdown. Lateral images of live 48 hpf (A) Control MO, (B) *rgs3* MO, (C) *rgs4* MO and (D) *rgs5* MO injected embryos.

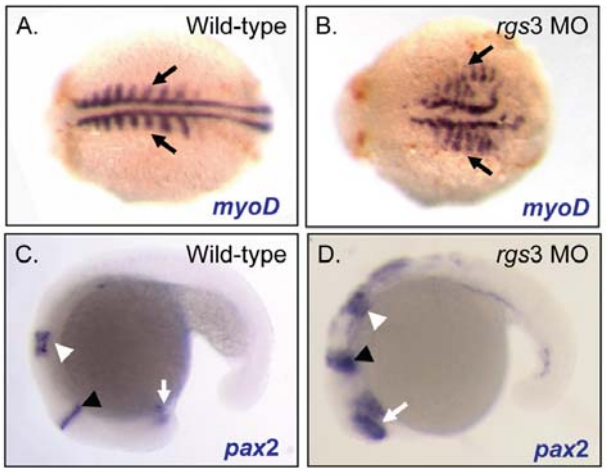

Figure 22: Analysis of Rgs3 Morphants Convergent-Extension Defect. WMISH with anterior to the left of (A and C) Wt and (B and D) rgs3 MO injected embryos hybridized with (A-B) MyoD at 14 hpf and (C-D) Pax2 at 20 hpf. (A-B) Black arrows indicate lateral somite extension, (C-D) white arrows indicate anterior retina, black arrow heads indicate midbrain/hindbrain boundary, and white arrow heads indicate the otic vesicle.

Figure 23: Analysis of *rgs3* Knockdown. (A-D)Lateral images of live 24 hpf (A) Control MO injected, (B) *rgs*3 MO injected and (C) *pipetail* embryos. Lateral and (F-G) dorsal images with anterior to the right of Whole mount in situ hybridization of (A-G) 8-10 somite wild-type embryos hybridized with (D and F) *rgs*3 and (E and G) *wnt5*.

CHAPTER 4

REGULATOR OF G PROTEIN SIGNALING 3 MODULATES WNT5B CA^{2+} DYNAMICS AND SOMITE PATTERNING

Introduction

Vertebrate development requires communication among cells of the embryo in order to define the body axis. The Wnt signaling network plays a key role in axis formation as well as a vast array of other cellular processes. The distinct phenotype associated with Rgs3 knockdown, in particular the lack of convergence to the midline and shortened anterior to posterior extension is reminiscent of defects associated with the Wnt signaling network, leading to the hypothesis that Rgs3 is an endogenous regulator of Wnt/Ca^{2+} signaling

To investigate potential roles of RGS proteins in vertebrate development, I utilize gene knockdown in zebrafish. I focus on *rgs*3, which was identified in an expression screen in zebrafish (Kudoh, Tsang et al. 2001). I find that *rgs3* is expressed in overlapping and adjacent domains with *wnt5b* at multiple stages of zebrafish development. Morpholino knockdown of *rgs3* in zebrafish embryos causes CE defects that resemble phenotypes observed in the *wnt5b* genetic mutant, *pipetail* (Rauch, Hammerschmidt et al. 1997). In addition, I have identified a genetic interaction between *rgs3* and *wnt5b*. Additionally, I describe endogenous Ca^{2+} release dynamics during somite stages and show that Rgs3 and Wnt5b impact the frequency of Ca^{2+} release. Moreover, I show that Rgs3 modulates the extent and duration of Wnt5b induced Ca^{2+} activity. Functional analysis shows that both the rescue of the *rgs3* knockdown defect and its impact on Wnt5-induced Ca^{2+} release requires a key asparagine in the RGS domain of Rgs3 that is necessary for Gα binding and acceleration of its GTPase activity.

This research identifies a link between Wnt5b signaling and Rgs3 activity relative to the frequency of Ca^{2+} release, thus revealing obligatory roles for RGS proteins in vertebrate development in the context of the whole animal. Our results also demonstrate that the biological outcome of Wnt signaling depends greatly upon regulating the duration of its signal, as shown here with Rgs3.

Rgs3 expression overlaps with Wnt5b

Zebrafish *rgs3* was identified in an expression screen during early somitogenesis stages (Kudoh, Tsang et al. 2001) and is poised to interact with the Wnt signaling network (Chapter3). Utilizing Reverse Transcriptase Polymerase Chain Reaction (RT-PCR), I determined that *rgs3* expression begins during the blastula period shortly after zygotic transcription initiates (2.5-5 hours post fertilization, hpf), and persists through the segmentation period (10-24hpf) (Figure 24A). Whole Mount *In Situ* Hybridization (WMISH) demonstrated ubiquitous *rgs3* expression during epiboly and gastrulation stages. During somite stages (10-28 hpf), *rgs3* expression resolves in the somites, tailbud, and brain (Figure 24B-I), with discrete *rgs3* expression in the midbrain/hindbrain boundary as demonstrated by overlap with the molecular marker engrailed 1 (*eng*1*)* at 28 hpf (Figure 24J-K), and enriched *rgs3* expression in the posterior (caudal) portion of developing somites (Figure 24G and L). Double label WMISH with Titin, which decorates the somite boundaries, indicates that *rgs*3 expression becomes diffuse in the somites after 30 hpf (Figure 24M).

Preliminary analysis of *rgs3* knockdown suggested that Rgs3 may function in the Wnt/Ca^{2+} pathway. Therefore, I compared the expression patterns of *wnt*5 and *wnt*11 to *rgs*3. In zebrafish, Wnt5 and Wnt11 function in Wnt/ Ca^{2+} signaling (Dale 1998; Kuhl, Sheldahl et al. 2000). Wnt11 is enriched in the anterior and mutants show anterior extension and eye fusion defects, while Wnt5b is enriched in the posterior and mutants

show altered cell movements during gastrulation (Sepich, Myers et al. 2000; Heisenberg and Solnica-Krezel 2008; Lin, Chen et al. 2009). Since *rgs3* was dynamically expressed in the posterior tail and developing somites (Figure 24B-I), I used double label WMISH to directly compare *rgs*3 and *wnt*5 expression during the segmentation period (Figure 25). I find that *rgs3* and *wnt5b* show both overlapping and adjacent expression domains in the somites and in the posterior tailbud (Figure 25C, F G-J). *rgs3* expression is enriched around the Kupffer's vesicle (Figure 25H), a ciliated organ in the zebrafish embryo that has been shown to influence left-right patterning, yet *rgs3* does not appear to be required for organ laterality (data not shown). As Wnt5b is a secreted ligand, the proximity of *rgs3* to *wnt5b* producing cells suggests that Rgs3 may function in modulating Wnt5b signaling.

Rgs3 inhibits Wnt5b induced Ca^{2+} dynamics

A mutation in Wnt5b has been shown to correspond to *pipetail* (*ppt*; (Rauch, Hammerschmidt et al. 1997). *ppt* zygotic mutants have axis extension defects, reflected in a shorter anterior-posterior length and kinks in the tail, resembling a pipe (Figure 22C; (Hammerschmidt, Pelegri et al. 1996)). Analysis of zygotic ppt mutant embryos revealed reduced Ca^{2+} levels in the YSL region (Westfall, Brimeyer et al. 2003).

In zebrafish, *wnt5b* over-expression induces increased Ca^{2+} release during the blastula stage in a G protein-dependent manner (Slusarski, Corces et al. 1997; Slusarski, Yang-Snyder et al. 1997; Westfall, Hjertos et al. 2003). To determine if *rgs3* over-expression is sufficient to negatively regulate Wnt5b signaling (Figure 26A), I tested the impact of *rgs3* on *wnt5b* induced Ca^{2+} release. In vivo imaging in blastula stage embryos is accomplished with the Ca^{2+} sensor Fura-2. Upon binding Ca^{2+}, Fura-2 exhibits an absorption shift that can be determined by collection at two wavelengths (340nm, Ca^{2+}-saturated and 380nm, Ca^{2+}-free). A ratio image is derived as the quotient of the 340-nm image divided by the 380-nm image on a pixel-by-pixel basis, and provides spatial and

temporal measurement of Ca^{2+} dynamics. Ca^{2+} release activity was monitored over a 75 minute time course during the blastula stage. Sequential ratiometric images were analyzed by a subtractive algorithm to identify changes in Ca^{2+} release activity (transients) over time as well as the location of the activity, as described previously (Lechleiter, Giraρd et al. 1991; Chang and Meng 1995; Slusarski and Corces 2000; Freisinger, Houston et al. 2008). Transients identified during the time course are presented as a composite image with location of Ca^{2+} release mapped on the embryo. The number of Ca^{2+} transients during the cellular blastoderm stage is represented by height of the peaks and color coded where purple is low and yellow/red is a high number of events. The composite image of a wild-type (wt) embryo during the blastula stage indicates endogenous Ca^{2+} levels throughout the embryo (Figure 26C) compared to those observed during increased Ca^{2+} release in an embryo injected with *wnt5b* (Figure 26B). Embryos were co-injected with *rgs3* and dextran-conjugated Texas Red (TxR) lineage tracer into a subset of cells in embryos uniformly expressing *wnt5b* co-mixed with Fura-2. The reduction of Ca^{2+} levels (Figure 26D) in the rgs3/TxR positive region (Figure 26F) supports the conclusion that *rgs3* is sufficient to suppress *wnt5b* induced Ca^{2+} release.

I next investigated if Rgs3's ability to suppress *wnt5b* induced Ca^{2+} release requires GAP activity. A conserved asparagine within the RGS domain of RGS proteins is necessary for GAP activity on Gα subunits (Tesmer, Berman et al. 1997; Natochin, McEntaffer et al. 1998; Srinivasa, Watson et al. 1998). Substitution of this key asparagine (N) with Alanine (A) results in a loss of the GAP activity of RGS proteins towards Gα subunits in cultured cells (Natochin, McEntaffer et al. 1998; Srinivasa, Watson et al. 1998). To elucidate the role of the GAP function of Rgs3, I created a N to A mutation in zebrafish *rgs3* (*rgs*3^{N109A})(Figure 27A). I evaluated the impact of *rgs*3^{N109A} expression on Wnt5b induced Ca^{2+} release. Unlike *rgs3*, the *rgs*3^{N109A} is unable to suppress *wnt5b* induced Ca^{2+} release (Figure 26E) as demonstrated by no

change in the Ca^{2+} activity in the *rgs*3^{N109A} /TxR positive region of embryos (Figure 26G). To rule out the possibility that lack of suppression by $Rgs3^{N109A}$ was due to differences in its expression or localization compared to Rgs3, I generated and expressed N-terminal myc-tagged *rgs*3 and *rgs*3^{N109A} constructs in embryos. Western analysis reveals robust and comparable expression of Rgs3 and $Rgs3^{N109A}$ at the time of Ca^{2+} imaging as well as through 24hpf (Figure 27B). Immunostaining for anti-myc in epiboly stage embryos also indicates that both proteins localize to the membrane and cytoplasm (Figure 26 H and I, respectively). Together these data strongly indicate that *rgs3* is sufficient to inhibit *wnt5*b-induced Ca^{2+} signaling and that this action requires the GAP activity of Rgs3.

Endogenous requirement of Rgs3 during embryogenesis

Since Rgs3 is sufficient to modulate Wnt5 activity in an over-expression assay, I next evaluated the necessary role of *rgs3* during development. To knockdown Rgs3, I utilized antisense morpholino oligonucleotides (MO) (Morcos 2000). Three separate MOs were designed to bind *rgs3* 5'UTR (MO and MOb) or splice junction (SA) (Figure 27A). All MOs designed to knockdown Rgs3 produced similar defects. Control-injected embryos at 28 hpf are fully extended with a characteristic anterior-posterior (A-P) length (Figure 27C). In contrast, *rgs3* MO-injected embryos have shorter A-P extension, a kinked tail (Figure 27D), and decreased somite spacing (Figure 27 F). The distinct phenotype associated with Rgs3 knockdown, in particular the lack of convergence to the midline and shortened anterior to posterior extension is reminiscent of defects observed in the *wnt5b* (*pipetail*) genetic mutant (Rauch, Hammerschmidt et al. 1997). Inhibition of Wnt5a has been shown to inhibit endothelial cell proliferation and migration (Masckauchan, Agalliu et al. 2006; Cheng, Yeh et al. 2008). We have previously reported that *pipetail*, displays vascular developmental defects consistent with endothelial migration defects caused by diminished PCP regulation.(Cirone, Lin et al. 2008). These

data suggest a mechanism whereby Wnt signaling can direct endothelial cell growth and coordination during angiogenesis.

Angiogenesis, the formation of new vasculature, involves the migration of endothelial cells from existing large vessels. In the zebrafish, the formation of intersegmental blood vessels serves as a paradigm to study angiogenesis *in vivo*. During the formation of intersegmental vessels, endothelial cells divide as they migrate out of the main vessel, the dorsal aorta (Leslie, Ariza-McNaughton et al. 2007). As intersegmental vessels form, endothelial cells rearrange extensively and eventually fuse producing fully formed intersegmental vessels which consist of 4–6 cells arranged in an overlapping and staggered fashion (Blum, Belting et al. 2008).

I compared intersegmental vessel formation in Rgs3 morphants to Wnt5 morphants. Vessel formation was evaluated *in vivo* by fluorescence microscopy of Tg(Fli1:EGFP) embryos. In control MO injected embryos; intersegmental vessels sprout from the dorsal aorta and extend to form the dorsal longitudinal anastomotic vessel (Figure 27G-H). Rgs3 morphants display disrupted intersegmental vessel formation characterized by reduced dorsal migration resulting in the appearance of stub-like structures (Figure 27I) where Wnt5 morphant vessel formation is characterized by abnormal vessel migration in which the path of migration is randomized (Figure 27J).

Given the need for cell-cell communication during angiogenesis, it is predicted that alterations in Wnt signaling in individual cells could influence the migration of neighboring cells. To investigate if alterations in Wnt signaling influence vessel migration of neighboring cells, I performed cell transplant experiments. Donor Tg(Fli1:EGFP) embryos were co-injected with Texas red and either Rgs3 MO, Wnt5 MO, *rgs3* RNA or $rgs3^{N\text{-}A}$ RNA at the one cell stage. Cells from the donor embryos were transplanted into a Tg(Fli1:EGFP) host embryos and intersegmental vessel outgrowth was characterized at 48hpf. My preliminary analysis indicates that an alteration in Wnt signaling in individual cells influences the migration of neighboring cells. I find that

intersegmental vessels outgrowth stops when a vessel approaches an Rgs3 morphant cell (Figure 27K), intersegmental vessels migrate into areas where Wnt5 is inhibited (Figure 27L), intersegmental vessels migrate toward, but not into cells overexpressing rgs3 RNA (Figure 27M) while intersegmental vessel formation is unaffected by cells over-expressing mutant rgs3^{N-A} RNA (Figure 27N). To confirm these results, additional cell transplantation experiment should be performed to obtain larger clone areas. Together these data support the conclusion that the intersegmental vessel defects observed in Rgs3 and Wnt5 morphant embryos are not secondary vascular defects, due to altered somite formation, and proper Wnt signaling is required for angiogenesis.

To evaluate anterior-posterior extension alterations at an earlier developmental stage (15 hpf), molecular markers were used. Control-injected embryos have a characteristic spacing of *krox20* expression in the hindbrain rhombomeres 3 and 5, as well as regular spaced blocks of *myoD* expression in the developing somites flanking the midline (Figure 28A-B and E-F). In contrast, *krox20* and *myoD* expression in *rgs3* morphants reveal a failure of cells to converge on the midline resulting in a lateral expansion of the rhombomeres and somites (Figure 28C and G). Additionally, *rgs3* morphants fail to extend along the anterior-posterior (A-P) axis leading to closer spaced *myoD* (Figure 28G, asterisks). The A-P extension defects were further confirmed with *pax2*, a marker expressed in the anterior retina, midbrain/hindbrain, and otic vesicle of 18 hpf embryos (Figure 28I). *rgs3* morphants display compression of these regions along the A-P axis (Figure 28J). Together these data strongly indicate that *rgs3* is required for normal anterior-posterior axis extension.

The specificity of the rgs3 knockdown as well as structural functional analyses was determined by RNA co-injection experiments. Injection of control 5bp mismatch MO resulted in negligible defects compared to *rgs3* MO which induced morphological somite defects (Figure 28L). Co-injection of *rgs3* MO with *rgs*3 RNA suppressed the MO-induced defects evaluated by molecular markers *krox20* (Figure 28D), *myoD* (Figure

28H, asterisks) and *pax2* (Figure 28K). Moreover, wild-type *rgs3* RNA leads to significant suppression of MO-induced defects (Figure 28L and Table 2). In contrast, *rgs3*^{N109A} mutant RNA does not suppress the MO-induced defect (Figure 28L and Table 2). These results demonstrate that Rgs3 GAP activity is required for its developmental functions.

rgs3 function is necessary for endogenous Ca^{2+} dynamics in somites

The functional requirement of *rgs3* during anterior-posterior axis extension and the finding that over-expression of *rgs3* is sufficient to inhibit *wnt5*b-induced Ca^{2+} signaling, raised the possibility that *rgs3* may negatively modulate Ca^{2+} release dynamics during somitogenesis. Ca^{2+} signals along the trunk of zebrafish embryos during somitogenesis have been described using the bioluminescent Ca^{2+} reporter R-aequorin (Creton, Speksnijder et al. 1998; Webb and Miller 2000; Webb and Miller 2006). In order to compare changes in Ca^{2+} release dynamics upon *rgs3* manipulation, I performed a detailed analysis of endogenous Ca^{2+} release in tissues that express both *wnt5b* and *rgs3*. To this end, we utilized Fura-2 imaging to monitor Ca^{2+} activity with a focus on the developing somites and tailbud in either a dorsal (Figure 29A) or a lateral (Figure 30A) orientation. The pseudocolored ratio image provides a spatial and temporal measurement of Ca^{2+} dynamics with low Ca^{2+} represented by blue and high Ca^{2+} represented by yellow/red. Representative pseudocolored ratio images from a time-lapse series of Ca^{2+} measurements, spanning the 3-13 somite stages are shown (Figure 29B-E). The notochord and forming somites can be identified in the grayscale fluorescence images (Figure 29B'-E'). Overlay of grayscale and ratio images illustrate the regions of increased Ca^{2+} levels relative to morphology (Figure 29B''-E'').

Ca^{2+} release activity during somitogenesis is dynamic with sustained Ca^{2+} levels in the presomitic mesoderm, lateral to the somite forming region and flanking the

midline/notochord (Fig 29C''-E''). As somitogenesis proceeds, sustained Ca^{2+} levels appear distinctly between the somites (Fig 29C''-E'', arrowheads). In addition, we observe localized short-lived increases in Ca^{2+} release (referred to as transients). To demonstrate a transient, a region of interest (ROI) is noted by dashed circle (Figure 31A-C). In the ROI, an increase in Ca^{2+} is observed from time 0s to time 15s and the local increase subsides by time 30s. Since *rgs3* may function to influence the frequency of Ca^{2+} release, we determined the number of transients as a function of developmental age (Figure 31D). In wt embryos, we observe an average of 5.3 Ca^{2+} transients per hour (n=3) (Figure 31E). A similar frequency is found when analyzing the data from a lateral view (Figure 30B-D and K).

Having defined endogenous Ca^{2+} release dynamics during somitogenesis, we next determined the impact of *rgs*3 knockdown. From the development of somite 6 to somite 12, *rgs*3 morphants have statistically more Ca^{2+} transients, with an average of 21.7 per hour (n=3), when compared to wt embryos (Figure 31D and E). *rgs*3 morphants have sustained Ca^{2+} levels in the lateral regions similar to wt. However the dynamics within the somite region frequently show initiating transients leading to responses in neighboring cells, resulting in larger areas of increased Ca^{2+} release (Figure 31I-K). These large and robust transients are not observed in wt embryos (Figure 31F-H) or in Wnt5b morphant embryos co-injected with *rgs3* RNA. The same dramatic increase in both the frequency of release and amplitude is observed in lateral views as well (Figure 30E-G and K). The change in Ca^{2+} release dynamics in *rgs3* morphants is consistent with a delayed shut-off of G protein signaling, i.e. normally mediated by the GAP activity of Rgs3. These data indicate that during the segmentation period Rgs3 functions to limit the extent and duration of the endogenous Ca^{2+} release activity.

Previously, we reported reduced Ca^{2+} release in blastula stage Wnt5b (*pipetail)* genetic mutants (Westfall, Brimeyer et al. 2003). When compared to wild-type embryos, *wnt5b* morphant embryos show a statistically reduced number of Ca^{2+} transients,

averaging 1.3 per hour (n=2) during the segmentation period (Figure 31D-E and L-M). A similar decrease in frequency is also observed in a lateral view (Figure 30H-K). The size and duration of Ca^{2+} transients observed in *wnt5b* morphants are comparable to wt embryos. In order to determine if the increased frequency of Ca^{2+} transients associated with *rgs3* knockdown is dependent upon *wnt5b* signaling, we simultaneously knocked down *wnt5b* and *rgs3*. Embryos co-injected with *wnt5b* MO and *rgs3* MO and imaged during the segmentation period show a statistically reduced number of Ca^{2+} transients, 1.8 per hour (n=5) (Figure 31D-E). The reduced Ca^{2+} release in the double knockdown is not significantly different than that in the *wnt5b* single knockdown, demonstrating that the *rgs3* morphant phenotype is dependent upon Wnt signaling.

Due to the fact that the *rgs3* morphant phenotype is dependent upon Wnt signaling I used WMISH to determine if Rgs3 morphants had altered *wnt5b* expression or if Wnt5b morphants had altered *rgs3* expression (Figure 32). I find that there is ectopic wnt5b expression in the anterior region of Rgs3 morphant embryos (Figure 32B) indicating that endogenous Rgs3 in the head may function to inhibit Wnt5 in a feedback loop. A future approach will be to determine if the ectopic *wnt5* expression alters Ca^{2+} dynamics in the anterior region of Rgs3 morphant embryos. Due to the defects in somite formation and anterior-posterior extension in Wnt5 morphants, I was unable to identify a difference in *rgs3* expression in wnt5b morphants compared to wild-type embryos (Figure 32C-D).

rgs3 and wnt5b interaction

To further explore interaction between Rgs3 and Wnt5b, we defined a low dose for *wnt5b* MO which results in a mild A-P extension phenotype and determined whether *rgs3* enhances or suppresses the *wnt5b* gene knockdown defects. Phenotypes were evaluated by morphology (Figure 33A, D, G and J) and molecular markers, *krox20* and *myoD* (Figure 33B-C, E-F, H-I and K-L). Compared to wt (Figure 33A-C), low dose

wnt5b MO (2 ng) results in a mild phenotype (Figure 33D-F). We next defined a sub-phenotypic dose for *rgs3* MOsa (0.8 ng), which produced a phenotype (Figure 33G-I) indistinguishable from wt (Figure 33A-C). Individual injection of low dose *rgs3* MOsa or *wnt5b* MO did not induce any severe defects (Figure 33M). However, *wnt5b* MO (2 ng) combined with *rgs3*MOsa (0.8 ng) resulted in a 92% penetrance of severe defects (Figure 33J-M). Our Ca^{2+} imaging implicated Rgs3 function in limiting the extent and duration of endogenous Ca^{2+} release activity and this was dependent upon Wnt5b. However, in the presence of low level Wnt5b activity (low-dose MO), partial knockdown of *rgs3* could lead to discordant changes in the frequency and amplitude of Ca^{2+} release that result in the dramatic phenotypic penetrance and severity.

rgs3 and the Wnt signaling network

Studies have shown that increased Wnt/Fz signaling leads to degradation of Dvl (Gao and Chen; Angers, Thorpe et al. 2006; Jung, Kim et al. 2009). In addition *Drosophila* genetics places active G protein signaling upstream of Dvl (Katanaev, Ponzielli et al. 2005). Because RGS is predicted to function at the level of G protein activation, I investigated if Rgs3 plays a role in modulation of Dvl levels. I find that *wnt5b* co-expression reduced Dvl2-Myc levels (Figure 34A). Reduction of Rgs3 function, via MO knockdown, also leads to decreased Dvl2-Myc levels. Interestingly, overexpression of Flag-*rgs*3 also resulted in decreased Dvl2-Myc levels. Overexpression of the mutant form of Flag-*rgs*3^{N-A} doesn't alter Dvl2-Myc levels (Figure 34A), indicating that the observed decrease in Dvl2-MT levels with overexpression of Flag-*rgs*3 is dependent upon Rgs3 function. In order to determine if activation of the Wnt signaling results in Rgs3 turnover, *wnt5*b RNA was co-injected with Flag-*rgs3*. Western blot analysis indicates that Wnt5b has no impact on Flag-Rgs3 or Flag-$Rgs3^{N-A}$ protein levels (Figure 34B). These data demonstrate that endogenous Rgs3 functions in the non-

canonical Wnt pathway upstream of Dvl, thereby functioning to modulate the duration and robustness of Wnt5 signaling.

Dvl is known to function as a key scaffolding protein and cell culture data supports that the βγ subunit of G proteins binds to Dvl (Angers, Thorpe et al. 2006). I therefore investigated the possibility that Rgs3 directly binds to Dvl. In the absence of an antibody to evaluate binding of endogenous Rgs3, I generated a Flag-tagged form of zebrafish Rgs3 that is readily detected by western blot. I performed co-immunoprecipitation experiments to determine if Flag-Rgs3 binds to Dvl2-Myc. With these methods, I found no evidence that there was a direct interaction between Flag-Rgs3 and Dvl2-Mt (Figure 35). A future direction would be to determine if in the presence of activated Gα, RGS and Dvl interact.

The observation that Flag-Rgs3 influences Dvl2-Myc levels led me to investigate Rgs3 function in the Wnt/β catenin pathway, which requires Dvl. It has been previously demonstrated that Wnt5 overexpression induces hyperdorsalization defects indicating that Wnt5 signaling is able to antagonize the Wnt/β-catenin pathway (Westfall, Brimeyer et al. 2003). Additionally, we have shown that depletion of intracellular Ca^{2+} stores in zebrafish embryos is sufficient to generate hyperdorsalized phenotypes (Westfall, Hjertos et al. 2003). From these results I predicted that Rgs3 knockdown would lead to increased Wnt5 signaling and therefore inhibit Wnt/β-catenin signaling. To test this hypothesis, I used double label WMISH to identify dorsal and ventral regions of shield stage zebrafish embryos. We have previously determined that Wnt5 overexpression results in a reduction of the presumptive dorsal region and expansion of presumptive ventral tissue. In shield stage Wt embryos, *chordin* expression is seen in a tight region on the presumptive dorsal side while *eve1* expression is seen on the ventral side (Figure 36A). I found that loss of Rgs3 results in a lateral expansion of *chordin* expression as well as an expansion of *eve-1* expression, resulting in an overlap of dorsal and ventral markers (Figure 36B). Although the dorsal marker *chordin* had expanded lateral expression the

chordin positive region was very narrow therefore, I was unable to determine if more cells were expressing *chordin*. From these results I was unable to conclude whether or not Rgs3 knockdown inhibited dorsal identity.

As an alternative approach to determine if Rgs3 knockdown impacts Wnt/β catenin signaling, I utilized a luciferase reporter system. Activation of the Wnt/β catenin pathway results in the stabilization of β catenin protein. In the luciferase reporter system, injected TopFlash plasmids are used to quantify the amount of β catenin dependent transcriptional activation. In the presence of Wnt activation, β catenin enters the nucleus and is able to bind the TCF/LEF response elements (TOPFLASH) and drive firefly luciferase expression. In order to quantify Wnt/β catenin activation, one cell zebrafish embryos were co-injected with a plasmid containing both Renilla luciferase as well TOPFLASH or the mutant sequence (FOPFLASH) driving the expression of a cDNA encoding the firefly luciferase gene and either Rgs3 MO or β catenin RNA. Wnt/β catenin signaling was measured at 50% epiboly. The activity of Wnt/β catenin signaling was quantified by measurement of normalized luciferase expression or relative luciferase activity units (RLUs), which is derived as the ratio of the absolute activity of firefly luciferase to that of renilla luciferase which serves as a control for injection efficiency. My preliminary results indicate that knockdown of Rgs3 leads to a significant decrease in Wnt/β catenin signaling when compared to Wt (Figure 36C). However, the results I obtained were inconclusive due to the fact that β-catenin overexpression did not significantly increase Wnt/β catenin signaling when compared to Wt (Figure 36C). The β catenin is translated into a functional product in this assay as it induced dorsalization (Figure 36F). Due to the fact that I was unable to obtain repeatable results from the luciferase assay I can not definitively conclude if Rgs3 impacts the canonical Wnt pathway. Future experiments using quantitative RT PCR will be essential in determining if Rgs3 function influences the canonical Wnt pathway.

Discussion and Future directions

In this chapter, I use rescue of gene knockdown and *in vivo* Ca^{2+} imaging assays, to demonstrate that the activity of Rgs3 requires its ability to interact with Gα subunits and function as a G protein GAP. Additionally, I provide data supporting that Rgs3 function is necessary for maintaining the appropriate frequency and amplitude of Ca^{2+} release during somitogenesis and is downstream of Wnt5 activity. These results provide the first evidence for an essential developmental role of RGS proteins in modulating the duration of Wnt/Ca^{2+} signaling.

I show that Rgs3 is necessary for proper gastrulation and somite patterning during zebrafish development. These actions of Rgs3 require its ability to interact with and accelerate the rate of GTP hydrolysis by G proteins, as revealed by studies employing an Rgs3 mutant defective in these activities. I describe endogenous Ca^{2+} release dynamics during somitogenesis. The frequency of Ca^{2+} transients as well as the observation of sustained Ca^{2+}activity in the trunk and tail region are consistent with previous reports of Ca^{2+} activity during zebrafish somitogenesis (Creton, Speksnijder et al. 1998; Webb and Miller 2000; Webb and Miller 2006; Webb and Miller 2007). Of particular significance is the dramatic increase in the frequency of endogenous Ca^{2+} release upon *rgs3* knockdown.

RGS proteins were identified as negative regulators of G protein signaling in the mid 1990s (Dohlman, Apaniesk et al. 1995; Koelle and Horvitz 1996) and the role of G proteins in Wnt/Ca^{2+} signaling was first demonstrated in 1997 (Slusarski, Corces et al. 1997). Subsequent reports further implicated G proteins in canonical Wnt signaling (Liu, Liu et al. 1999; Liu, DeCostanzo et al. 2001; Ahumada, Slusarski et al. 2002). Heterotrimeric G protein activation and inactivation are tightly regulated to provide precise control of the amplitude and duration of G protein signaling. Receptor-stimulated GTP binding activates G proteins, while their intrinsic GTPase activity functions to terminate signaling. RGS proteins by definition accelerate this GTPase activity. Over-

expression studies in cell culture (Feigin and Malbon 2007) and in Xenopus embryos (Wu, Zeng et al. 2000) have indicated that specific RGS proteins are sufficient to regulate canonical Wnt signaling. Although G protein signaling is required for normal cell movement during zebrafish gastrulation (Lin, Chen et al. 2009), the role of RGS proteins in noncanonical Wnt signaling has not been investigated. Our current study identifies a member of the RGS protein family that has a direct impact on frequency and amplitude of Wnt5b signaling. I find that Rgs3 activity is sufficient to modulate *wnt5b* induced Ca^{2+} release and this ability requires GAP activity consistent with the known role of G proteins in the activation of Wnt signal transduction pathways (Kohn and Moon 2005; Force, Woulfe et al. 2007; Schulte and Bryja 2007). I report two key novel findings, that knockdown of Rgs3 results in increased frequency and amplitude of Ca^{2+} release and that this dramatic impact on Ca^{2+} dynamics in the somites is dependent upon Wnt5. These two together support the conclusion that Wnt/Ca^{2+} signaling activity is an *in vivo* target of RGS proteins. Moreover, *rgs3* demonstrates a complex genetic interaction with *wnt5b*. *rgs3* is expressed in and near *wnt5b* expressing tissues, and I find that combined low doses of *wnt5b* MO and *rgs3* MOsa results in a large penetrance of severe somite defects, which is not observed during their individual knockdown. Our data suggest that both the frequency and amplitude of *wnt5b* signaling must be tightly regulated to result in correct cell movement and somite patterning.

Wnt5b modulates both transient Ca^{2+} release activity in small populations of cells, as well as sustained activity in a large region of cells (Freisinger, Schneider et al. 2008). While the transient release correlates with limiting β-catenin activity (Westfall, Hjertos et al. 2003; Schneider, Houston et al. 2008), I hypothesize that the sustained activity correlates with polarized cell movement, for example in convergence-extension movements during gastrulation or neural and vascular outgrowth (Freisinger, Schneider et al. 2008). This concept is supported by vascular outgrowth defects in *pipetail* genetic mutants (Cirone, Lin et al. 2008) as well as the observation of a reduction in sustained

Ca^{2+} activity at the somite boundaries (data not shown). It is of interest to determine if interactions between *rgs*3 and *wnt5b* influence directed vascular outgrowth.

Modulation of G protein signaling (impacting frequency as well as duration) is likely to influence directed cell migration, vascular development as well as numerous other developmental processes (Albig and Schiemann 2005; Parmalee and Kitajewski 2008; Zerlin, Julius et al. 2008). Our findings clearly justify the need for further investigations into the role of RGS proteins in this process and in other interactions between Rgs3 and Wnt signaling to provide new insights into their mechanistic role in directed cell movement and disease.

Materials and Methods

Zebrafish

Adults were maintained in a 14-hour light / 10-hour dark cycle at 28°C. Embryos were collected from natural pairwise matings and staged by hpf at 28.5ºC and morphological criteria described in Kimmel et al. (Kimmel, Ballard et al. 1995; Westerfield 1995). Animal welfare assurance number: A3021-01

Zebrafish rgs3 point mutant

*rgs*3 (clone IBD5096) was isolated in an expression screen in zebrafish (Kudoh, Tsang et al. 2001) and generously provided by Dr. I. Dawid. MO-resistant *rgs*3 was generated by RT-PCR and directionally cloned (5'-3') into the pCS^{2+}, pCS^{2+} myc or pCS^{2+} Flag expression vector. The Quick Change II site-directed mutagenesis kit (Stratagene) was used to generate an Asparagine (N) to Alanine (A) substitution at amino acid 109 which is located in the RGS domain of Rgs3. Synthetic RNA was then *in vitro* transcribed using SP6 RNA polymerase and the mMessage mMachine system (Ambion).

Micro-Injections

Antisense morpholino oligonucleotides (MO) were designed to target the 5'-UTR/ATG (*rgs3* MO and *rgs3* MOb) to inhibit translation and an intron-exon junction in the RGS domain (*rgs3* MOsa) to alter splicing. As a control *rgs3* MOmm (5 bp mismatch in lowercase letters) was designed (Gene-Tools):

rgs3 MO 5'-AGTCGGTTCTTCATGTCTTTGGCCC-3',

rgs3 MOb 5'-TCTCCGAGAAATCCACCATAGTGTG-3',

rgs3 MOsa 5'-CCAGTCCATCTGATGAGGGAGAGAG-3'.

rgs3 MOmm 5'-TCaCCcAGAAATCCtCCATtGTcTG-3'.

MOs (5-20ng) were pressure-injected into one cell-stage embryos. For low-dose knockdown, 0.8ng *rgs3* MOsa and/or 2 ng *wnt5b* MO (Cirone, Lin et al. 2008) were injected into one cell zebrafish embryos. Control *rgs3* MOmm did not produce any phenotype at 25 ng. For rescue, *in vitro*-transcribed MO-resistant *rgs3* (500 pg) was co-injected with 20 ng *rgs3* MO. Injected embryos were characterized by morphological and molecular analysis.

Cell Transplantation

Donor Fli1:EGFP embryos were microinjected with 30ng lineage marker (dextran-conjugated Texas Red, Molecular Probes) mixed with either Rgs3 MO or Wnt5 MO at the 1–2 cell stage. Donor and host Fli1:EGFP embryos were manually dechorionated prior to transplantation. At sphere/dome stage, 25–35 cells were removed from donor embryos and transplanted into the blastodermal margin of a Fli1:EGFP host embryo.

48 hpf host embryos with transplanted cells incorporated into the somite region were visualized by florescent moicrosopy to analyze vessel defects.

TopFlash luciferase assay

The TopFlash plasmid has a TCF optimal promoter consisting of multimerized TCF-binding sites driving the expression of a cDNA encoding the firefly luciferase gene. One cell zebrafish embryos were co-injected with a plasmid containing both Renilla luciferase as well TOPFLASH or the mutant sequence FOPFLASH (the 12 TCF-binding sites are mutated) driving the expression of a cDNA encoding the firefly luciferase gene and with either Rgs3 MO or β-catenin RNA. Embryos were incubated until 50% ebiboly. At 50% epiboly embryos were flash frozen. Triplicate samples of 15 embryos were then used for TopFlash/FopFlash dual luciferase assays. Luminescence was detected in a Turner Biosystems 20/20n luminometer. Wnt/β catenin signaling was determined by a measurement of normalized luciferase expression or relative luciferase activity units (RLUs), which is derived as the ratio of the absolute activity of firefly luciferase to that of renilla luciferase which serves as a control for injection amount.

Whole mount in situ hybridization

Embryos were fixed overnight in 4% paraformaldehyde and dechorionated. Single label WMISH was performed as previously described (Thisse, Thisse et al. 1993; Westfall, Brimeyer et al. 2003), using digoxigenen (Dig)-labeled or dinitrophenyl (DNP)-labeled antisense and sense RNA probes. Detection was carried out using BM purple (Roche Applied Science). Double label WMISH was performed as previously described (Long and Rebagliati 2002), using both Dig and DNP-labeled antisense probes. Purple color was developed with AP-conjugated anti-Dig and BM purple (Roche Applied Science), and red color was developed with AP-conjugated anti-DNP and INT RED (Roche Applied Science). Reactions were stopped in PBS. Embryos were mounted on bridged coverslips and photographed using a Zeiss Stemi M13 Stereoscope and an Axiocam digital camera.

Western Analysis

To compare levels of myc-Rgs3 and mutant myc-Rgs3, embryos were injected with either *myc-rgs3* or *myc-rgs3*$^{(N109A)}$ (750 pg). To investigate Rgs3's impact on Dvl, C-terminal myc tagged zebrafish *dvl2* (300 pg) was injected alone, with *rgs3* MOsa (5ng), with *wnt5b* (250pg), and with both *rgs3* MOsa (5ng) and *wnt5b* (250pg). Injected Embryos were allowed to develop to the appropriate stage (5 hpf and 24 hpf) before incubating in lysis stock buffer (20 mM Tris, 100mM NaCl, 1mM EDTA, 5% Triton, .5%SDS, 10% Leupeptin and 0.1mM PMSF) at room temperature for 3 minutes. Embryos were then disrupted using a pestle, centrifuged at 13,000 rpm for 10 minutes at 4°C and the clear supernatant containing whole zebrafish protein was collected. Approximately 10µg of protein was loaded in each well and separated with SDS-PAGE gel electrophoresis. Proteins were transferred onto nitrocellulose membrane (Li-Cor) and incubated with the following primary antibodies: mouse anti-myc (1:2,000; Cell Signaling Technology) and rabbit anti-βactin (1:2,000; Sigma), and then incubated with the following secondary antibodies: IRDye800 anti-mouse (1:20,000; Li-Cor) and IRDye680 anti-rabbit (1:20,000; Li-Cor). The signal was visualized using the Odyssey Infrared Imaging System (Li-Cor).

Immunohistochemistry

Embryos injected with either *myc-rgs3* or *myc-rgs3*$^{(N109A)}$ (200 pg) were fixed 1-3 hrs in 4% PFA/1× PBS at sphere/dome stage. Mouse anti–myc antibody (1:1,500; Cell Signaling Technology), followed by goat-anti-mouse Alexa488 conjugated secondary antibody (1:400; Molecular Probes) was used to detect the rgs3 products. Nuclei were identified with 5 µM TOPRO3 (Molecular Probes). Embryos were mounted in an animal pole orientation in bridged coverslips and optically sectioned using two-channel imaging on a scanning laser confocal microscope, Leica TCS SP2. Wide-field fluorescence and bright–field images from a Zeiss Stemi M13 Bio Stereoscope were photographed using

Axiovision (Zeiss) software and an Axiocam 5000 camera. Images were merged using Adobe Photoshop CS.

Intracellular Calcium Imaging

The ratiometric Ca^{2+}-sensing dye Fura-2 or Bis-Fura-2 (Molecular Probes) was injected into 1-cell zebrafish embryos. The excitation spectra are different between Ca^{2+} bound Fura-2 (340-nm) and Ca^{2+} free (380-nm) forms. By taking the ratio of the fluorescence intensity at these wavelengths an estimate of intracellular-free Ca^{2+} can be derived. To stimulate Wnt signaling, *in vitro* transcribed *wnt*5b RNA (400 pg) was co-injected with Fura-2 at the one cell stage. *rgs*3 or *rgs*3^{N109A} RNA (400 pg) was unilaterally injected at the 16-cell stage mixed with dextran-conjugated Texas Red (TxR) lineage tracer. TxR distribution was determined by collecting a reference exposure at 540-nm excitation. For cellular blastoderm stage imaging, embryos were oriented in a lateral position in a glass-bottomed dish on a Zeiss axiovert epifluorescence microscope. Image pairs at 340 and 380-nm excitation wavelengths (510-nm emission) were collected at 15-second intervals. Each imaging session collected 300 image pairs. The ratio image, a pixel by pixel match of both excitation wavelengths, is calculated by computer software (RatioTool, Inovision). The sequence of ratio images was processed and the Ca^{2+} fluxes (transients) were determined by a subtractive analog patterned after (Lechleiter, Girard et al. 1991; Chang and Meng 1995) and described in (Slusarski and Corces 2000; Freisinger, Houston et al. 2008). The ratio image (340nm, Ca^{2+}-saturated and 380nm, Ca^{2+}-free) imported for publication is encoded in 8 bits and converted to pseudocolor with low ratio (low Ca^{2+}) represented by blue and high ratio (high Ca^{2+}) represented by yellow/red.

For somite imaging, 2-6 somite stage embryos were oriented in low melt agarose (.38%) in a dorsal or lateral orientation. Time courses collected images pairs until 12-15 somite stage at 15-second intervals (Approximately 1000 images pairs). Image pairs

were converted to ratio images as described above. Sequential ratio images were manually analyzed for changes in Ca^{2+} transients. Somite stage Ca^{2+} transients were defined as a localized increase in Ca^{2+} which persists no longer than thirty seconds.

Statistical analysis

Calculations for MO rescue experiments were made using the Fisher's exact test and the two-tailed p-value was reported. Calculations for analysis of somite stage Ca^{2+} transients in morphant embryos were made using One-Way Analysis of Variance (one-way ANOVA) with Tukey HSD test p-values reported.

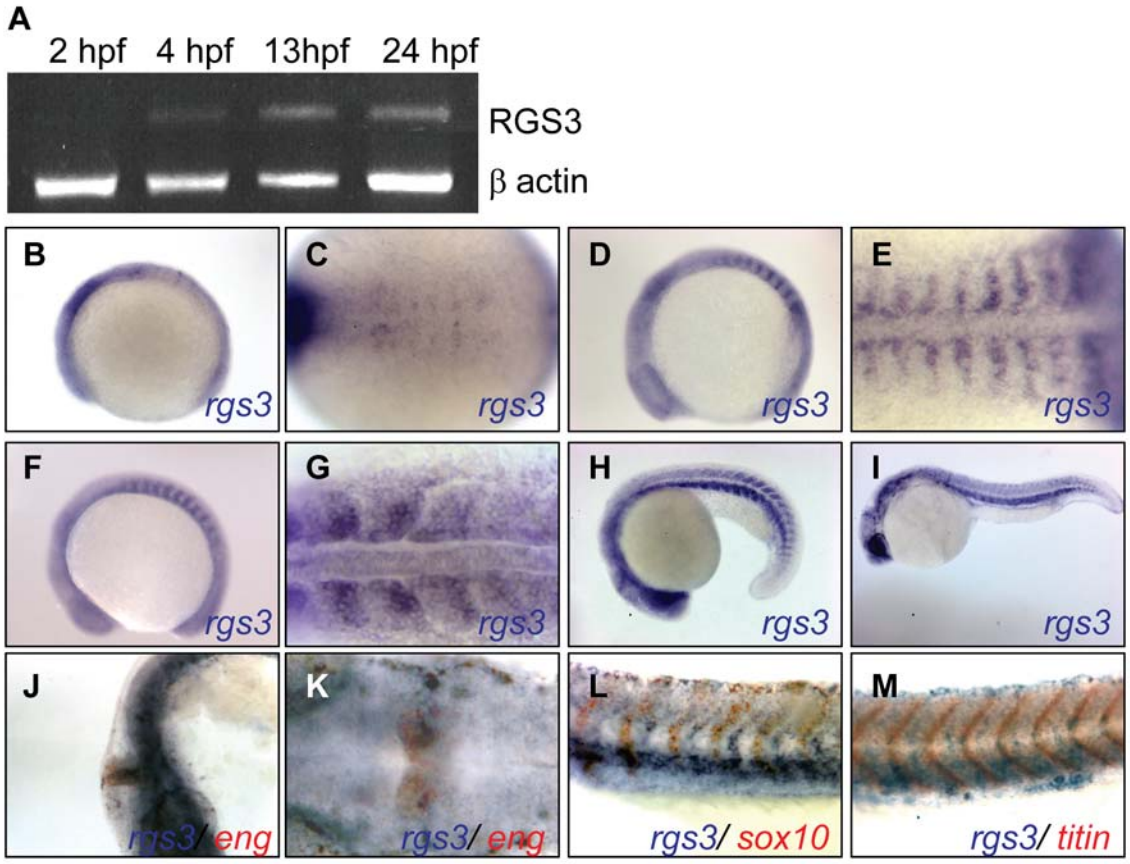

Figure 24: Temporal and Spatial Expression of *rgs3* Throughout Zebrafish Development. (A) RT-PCR was used to determine the temporal expression of *rgs3* from 2 hpf to 24 hpf. Whole Mount *In Situ* Hybridization was utilized to determine the spatial expression of (B-I) *rgs3* in (B-C) 10hpf, (D-E) 12 hpf, (F-G) 14 hpf, (H) 18 hpf, (I-L) 28hpf and (M) 30hpf wild type embryos. (B, D, F, H-J and L-M) Lateral and (C, E, G, and K) dorsal views illustrate that *rgs3* is expressed in the developing somites and posterior tail. (G) At 14 hpf *rgs3* expression is enriched in the posterior (caudal) portion of the developing somites. (J-M) Double label WMISH with *rgs3* (blue) and either *eng* (J-K), *sox10* (L) or *titin* (M) in red.

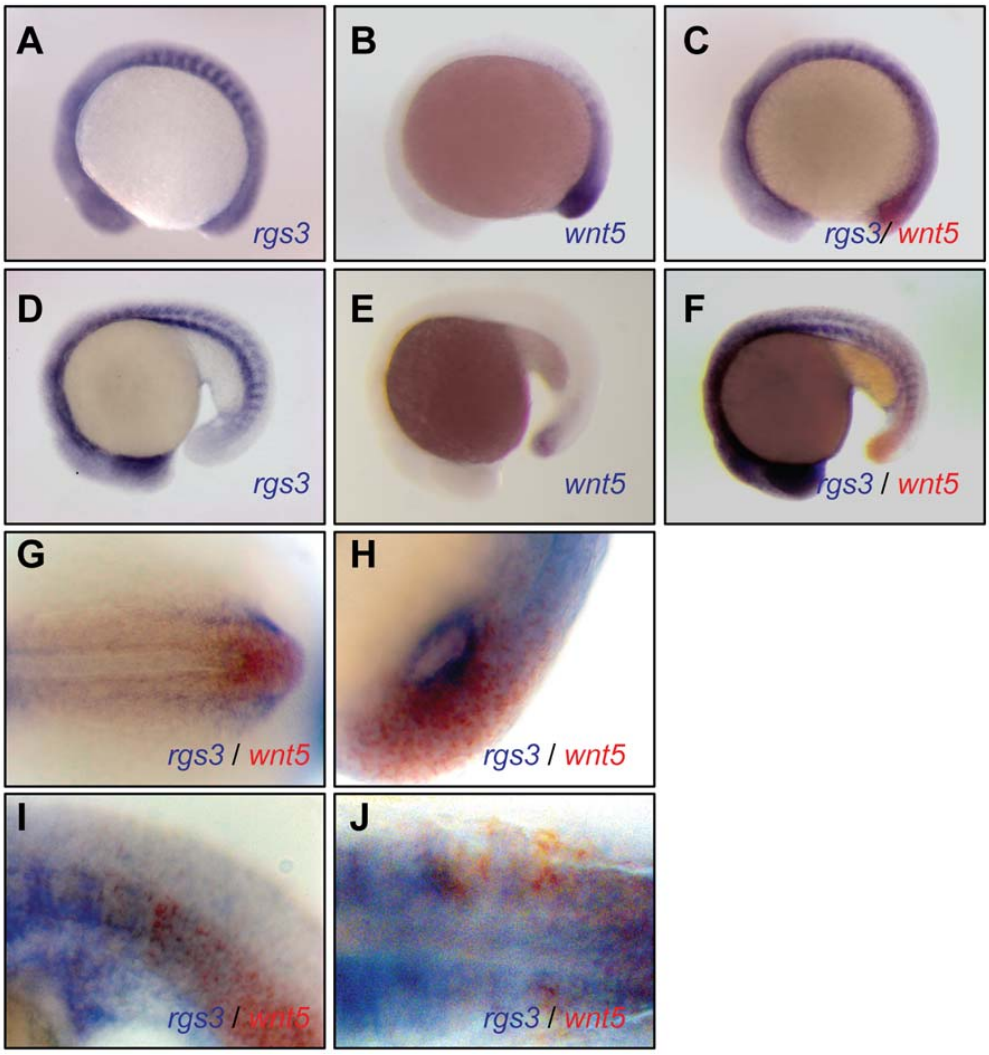

Figure 25: *rgs3* Expression is Adjacent and Overlapping with *wnt5*. Temporal and spatial expression of *rgs3* compared to *wnt5b* in zebrafish development. Whole Mount *In Situ* Hybridization was utilized to compare the spatial expression of (B and E) *wnt5b* to (A and D) *rgs3*. WMISH of (A-C and G-H) 14hpf and (D-F and I-J) 17hpf wild-type zebrafish embryos. (A-F, H and I) Lateral and (G and J) dorsal views. (C, F and G-J) Double label WMISH with *wnt5b* (red) and *rgs3* (blue) (C, F and G-J), shows adjacent and overlapping expression domains around Kupffer's vesicle and in the tailbud and somites.

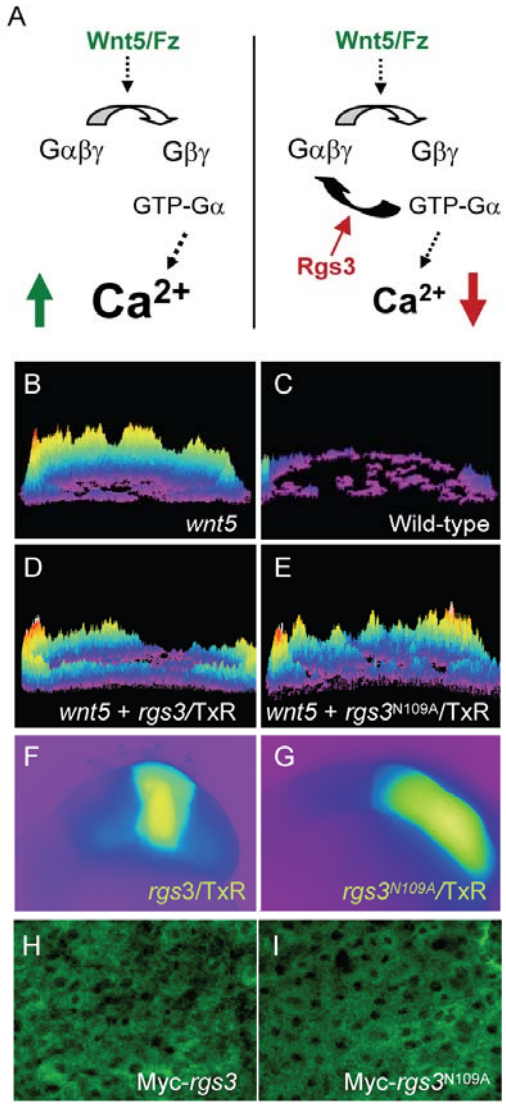

Figure 26: *rgs3* Inhibits *wnt5*b Induced Ca^{2+} Dynamics. (A left side) Schematic representation illustrating that *wnt5*b overexpression results in intracellular calcium release in a G protein dependent manner and (A right side) the predicted negative effect overexpression of Rgs3 will have on the Wnt/Ca^{2+} pathway. (B-E) Representative Ca^{2+} release profiles (composite image) of (B and D-E) *wnt5*-overexpressing and (C) wild-type blastula stage zebrafish embryos. Panels B-E are composites of fura-2 ratiometric imaging time course showing total calcium release activity as peaks and colors mapped topographically. (C) Wt Ca^{2+} release profile. (B-E) *wnt5b* expressing embryo with localized (D) TxR/*rgs3* or (E) Txr/$rgs3^{N109A}$. Corresponding fluorescent images illustrate the location of (F) TxR/*rgs3* and (G) TxR/$rgs3^{N109A}$. Immunohistochemistry of (H) myc-rgs3 and (I) myc-$rgs3^{N109A}$ embryos at 80% epiboly indicate that both proteins are stable.

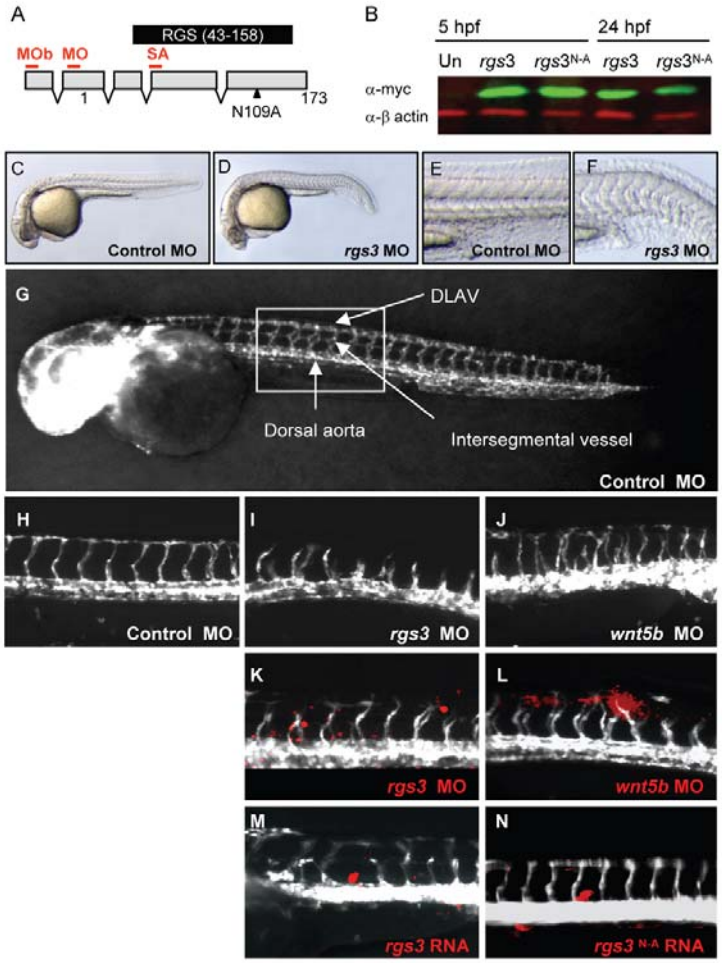

Figure 27: Rgs3 Knockdown is Reminiscent of Altered Wnt Signaling. (A) Schematic of zebrafish rgs3 mRNA/protein composite. Numbers refer to the amino acid number of the encoded Rgs3 protein, while the locations of morpholino binding sites employed in later experiments are indicated by red lines above the transcript. MO = rgs3 MO, MOb = rgs3 MOb and SA = rgs3 MOsa. The RGS domain of Rgs3, amino acids 43-158, is highlighted by the black box. (B) Western analysis demonstrates that myc-tagged rgs3 and rgs3^{N109A} proteins are detectable from 5 hpf to 24 hpf . (C-F) Antisense morpholino-mediated gene knockdown of rgs3 results in embryonic defects. Lateral views of 28 hpf (C-E) wild-type and (D and F) *rgs3* MO injected embryos illustrate that rgs3 morphants have (D) a reduced body length and (F) altered somite formation. *rgs3* and *wnt5b* morphant embryos display cardiovascular defects. (A-H) Fluorescence images of 48 hpf Tg(Fli1:EGFP) embryos. Embryos injected with (G and H) Control MO, (I) *rgs3* MO and (J) *wnt5*b MO. Control injected embryo with mosaic (K) rgs3 morphant, (L) wnt5 morphant, (M) rgs3 overexpressing or (N) rgs3^{N-A} overexpressing cell transplants in red. Box in panel G indicates region magnified in panels H-N.

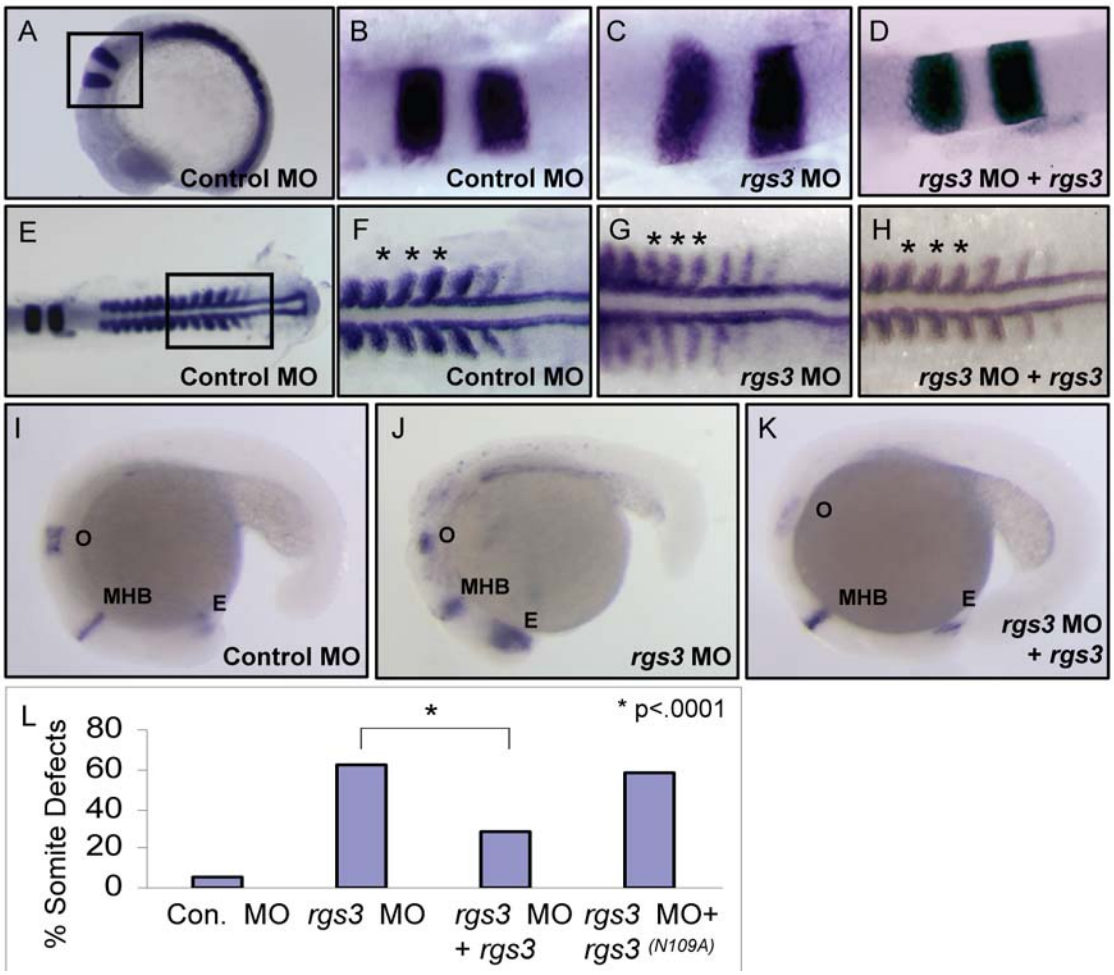

Figure 28: *rgs3* Morphant Phenotypes and Functional Rescue. *rgs3* was co-injected with *rgs3* MO to monitor rescue of gene knockdown. (A-K) The molecular markers *krox20*, *myoD* and *pax2* were used to evaluate rgs3 morphant rescue. *kro*x 20 labels rhombomeres 3 and 5, *myoD* labels the developing somites and adaxial cells while, *pax2* labels the otic vesicle (o), midbrain-hindbrain boundary (MHB) and eye (E). (A and I-K) Lateral and (B-H) dorsal views, anterior to the right, of (A-H) 15 hpf and (I-K) 20 hpf wild-type embryos injected with (A, B, E, F and I) Control MO, (C, G and J) *rgs3* MO and (D, H and K) *rgs3* MO + *rgs*3. Boxed regions in A and E represent the areas magnified in B-D and F-H respectively. (F-H) Asterisks indicate the spacing and width of three representative somites. (D, H and K) *krox20*, *myoD* and *pax2* expression patterns indicate that *rgs3* is able to suppress the morpholino-induced defect. For structural functional analyses, $rgs3^{N109A}$ was evaluated for rescue of knockdown. Morphological analyses reveals that (L) *rgs3* is able to suppress the MO induced defect while, (L) $rgs3^{N109A}$ is unable to suppress the MO induced defect.

	Morphological Analysis			MyoD/Krox20 WMISH		
	n	% WT-like	% Somite defects	n	% WT-like	% Expanded somites
Wild Type	175	100	0	75	100	0
Control MO	140	100	0	43	100	0
***rgs3* MO**	340	38	62	50	41	59
rgs3* MO + *rgs3	152	71	29	35	72	28
***rgs3* MO + *rgs3*$^{N-A}$**	207	42	58	40	42	58

Table 2: Morphological (48hpf) and Molecular (15hpf) Analysis of rgs3 Knockdown and Rescue.

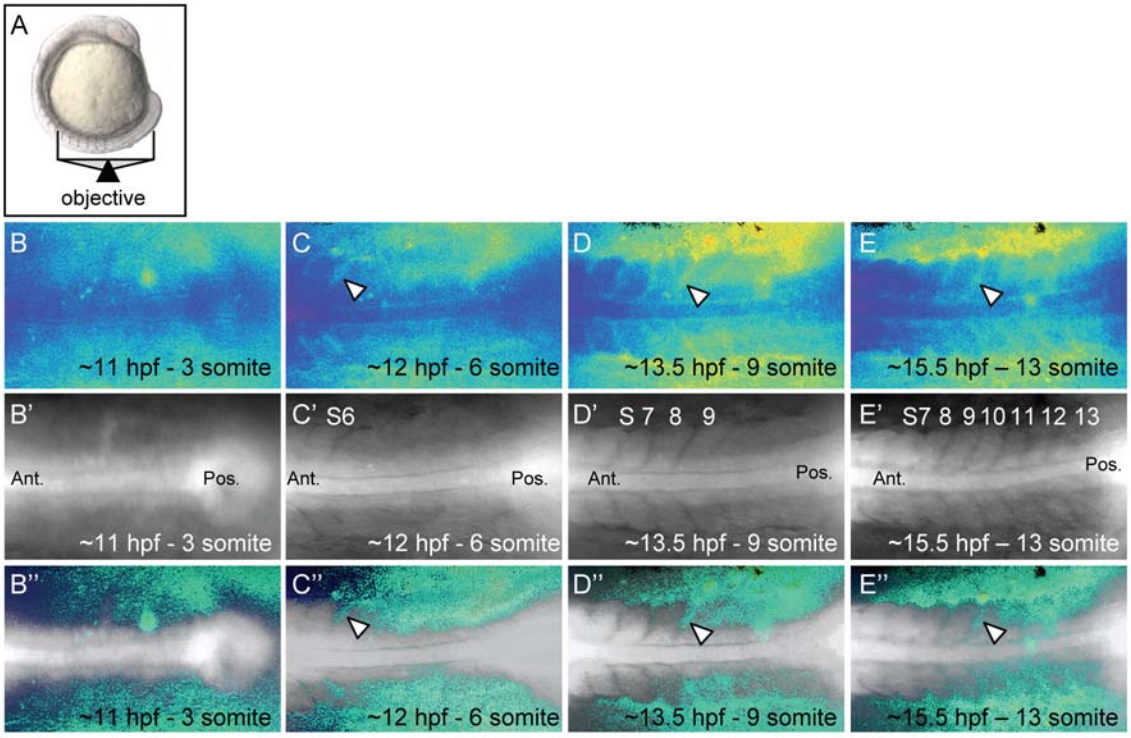

Figure 29: Calcium Dynamics During Zebrafish Somitogenesis. (A) Illustration of the position of a 10 somite stage (14 hpf) zebrafish embryo relative to the objective during calcium imaging. (B-E) Representative ratio images, pseudocolored with low ratio (low calcium) represented by blue and high ratio (high calcium) represented by yellow/red, of (B) 3, (C) 6, (D) 9 and (E) 13 somite stage embryos. (B'-E') Grayscale fluorescence images highlighting the morphology of the forming somites and notochord. (B''-E'') Overlay of grayscale and ratio images illustrate the regions of calcium release activity relative to morphology. Arrowheads indicate areas of sustained Calcium activity between forming somites. Ant. is Anterior, Pos. is Posterior and S is somite number.

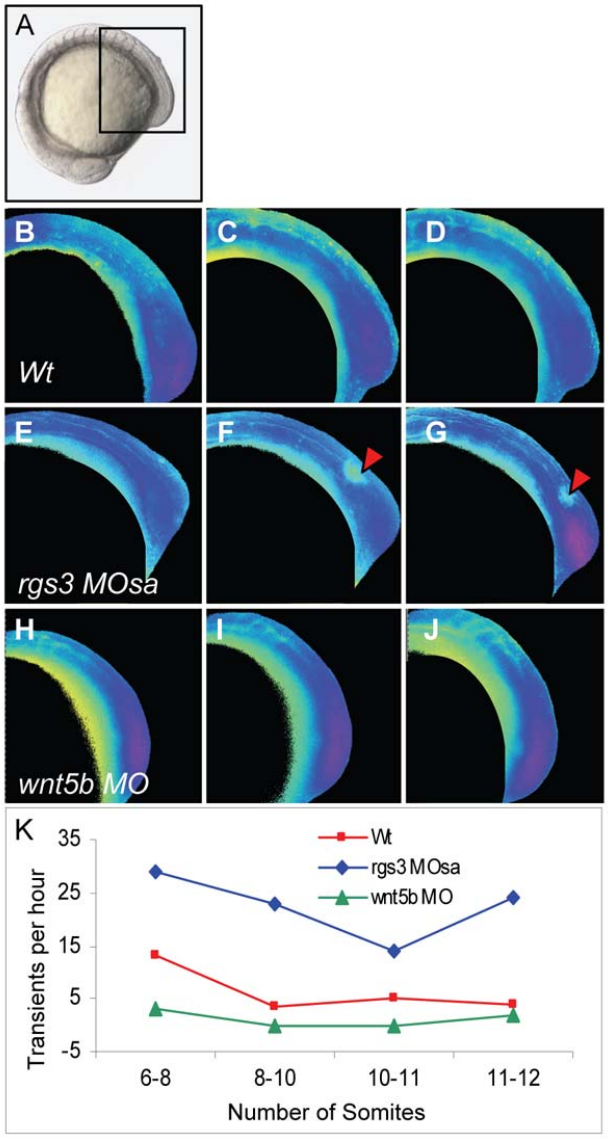

Figure 30: rgs3 Impacts Segmentation Stage Calcium Dynamics. (A) Zebrafish embryos injected with Fura-2 oriented in a lateral posterior view with a focus on the developing somites and tail (boxed region). (B-J) Ratio images, pseudocolored to represent low Ca^{2+} as blue and high Ca^{2+} as yellow/red. (B-J) Representative ratio images of (B, E and H) 6 somite stage, (C, F, and I) 8 somite stage and (D, G and J) 10 somite stage embryos. (E-G) Arrowheads indicate large Ca^{2+} transients in rgs3 morphant embryos that are not observed in (B-D) Wt or (H-J) *wnt5b* morphant embryos. (K) The number of Ca^{2+} transients per hour observed, in embryos oriented in a lateral posterior view from 6 to 12 somite stage, is represented graphically as a function of developmental age.

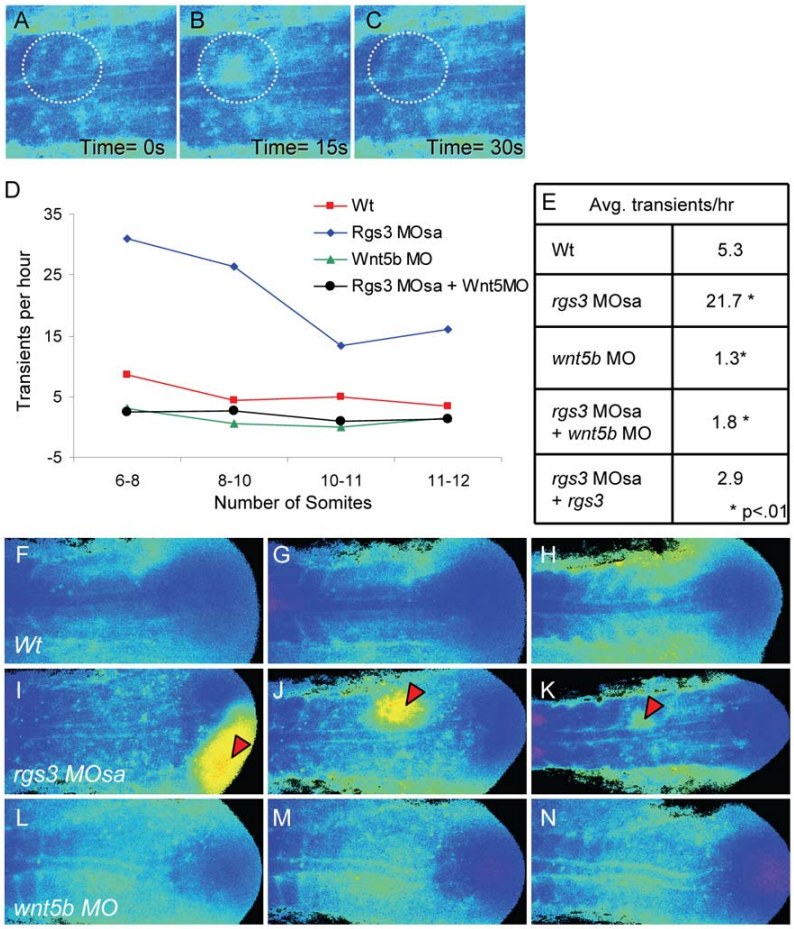

Figure 31: *rgs3* Functions Downstream of *wnt5* to Impact Segmentation Stage Calcium Dynamics. Zebrafish embryos injected with Fura-2 were oriented in a dorsal posterior view. (A-C and F-N) Representative ratio images, pseudocolored with low Ca^{2+} represented by blue, and high Ca^{2+} represented by yellow/red. During somitogenesis, Ca^{2+} transients are identified as a local short-lived increase in intracellular Ca^{2+} levels. (A-C) A region of interest (ROI) is noted by a dashed circle highlighting a representative Ca^{2+} transient. In the ROI from time 0s to time 15s, (B) an increase in Ca^{2+} levels is observed that (C) subsides by time 30s. (D) Graphical representation of the number of transients as a function of developmental age. (E) Table depicting the average number of Ca^{2+} transients per hour from 6 to 12 somite stage for each treatment. Representative ratio images of (F) 5 somite stage, (G) 7 somite stage and (H) 10 somite stage wt embryos taken from Movie S1. Representative ratio images of (I) 5 somite, (J) 7 somite and (K) 10 somite stage rgs3 MOsa injected embryo taken from Movie S2. Representative ratio images of (L) 5 somite, (M) 7 somite stage and (N) 10 somite stage wnt5b MO injected embryo taken from Movie S4. (I-K) Red arrowheads indicate large Ca^{2+} transients in *rgs3* morphant embryos that are not observed in (F-H) wt or (L-N) *wnt5b* morphant embryos.

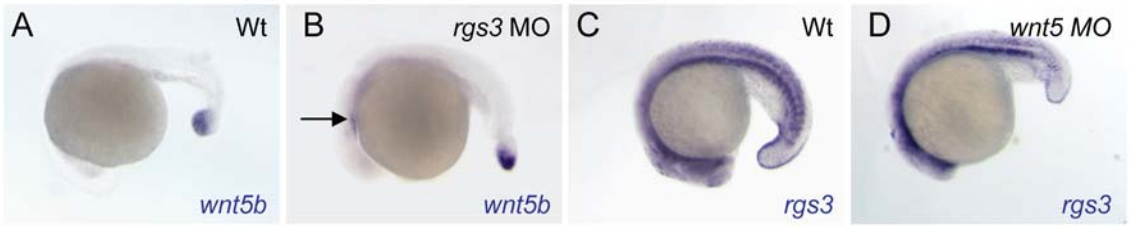

Figure 32: *rgs3* and wnt5 Expression in Morphant Embryos. Whole Mount *In Situ* Hybridization was utilized to determine the spatial expression of (A-B) *wnt5* and (C-D) *rgs3* in (A and C) Wt, (B) *rgs3* morphant and (D) *wnt5* morphant embryos. Lateral views illustrate that at 18 hpf, ectopic wnt5b expression is observed in the anterior region (arrow) of (B) Rgs3 morphants while rgs3 is unchanged in (D) Wnt5b morphant embryos.

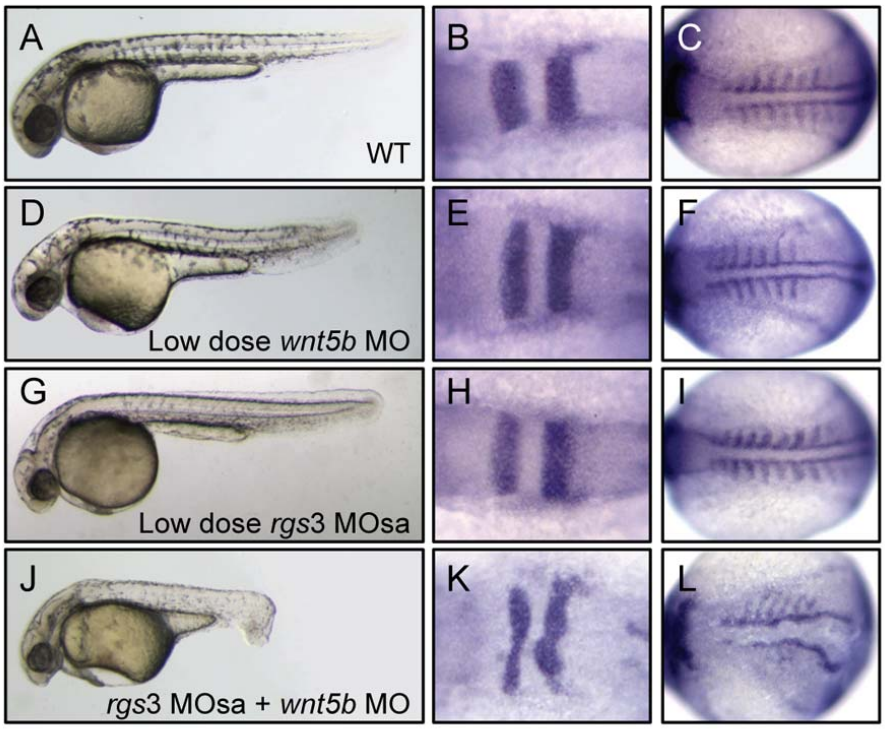

M	n	Mild defect (%)	Severe defect (%)
Wild Type	86	0	0
Control MO	113	0	0
wnt5b MO	119	45	0
rgs3 MOsa	141	5	0
rgs3 MOsa + *wnt5b* MO	155	0	92

Figure 33: *rgs3* Interacts with the Wnt Signaling Network. Low doses of *rgs3* and *wnt5b* MOs were used to test genetic interaction. Phenotypes were characterized by (A, D, G, J and M) morphology and the molecular markers (B, E, H and K) *krox20* and (C, F, I and L) *myoD*. Lateral images of 34 hpf (A) wt, low dose (D) *wnt5b* MO, (G) low dose *rgs3* MOsa, and (J) *wnt5b* MO + *rgs3* MO injected embryos. Dorsal images of 13hpf (B-C) Wt, (E-F) low dose *wnt5b* MO, (H-I) low dose *rgs3* MOsa, and (K-L) *wnt5b* MO + *rgs3* MO injected embryos. (M) Low dose *wnt5b* MO + *rgs3*MOsa resulted in a 92% penetrance of severe defects which were not observed with low dose *wnt5b* MO or low dose *rgs3*MOsa alone.

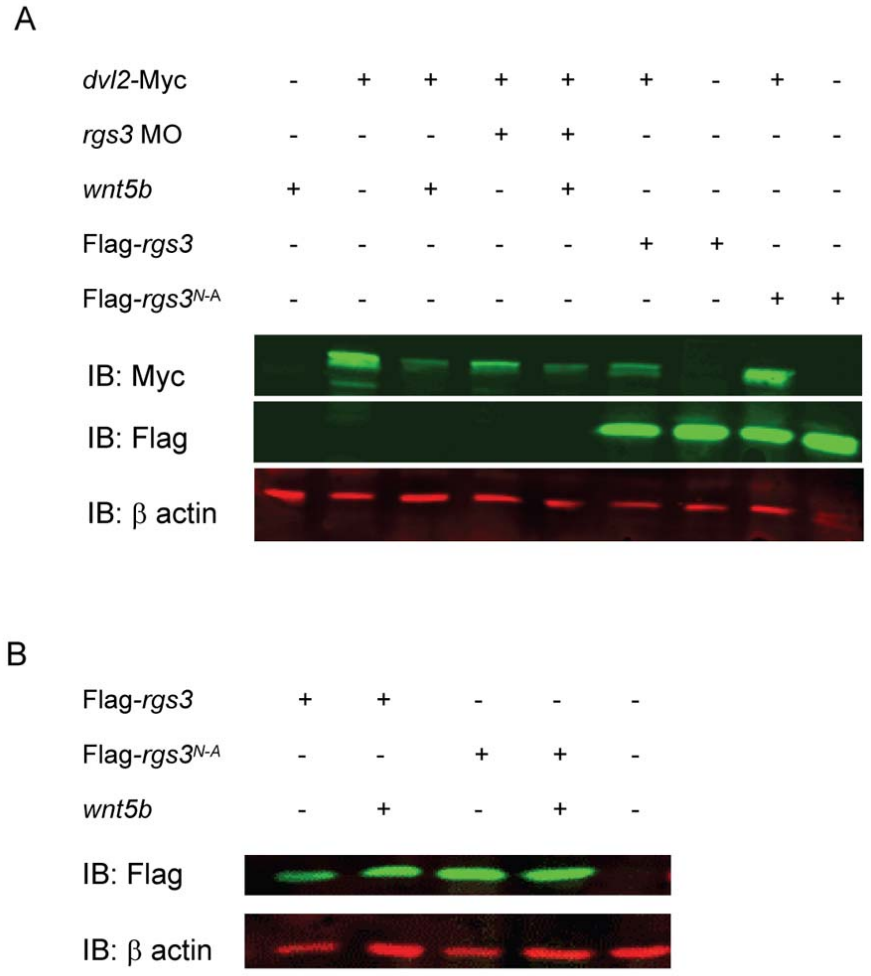

Figure 34: Flag-*rgs3* Results in Decreased Dvl2-Myc expression. (A) Western analysis of 24 hpf embryos demonstrates that Dvl2-Myc levels are reduced by *wnt5b* overexpression, *rgs3* knockdown, *rgs3* overexpression but remain unchanged with rgs3^{N-A} overexpression. (B) *wnt5b* overexpression has no impact on Flag-*rgs3* or Flag-*rgs3*$^{N-A}$.

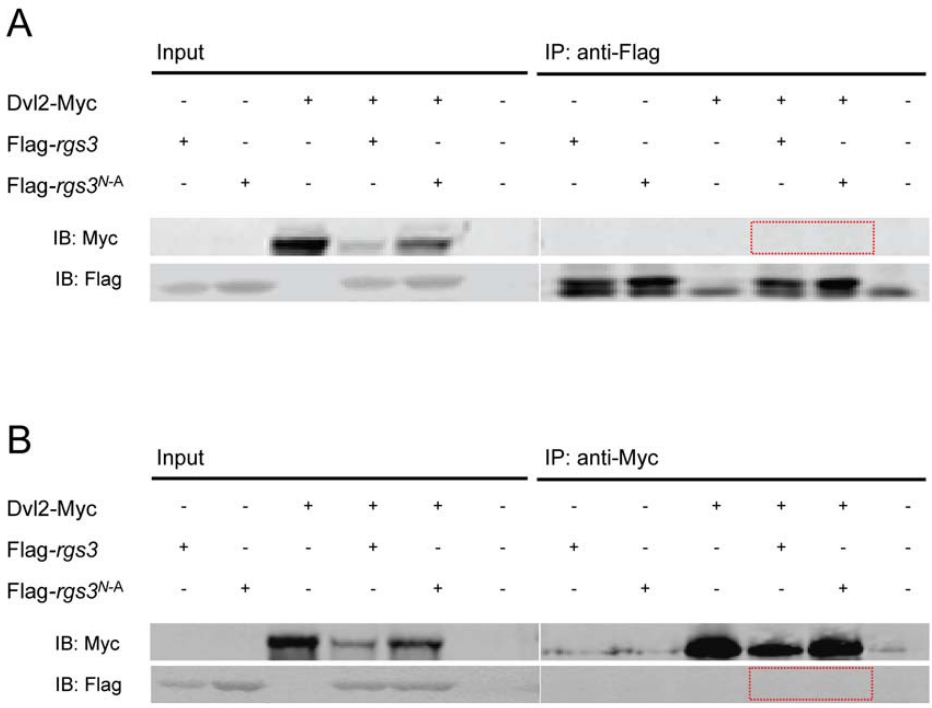

Figure 35: *rgs3* Does Not Directly Bind to Dvl2-Myc. (A-B) Co-IP and western analysis of 24 hpf embryos demonstrates that Flag-rgs3 does not bind Dvl2-Myc. (A) Anti-Flag immunoprecipitates and (B) Anti-Myc immunoprecipitates blotted with anti-Myc and anti-Flag. Red box in A indicates that neither Flag-rgs3 or Flag–rgs3^{N-A} pulled down Dvl2-Myc. Red box in B indicates that Dvl2-Myc did not pull down either Flag-rgs3 and Flag–rgs3^{N-A}.

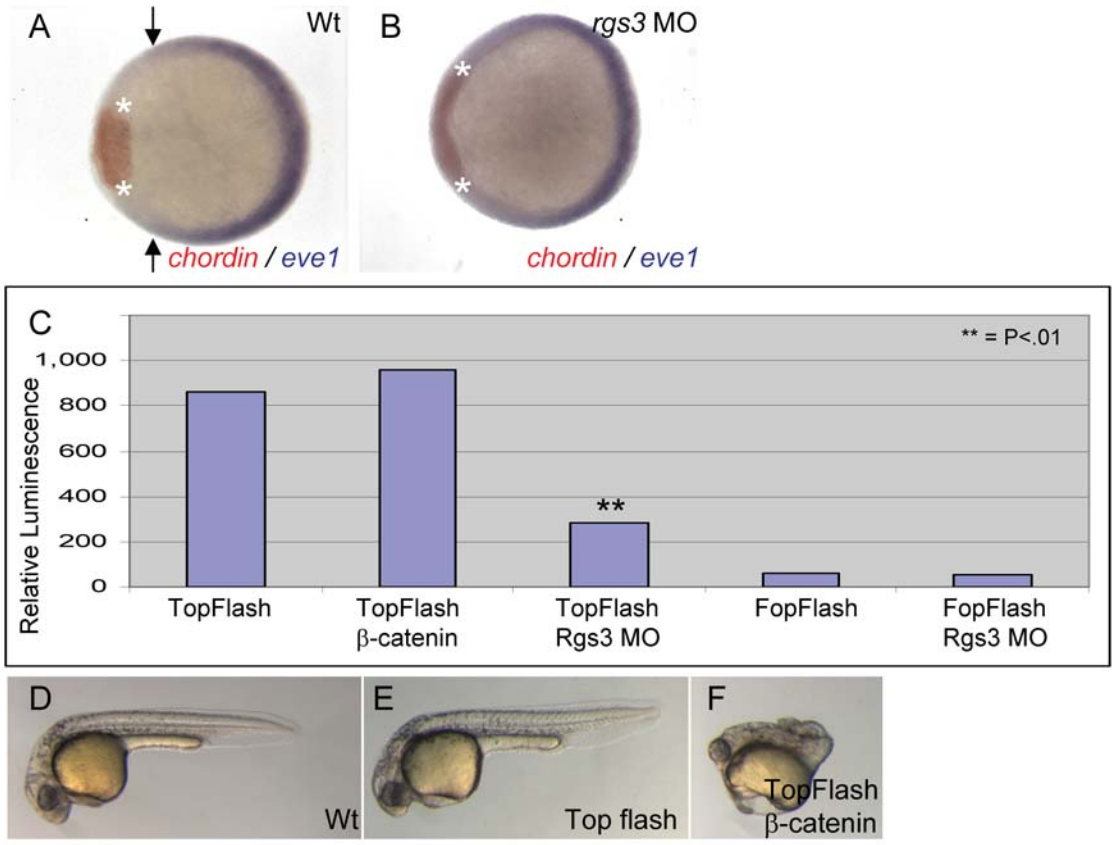

Figure 36: *rgs3* Knockdown Influences Wnt/β-catenin Signaling. (A-B) WMISH was utilized to compare the dorsal-specific chordin (red) expression domain denoted by asterisks flanked by the ventral-specific eve (blue) expression domain denoted by arrows. Expansion of both the dorsal domain as well as the ventral domain is observed in (B) *rgs3* morphant embryos when compaired to (A) wild-type. (C) TopFlash and FopFlash luciferase reporter constructs analyzed for relative luminescence in β-catenin overexpressing and Rgs3 morphant embryos. Lateral images of live 48hpf (D) Wt and (E) TopFlash, (F) TopFlash plus β-catenin.

CHAPTER 5

IDENTIFICATION OF RGS3B IN ZEBRAFISH

Introduction

To investigate potential roles of RGS proteins I identified RGS genes that are expressed in the embryo, and utilized gene knockdown in zebrafish to evaluate their necessary function. In chapter 4, I described results that show that Rgs3 activity is sufficient to modulate Wnt5b induced Ca^{2+} release, and this ability requires a key amino acid in the RGS domain which is required for GAP activity. Moreover, Rgs3 demonstrates a genetic interaction with Wnt5b supporting the conclusion that Wnt/Ca^{2+} signaling activity is an *in vivo* target of Rgs3 in somite development. Consistent with the known role of G proteins in the activation of Wnt signal transduction pathways, I hypothesize that other RGS genes may have a role in modulating Wnt/Ca^{2+} signaling in different tissues or different stages. This chapter describes the unique function of a related family member Rgs3b which contains a Ca^{2+} binding EF-hand domain and an N-terminal PDZ domain implicated in protein-protein interactions. To date, I have cloned and characterized the expression pattern of Rgs3b. The expression pattern suggests that Rgs3 and Rgs3b may have different functions in vivo however, the function of Rgs3b in zebrafish is not known.

EF hand Motif

Since the identification of EF hand motifs in 1973, EF hands have been identified in more than 50% of characterized Ca^{2+} binding proteins. EF hands are characterized by the presence of a twelve residue loop which is flanked by two twelve-residue alpha-helical domains (Kawasaki, Nakayama et al. 1998). Within the conserved loop region, residues 1, 3, 5, 7, 9, and 12 provide oxygen ligands to the Ca^{2+} ion, which are essential for binding. Proteins containing EF hands have been shown to function as either regulatory proteins or as structural proteins. In the presence of Ca^{2+}, regulatory EF hand

containing proteins undergo a conformational change which allows them to influence downstream targets, while structural EF hand containing proteins function by buffering intracellular Ca^{2+} (Levine, Dalgarno et al. 1983; Schroder, Schlumbohm et al. 1996).

Additional 5' exons in RGS3 splice variants have been shown to include an EF-hand domain as well as a PDZ domain (Druey, Blumer et al. 1996; Kehrl, Srikumar et al. 2002; Tosetti, Pathak et al. 2003). Among the structures reported to date, a majority of EF-hand motifs have been show to occur in pairs; however, RGS3 only contains one EF hand motif. Even though only a single EF hand motif is present, Tosetti and colleagues have demonstrated, by a gel shift assay, that the splice form of RGS3 containing the EF hand motif is able to bind Ca^{2+} while the isoform without the EF hand motif is unable to bind Ca^{2+} (Tosetti, Pathak et al. 2003). Due to its potential to bind Ca^{2+}, the Rgs3 splice variant containing an EF hand was of interest for my thesis.

Identification of Rgs3 splice variants

All identified forms of RGS3 contain the conserved RGS domain; however, longer forms have been identified in humans (Kehrl, Srikumar et al. 2002). Longer forms of RGS3 contain extra 5' exons, which encode additional protein domains such as an EF-hand motif and a PDZ domain have been identified in human, mouse and chick. RGS3 containing a PDZ domain has been shown to mediate a Ca^{2+}-dependent termination of G protein signaling in sensory neurons (Tosetti 2003) while RGS3 containing a PDZ domain is expressed in the human atria (Cho et al., 2003). Interactions between the PDZ domain of RGS3 with the Eph-B/ephrin-B system of tyrosine kinase receptors strongly implicates PDZ-RGS3 in ephrin signaling leading to blood-vessel sprouting and remodeling during vascular development (Lu et al., 2004; Lu et al., 2001).

In order to determine if a splice variant of Rgs3 containing a PDZ domain or an EF hand motif exists in zebrafish, I used the 5' RACE-PCR technique (Frohman 1993) to amplify Rgs3 cDNAs using nested primers targeted to the 5' end of the RGS domain.

I have used this approach to obtain six Rgs3 cDNAs. Unfortunately, none of the identified transcripts had any protein domains in addition to the RGS domain. After extensive 5' RACE, I was unable to identify an Rgs3 transcript encoding either an EF hand motif or a PDZ domain.

Gene duplicates

The fact that additional 5' exons in RGS3 splice variants have been shown to include an EF-hand domain as well as a PDZ domain (Druey, Blumer et al. 1996; Kehrl, Srikumar et al. 2002; Tosetti, Pathak et al. 2003) led me to investigate the possibility that a paralogue to Rgs3 exists in zebrafish.

During the evolution of vertebrates there have been multiple gene duplication events, including a very early duplication event, before the divergence of ray-finned fishes and tetrapods 420 million years ago, as well as a duplication event over 300 million years ago in the ray-finned fish lineage leading to zebrafish (Christoffels, Koh et al. 2004; Vandepoele, De Vos et al. 2004; Christoffels, Brenner et al. 2006). Whole genome duplications as well as individual gene duplication events have resulted in the existence of gene duplicates. The classical model for the evolution of gene duplicates predicts that for duplicate genes, one gene copy protects the other from natural selection allowing degenerative mutations to occur. Accumulation of mutations can then lead to two possible outcomes for duplicate genes. The first, most probable, possibility is that the accumulation of degenerative mutations in duplicated genes will result in gene silencing (nonfunctionalization). The second outcome, which is predicted to be very rare, is that mutations will result in the gene acquiring a new function (neofunctionalization) (Ohno, Wolf et al. 1968). Contrary to the predictions of the classical model, a substantial number of duplicated genes (20-50%) have been preserved throughout evolution (Lynch, O'Hely et al. 2001).

Interestingly, many preserved gene duplicates, such as the engrailed and Notch genes in zebrafish, have distinct expression patterns despite the fact that their coding sequences have been highly conserved. This reveals the possibility that one mode in preserving gene duplicates may involve the partitioning of their original expression patterns. To investigate the preservation of gene duplicates, as well as the evolution of gene expression patterns, researchers have proposed the duplication/degeneration/ complementation (DDC) model. In addition to the possibilities outlined in the classical model, nonfunctionalization and neofunctionalization, the DDC model includes an additional fate of duplicate genes based on subfunctionalization (Lynch, O'Hely et al. 2001).

Subfunctionalization is defined as "the fixation of complementary loss-of-function alleles that results in the preservation of duplicate loci" (Lynch and Force 2000). Subfunctionalization is possible when a gene has multiple distinct cis-regulatory regions. It is expected that as the number of mutatable subfunctions increases, gene preservation will also increase. Subfunctionalization is expected to be a mechanism for the preservation of duplicate genes when both the effective population size and the coding null mutation rate are low enough that new loss-of-function mutations arise less often than every five generations. These conditions, which are not uncommon for vertebrates, allow random genetic drift to drive changes in gene frequencies. Thus, subfunctionalization can be described as a neutral process. On the other hand, subfunctionalization is not likely to occur when selection is the driving force, as in populations with very large effective population sizes (Lynch and Force 2000). In this case the classical model for the evolution of gene duplicates is likely to occur.

Through subfunctionalization, the DDC model suggests that degenerative mutations lead to gene preservation allowing duplicated genes to be maintained by natural selection (Stoltzfus 1999). This leads to duplicate genes having distinct developmental functions although protein function is conserved.

In order to investigate subfunctionalization, researchers have focused on gene duplicates that currently exist in genomes. Experiments analyzing engrailed genes in zebrafish (Gardner and Barald 1992), cellular retinoid-binding genes in zebrafish (Liu, Sun et al. 2005; Sharma, Saxena et al. 2005) , ZAG1 and ZMM2 in maize (Gardner and Barald 1992), as well as Hoxa 1 and Hoxb1 in mouse (Krumlauf 1994; Vesque, Maconochie et al. 1996) provide data consistent with the DDC model. Lynch and colleagues provide further statistical evidence indicating that with "reasonable parameters" the DDC model can account for a significant number of preserved duplicate genes (Lynch, O'Hely et al. 2001).

Identification of Rgs3b

To date, evidence supports the hypothesis that subfunctionalization has played a key role in evolution. In order to determine if a gene duplicate of Rgs3 exists in zebrafish, I performed a blast analysis of the coding sequence of Rgs3 to identify a predicted paralogue in the zebrafish genome. Here, I report the identification and characterization of Rgs3b, a paralogue to Rgs3, in zebrafish. Rgs3b contains a putative Ca^{2+} binding EF-hand motif, as well as a PDZ domain.

Using the sequence for the predicted paralogue I designed gene specific primers, generated embryonic RACE ready cDNA pools and performed 5' RACE analysis (Frohman 1993). I was able to amplify the predicted paralogue and confirm that the RGS domain it is 78% identical to Rgs3. Due to the fact that the RGS domain of Rgs3 has an 83% identity to human RGS3 and the identified paralogue only has a 75% identity to human RGS3, the latter will be referred to as Rgs3b (Figure 37A-B).

I was able to identify three splice variants of Rgs3b (Rgs3b-1, Rgs3b-2 and Rgs3b-3). All identified transcripts include an RGS domain and a Ca^{2+} binding EF-hand domain, one transcript (Rgs3b-3) includes an N-terminal PDZ domain implicated in protein-protein interactions (Figure 38A).

In order to determine the temporal expression pattern of each transcript, I designed primer pairs that are specific for Rgs3b-1 and Rgs3b-3. Unfortunately, I was unable to design a primer set that was specific to Rgs3b-2, however I was able to design a primer set that recognized both Rgs3b-2 and Rgs3b-3 allowing me to deduce the expression of Rgs3b-2. I found that Rgs3b-1 expression begins after 17hpf, Rgs3b-2 is expressed maternally and throughout early development while Rgs3b-3 is expressed during early somite stages as well as at 36hpf (Figure 38B).

To further analyze Rgs3b expression I performed whole-mount *in situ* hybridization using an antisense probe that recognizes all three transcripts of Rgs3b (Figure 38C-L). Rgs3b displays dynamic expression patterns during somite stages. From 10-12hpf, Rgs3b is enriched in the developing midbrain and hindbrain (Figure 38C-D and H-I). At 10 somite stage, Rgs3b expression is strongest in the forebrain as well as in regions of the hindbrain (Figure 38E and J). After 18hpf, Rgs3b expression is strongest around the eyes and in the hindbrain (Figure 38 F-G and K-L). Of interest is the fact that while Rgs3b is enriched in brain during somite stages, Rgs3 is enriched in the posterior tail and developing somites (Figure 38M-N). Comparative analysis, by whole-mount in situ hybridization in zebrafish, has revealed that zebrafish paralogs have distinct mRNA expression patterns which when combined mimics the ubiquitous expression of its mammalian ortholog. These complementary expression patterns indicate that subfunctionalization may have occurred. Due to the fact that Rgs3b-2 is maternally expressed I chose to investigate the endogenous requirement of Rgs3b-2

Endogenous requirement of Rgs3b-2

To investigate necessary roles of Rgs3b in vertebrate development, I utilized gene knockdown. I designed a MO to target the initiator methionine (Met) of Rgs3b-2 (Figure 39A). Control-injected embryos at 28hpf are fully extended with a characteristic anterior-posterior (A-P) length (Figure 39B). In contrast, *rgs3b-2* MO-injected embryos

have shorter A-P extension and smaller heads and eyes (Figure 39H). In order to investigate brain defects at an earlier stage the molecular markers *dlx2*, *krox20* and *pax2* were used to identify developing brain structures. *dlx2* expression is observed in the anterior forebrain neuromere (telencephalon), the posterior forebrain neuromere (diencephalon), the hypothalamus as well as in brachial arches (Figure39 D-E) while, *pax2* expression is observed in the optic stalk and midbrain hindbrain boundary and *krox20* is expressed in rhombomere 3 and 5 in the hindbrain (Figure 39 F-G). When compared to control injected embryos (Figure 39B-G), *rgs3b-2* morphants have reduced forebrain structures such as the telencephalon and diencephalon and optic stalk (Figure 39J-M). More posterior structures such as the mandubular arch, hyoid arch and brachial arches, rhombomeres as well as overall patterning of the brain does not appear to be altered in morphants (Figure 39K-M). To further characterize eye/forebrain defects the transgenic ath5:GFP embryos were used to highlight eye morphology and retino-tectal patterning (Figure 40 E-F). Although overall eye size was reduced in *rgs3b-2* morphants retino-tectal patterning appeared Wt-like (Figure 40G) and a distinct optic chiasm was formed (Figure 40H) indicating that overall brain patterning was normal in rgs3b-2 morphants.

The specificity of the *rgs3*b knockdown as well as structural functional analyses was determined by RNA co-injection experiments. Exogenous Rgs3b-1 was co-injected with Rgs3b-2 met MO to overcome the effects of MO-induced knockdown. Rgs3b-1 RNA is MO-resistant because it does not contain the same initiator methionine as RGS3b-2 (Figure 39A). Like Rgs3b-2, Rgs3b-1 contains both an EF hand motif as well as an RGS domain. Injection of control MO resulted in negligible defects (Figure 39B-G) compared to *rgs3b* MO which induced eye and forebrain defects (Figure 39H-M). Co-injection of *rgs3b-2* MO with *rgs*3b-1 RNA suppressed the MO-induced defects evaluated by both morphology as well as molecular analysis (Figure 39 N-S and Figure 40A).

I next investigated if rgs3b-1 required a functional RGS domain in order to suppress the Rgs3b-2 morphant phenotype. A conserved asparagine within the RGS domain of RGS proteins is necessary for GAP activity on Gα subunits (Tesmer, Berman et al. 1997; Natochin, McEntaffer et al. 1998; Srinivasa, Watson et al. 1998). To elucidate the role of the GAP function of Rgs3, I created a N to A mutation in zebrafish *rgs3b-1* (*rgs*3b-$1^{N\text{-}A}$)(Figure 39A). *rgs*3b-$1^{N\text{-}A}$ mutant RNA does not suppress the MO-induced defect (Figure 39T-Y and Figure 40A). To rule out the possibility that lack of suppression by *rgs3b-1*$^{N\text{-}A}$ was due to differences in its expression or localization compared to *rgs3b-1*, I generated and expressed N-terminal myc-tagged *rgs*3b-1 and *rgs*3b-$1^{N\text{-}A}$ constructs in embryos. Immunostaining for anti-myc in epiboly stage embryos also indicates that both proteins localize to the membrane and cytoplasm (Figure 40C-D). The fact that *rgs*3 results in a statistically significant suppression of the morphant phenotype (Figure 40A) while *rgs*3b-$1^{N\text{-}A}$ is not sufficient to rescue the morphant phenotype (Figure 40A) indicates that Rgs3b-2 GAP activity is required for its developmental functions.

Endogenous requirement of Rgs3b

To morefully elucidate the function of Rgs3b, I next designed an initiator Met MO to Rgs3b-3 and two splice blocking MOs which target all three transcripts (Figure 41A). Rgs3b-3 has two possible initiator methionines. Due to an alignment with human and mouse RGS3 (Figure 41B), I choose to design the MO to the first methionine. The SA MOs were designed to either drop out the Ca^{2+} binding EF hand motif in frame (772 sa MO) or to induce a stop codon at the beginning of the RGS domain (71 sa MO).

I found that Rgs3b knockdown results in varying penetrance of C-E defects (Figure 41C). In order to test the specificity of the *rgs3* knockdown, RT-PCR was used to identify aberrant gene products and RNA "rescue" experiments were performed. RT-PCR indicates that both 772 sa MO and 71 sa MO injections result in production of an

aberrant product through 24hpf (Figure 41C and D respectively). Sequence analysis of the aberrant products supports the conclusion that injection of the 772sa MO results in loss of the EF hand motif in frame while injection of the 71sa MO induces a stop codon at the beginning of the RGS domain.

Due to the fact that the 772sa MO had the largest penetrance of C-E defects, I performed RNA rescue experiments on 772sa MO injected embryos. Co-injection of myc-*rgs3b*-1, myc-*rgs3b-2* or myc-*rgs3b-3* with the 772sa MO is insufficient to suppress the MO-induced defect. Immunohistochemistry confirms that myc-*rgs3b*-1, myc-*rgs3b*-2 and myc-*rgs3b*-3 exogenous proteins are being produced (Figure 41F-I). I next examined if the aberrant product impacts development.

Rgs3b 772 sa MO results in the loss of the exon encoding the EF hand motif. Sequence analysis supports that there is not a frame shift and the aberrant Rgs3b-2 product contains an RGS domain and the aberrant Rgs3b-3 product contains a PDZ domain as well as an RGS domain (Figure 42A). I synthesized myc-*rgs3b-2* (ΔEF) as well as myc-*rgs3b-3* (ΔEF). Injection of myc-Rgs3b-2 (ΔEF) results in no obvious defects (Figure 42C) while, injection of myc-Rgs3b-3 (ΔEF) results in 79% penetrance of a dorsalized-like phenotype (Figure 42D). Immunostaining for anti-myc in epiboly stage embryos indicates that both proteins are synthesized and localize to the membrane and cytoplasm (Figure 42F-G). These data support that the EF hand motif in Rgs3b-3 may help to regulate its function.

In order further characterize Rgs3b gene knockdown I investigated C-E defects at an earlier developmental stage and characterized left/right patterning. Using the molecular markers *pax2* and *krox20* I find that Rgs3b knockdown results in 14-24% penetrance of C-E defects (Figure 43A) and 4-9% penetrance of left/right defects when examined with *lefty1/2* at 20hpf (Figure 43B). WMISH with *nkx* at 30 hpf was used to further characterize left/right defects by investigating heart jogging. In control injected embryos the heart jogs left 90% of the time while in Rgs3b morphant embryos heart

jogging is affected in 7-30% of the embryos (Figure 43C). The fact that the 772 sa results in a 69% penetrance of C-E defects at 30 hpf (Figure 41C) but only a 19% penetrance at 15 hpf (Figure 43A) is most likely the result of Rgs3b-3 (ΔEF). Due to the fact that *rgs3b-3* is not expressed until 12hpf the developmental defects from *rgs3b-3* (ΔEF) can not occur before 12hpf. Further characterization of Rgs3b knockdown is required to elucidate its function in development.

This preliminary analysis of rgs3b knockdown suggests that Rgs3 may function in the Wnt/Ca^{2+} pathway. I compared the expression patterns of *wnt*5 and *wnt*11 to *rgs*3b and find that like Wnt11; Rgs3b is enriched in the brain during somite stages. Wnt11 is enriched in the anterior and mutants show anterior extension and eye fusion defects, while Wnt5b is enriched in the posterior and mutants show altered cell movements during gastrulation (Sepich, Myers et al. 2000; Heisenberg and Solnica-Krezel 2008; Lin, Chen et al. 2009). The expression pattern of *rgs3b* as well as the smaller eyes observed with *rgs3b*-2 knockdown and the C-E defects observed with Rgs3b knockdown indicate that Rgs3b may function to regulate Wnt11 signaling in the forming brain. It is of interest to investigate Ca^{2+} dynamics in the developing forebrain of Rgs3b morphant embryos.

Discussion

In this chapter, I report the identification and characterization of Rgs3b, a paralogue to RGS3, in zebrafish. I have identified three *rgs3b* transcripts which all include an EF-hand like motif and one includes a PDZ domain. I find that *rgs3b* is expressed in the brain during somite stages and that knockdown of *rgs3b-2* results in reduced forebrain structures and small eyes. In contrast, *rgs3* is expressed in the somites and posterior tail during somite stages and knockdown of Rgs3 results in altered somite formation and C-E defects. Having already found a genetic interaction between *rgs3* and *wnt5b,* it is of interest to investigate a possible genetic interaction between Rgs3b and Wnt11.

Taken together these data support subfunctionalization of duplicated zebrafish Rgs3 genes. Clearly, the regulatory elements responsible for the expression pattern of Rgs3 and Rgs3b need to be identified and compared to the regulatory elements responsible for the expression pattern of their mammalian orthologs. After the identification of regulatory regions, it will be necessary to address the complexity of the regulatory regions. This requires the molecular characterization of the regulatory regions.

Materials and Methods

Zebrafish

Adults were maintained in a 14-hour light / 10-hour dark cycle at 28^{o}C. Embryos were collected from natural pairwise matings and staged by hpf at 28.5ºC and morphological criteria described in Kimmel et al. (Kimmel, Ballard et al. 1995; Westerfield 1995). Animal welfare assurance number: A3021-01

5’ rapid amplification of cDNA ends (RACE)

Total RNA from zebrafish was isolated using TRIzol (Invitrogen, Carlsbad, Calif.). For 5’ rapid amplification of cDNA ends (RACE) PCRs, cDNA was prepared by incorporating a SMART oligo (BD SMART RACE cDNA amplification Kit) at the 5’ end and using CDS III–modified oligo-dT, according to the instructions of the manufacturer. PCRs were performed with the following primer pairs: 5’ RACE, 5’-CTAATACGACTCACTATAGGGCAAGCAGTGGTATCAACGCAGAGT-3’

Rgs3b gene specific primer, 5’-ACTAAACCTGTGTCTCCAGCAATAC-3’. Gel-purified PCR bands were subjected to automated DNA sequencing.

Zebrafish rgs3b point mutant

*rgs*3b-1 was identified by 5’RACE. *rgs3b-1* was directionally cloned (5’-3’) into the pCS^{2+} or pCS^{2+} myc expression vector. The Quick Change II site-directed

mutagenesis kit (Stratagene) was used to generate an Asparagine (N) to Alanine (A) substitution within the RGS domain of Rgs3b-1. Synthetic RNA was then *in vitro* transcribed using SP6 RNA polymerase and the mMessage mMachine system (Ambion).

Micro-Injections

Antisense morpholino oligonucleotides (MO) were designed to target the 5'-UTR/ATG (*rgs3b-2 met* MO and *rgs3b-3 met* MO) to inhibit translation and an intron-exon junction in the EF hand motif (rgs3b 772sa MO) which drops out the EF hand motif in frame as well as to the RGS domain (*rgs3b* 71sa MO) which alters splicing and induces a premature stop. As a control *rgs3* MOmm (5 bp mismatch in lowercase letters) was designed (Gene-Tools):

rgs3b-2 met MO 5'-GACAACATCAGGACTCTCTCTGGGC-3',

rgs3b-3 met MO 5'-TGACAGACCGCTCTTTGAGTACATC-3',

rgs3b 772sa MO 5'-AGCATCTGTCAAGTGAAATCAACAG-3',

rgs3b 71sa MO 5'-TTGCCACAAACCTGTGAAAGATTTA-3'

rgs3 MOmm 5'-TCaCCcAGAAATCCtCCATtGTcTG-3'.

MOs (5-20ng) were pressure-injected into one cell-stage embryos. Control *rgs3* MOmm did not produce any phenotype at 25 ng. For rescue, *in vitro*-transcribed MO-resistant *rgs3b-1* (500 pg) was co-injected with 20 ng *rgs3b-2* met MO. Injected embryos were characterized by morphological and molecular analysis.

Whole mount in situ hybridization

Embryos were fixed overnight in 4% paraformaldehyde and dechorionated. Single label WMISH was performed as previously described (Thisse, Thisse et al. 1993; Westfall, Brimeyer et al. 2003), using Dig-labeled antisense and sense RNA probes. Detection was carried out using BM purple (Roche Applied Science). Purple color was developed with AP-conjugated anti-Dig and BM purple (Roche Applied Science.

Reactions were stopped in PBS. Embryos were mounted on bridged coverslips and photographed using a Zeiss Stemi M13 Stereoscope and an Axiocam digital camera.

Immunohistochemistry

Embryos injected with either *myc-rgs3b-1, myc-rgs3b-2, myc-rgs3b-3, myc-rgs3b-1*$^{(N\text{-}A)}$, *myc-rgs3b-2ΔEF, myc-rgs3b-3ΔEF* (200 pg) were fixed 1-3 hrs in 4% PFA/1× PBS at sphere/dome stage. Mouse anti–myc antibody (1:1,500; Cell Signaling Technology), followed by goat-anti-mouse Alexa488 conjugated secondary antibody (1:400; Molecular Probes) was used to detect the rgs3 products. Nuclei were identified with 5 μM TOPRO3 (Molecular Probes). Embryos were mounted in an animal pole orientation in bridged coverslips and optically sectioned using two-channel imaging on a scanning laser confocal microscope, Leica TCS SP2. Wide-field fluorescence and bright–field images from a Zeiss Stemi M13 Bio Stereoscope were photographed using Axiovision (Zeiss) software and an Axiocam 5000 camera. Images were merged using Adobe Photoshop CS.

Statistical analysis

Calculations for MO rescue experiments were made using the Fisher's exact test and the two-tailed p-value was reported.

A.

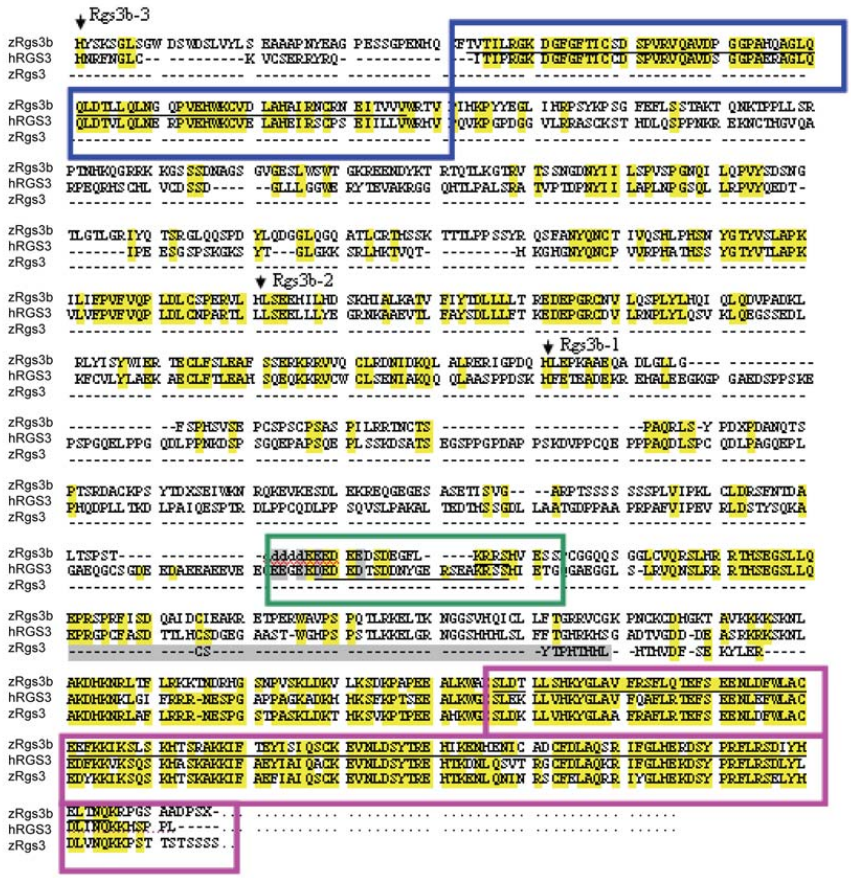

B.

	PDZ	EF Hand	RGS	Whole
hRGS3 to zRgs3			83%	70%
hRGS3 to zRgs3b	84%	33%	75%	40%
zRgs3b to zRgs3			78%	63%

Figure 37: Alignment of Human and Zebrafish Rgs3. (A) Alignment of zRgs3b, hRgs3 and zRgs3. Blue box indicates the PDZ domain, Green box indicates the EF Hand motif and pink box indicates the RGS domain. Arrows indicate where each of the three isoforms of zRgs3b begins. (B) Percent identity of Rgs3 proteins within the conserved protein domains as well as comparison of the whole protein. h=human z=zebrafish

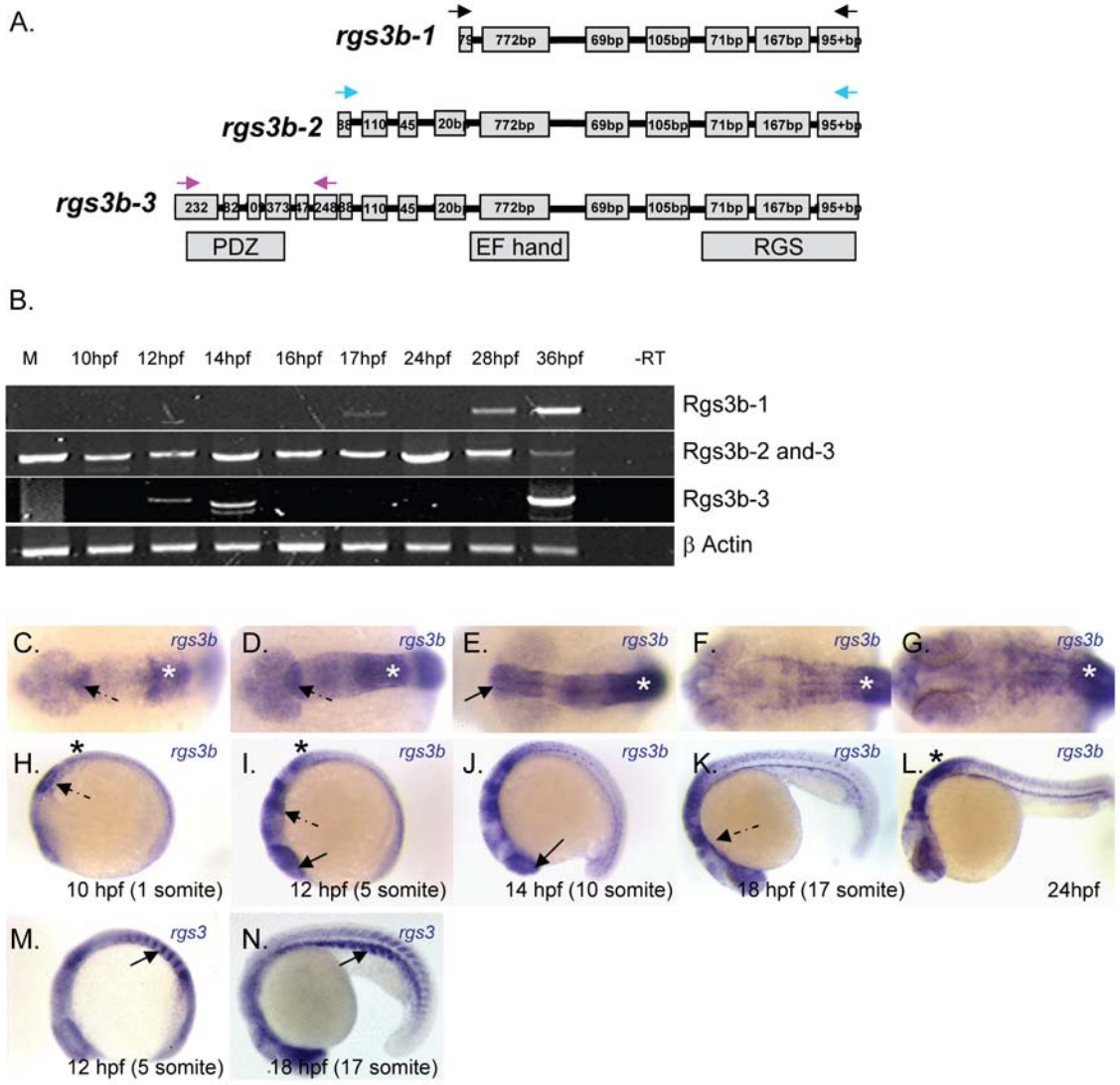

Figure 38: Temporal and Spatial Expression of Rgs3b Throughout Zebrafish Development. (A) Schematics illustrating the three splice variants of Rgs3b which were identified by 5' RACE. Arrows indicate the location of primers used for RT-PCR. Black arrows are specific for Rgs3b-1, blue arrows are specific for Rgs3b-2 and b-3 and pink arrows are specific for Rgs3b-3. (B) RT-PCR was used to determine the temporal expression of specific *rgs3b* isoforms from 0 hpf to 36 hpf. (C-N) WMISH was utilized to determine the spatial expression of (C-L) *rgs3b* and (M-N) *rgs3* in wild type embryos. (C-G) Dorsal views and (H-N) lateral views illustrate that *rgs3b* is expressed in the forebrain (arrow), midbrain (dashed arrow) and hind brain (asterisk) while (M-N) *rgs3* is expressed in the posterior tail and developing somites (arrow).

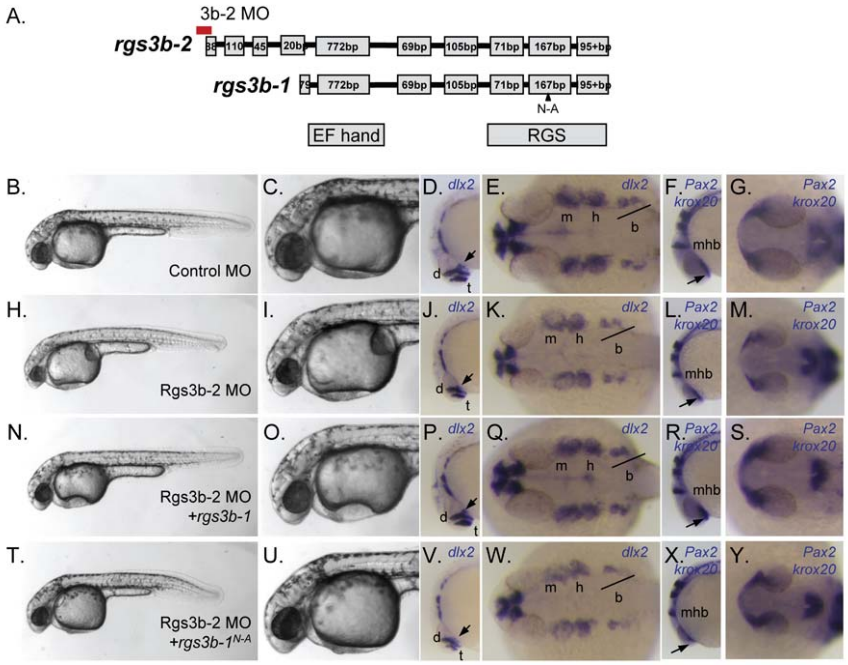

Figure 39: rgs3b-2 Morphant Phenotypes and Functional Rescue. (A) Schematic of zebrafish rgs3 mRNA/protein composite. The location of the morpholino binding site is indicated by a red line above the transcript. The EF hand motif as well as the RGS domain of Rgs3b is indicated by the grey box. Morphology of (N-O and T-U) 30hpf embryos as well as WMISH of 24 hpf embryos with the molecular markers (D-E, J-K, P-Q and V-W) dlx2 and (F-G, L-M, R-S and X-Y) pax2/krox20 were used to evaluate phenotypes of (B-G) Control MO, (H-M) rgs3b-2 MO, (N-S) rgs3b-2 MO + rgs3b-1 as well as (T-Y) rgs3b-2 MO + rgs3b-1N-A injected embryos . dlx2 labels the telencephalon (t), diencephalon (d), hypothalamus (arrow), mandibular arch (m), hyoid arch (h) and brachial arches (b) while pax2 labels the midbrain-hindbrain boundary (mhb) and optic stalk (arrow) and krox20 labels rhombomere 3 and 5. (A and I-K) Lateral and (B-H) dorsal views, anterior to the right, of (A-H) 15 hpf and (I-K) 20 hpf wild-type embryos injected with (A, B, E, F and I) Control MO, (C, G and J) rgs3 MO and (D, H and K) rgs3 MO + rgs3. (B-D, F, H-J, L, N-P, R, T-V and X)Lateral and (E, G, K, M, Q, S, W and Y) dorsal views are shown with anterior to the left. (N-O) Morphology, (P-Q) dlx2 and (R-S) krox20 /pax2 expression patterns indicate that rgs3b-1 is able to suppress the morpholino-induced defect. For structural functional analyses, rgs3b-1N-A was evaluated for rescue of knockdown. (T-U) Morphological and (V-Y) molecular analyses reveals that rgs3b-1N-A is unable to suppress the MO induced defect.

A.

	n	Wt-like	Reduced forebrain	% Reduced forebrain	
Control Mo	65	64	1	2	
***rgs3b-2* M0**	110	41	69	63	*
rgs3b-2* M0 + *rgs3b-1	86	49	37	43	
***rgs3b-2* M0 + *rgs3b-1* N-A**	87	32	54	62	

*p-value = 0.006442

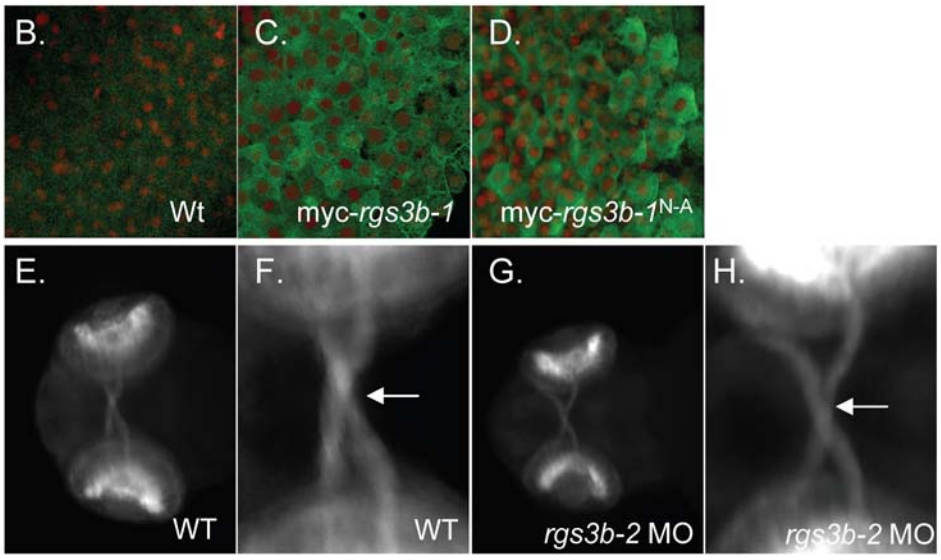

Figure 40: Statistically Significant Suppression of *rgs3b-2* Knockdown Requires a Functional RGS Domain. Morphological and molecular analyses reveals indicate that (A) *rgs3b-1* is able to statistically significantly suppress the morpholino-induced defect while *rgs*3b-1^{N-A} is unable to suppress the MO induced defect. Immunohistochemistry of (C) myc-rgs3b-1 and (D) myc-*rgs3b-*1^{N-A} embryos at 80% epiboly indicate that both proteins are stable. Expression of *ath5*:GFP in 3 dpf (E-F) wild-type or (G-H) *rgs3b-2* MO injected embryos. *ath5*:GFP is expressed in the eye and retino-tectal projection. Arrows indicate the optic chiasm.

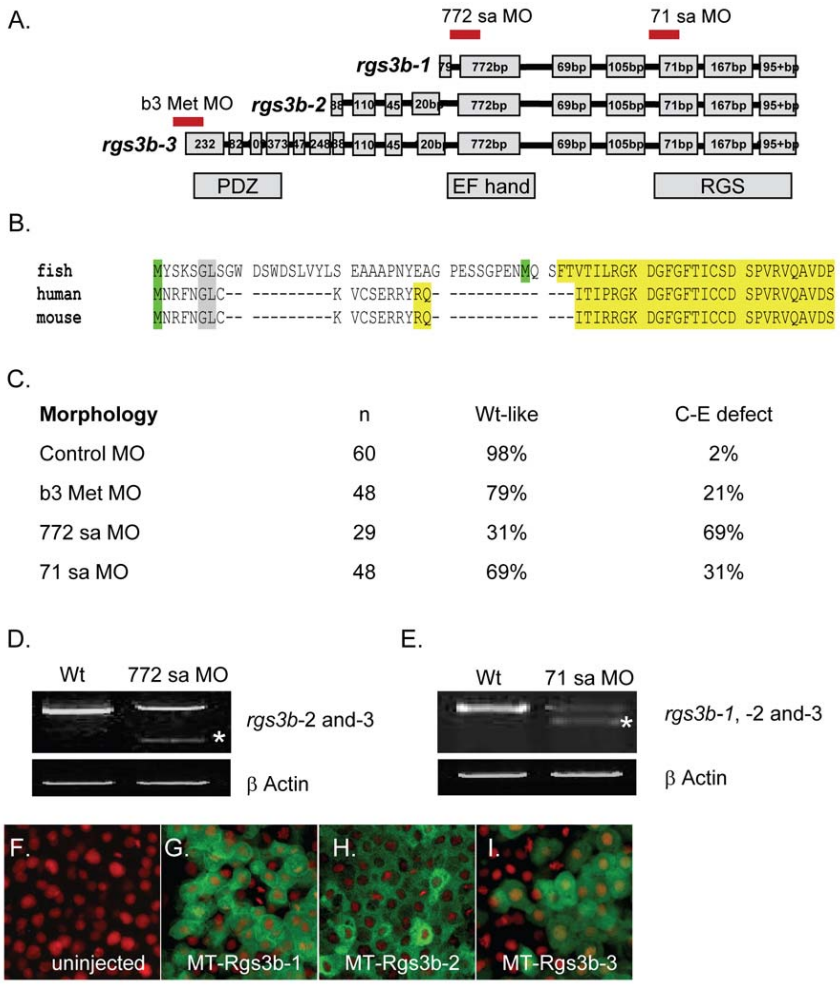

Figure 41: *rgs3b* Gene Knockdown. (A) Schematic of zebrafish rgs3b-1, b-2 and b-3 mRNA/protein composite. The location of the morpholino binding sites are indicated by a red line above the transcript. The PDZ domain, EF hand motif as well as the RGS domain of Rgs3b are indicated by the grey boxes. (B) Alignment of zebrafish Rgs3b-3, human Rgs3 and mouse Rgs3. Green Highlighted M indicates two possible initiator methionines in zebrafish *rgs3b*-3 and the identified initiator methionine in human and mouse. (C) *rgs3b* knockdown results in varying penetrance of C-E defects. (D) RT-PCR of 24hpf Wt and *rgs3b* 772 MO injected embryos. Asterisk indicates aberrant product. (E) RT-PCR of 24hpf Wt and Rgs3 71 MO injected embryos. Asterisk indicates aberrant product. Immunohistochemistry of (F) control (G) myc-*rgs3b-1*, (H) myc-*rgs3b-2* and (I) myc-*rgs3b-3* injected embryos at 80% epiboly indicate that all proteins are stable.

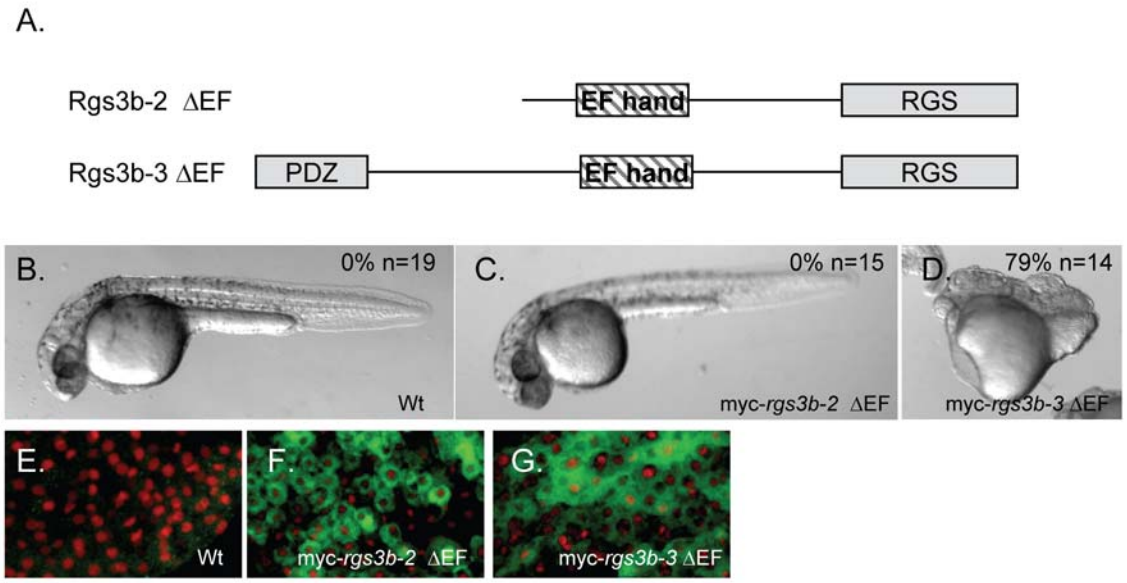

Figure 42: Characterization of the Aberrant Transcript Produced by *rgs3b 772*sa MO Injection. (A) Schematic of the zebrafish Rgsb-2 and Rgsb-3 mRNA/protein composite after altered splicing from the 772sa MO. Diagonal marks indicate that the EF hand motif is removed in frame. (B-D) Lateral brightfield images of 48 hpf embryos injected with (B) Control MO, (C) myc-*rgs3b-2* ΔEF or (D) myc-*rgs3b-3* ΔEF. (E-G) Immunohistochemistry of (E) Control, (F) myc-*rgs3b-2* ΔEF, and (G) myc-*rgs3b-3* ΔEF injected embryos at 80% epiboly.

A.

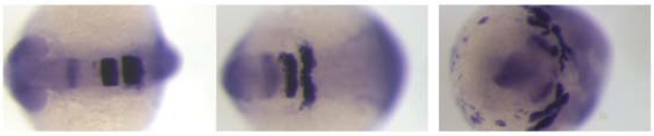

pax2/krox20	n	Wt-like	Expanded	Radial
wt	31	96%	4%	0%
b3 Met MO	23	83%	4%	13%
772 sa MO	21	80%	9.5%	9.5%
71 sa MO	25	76%	12%	12%

B.

lefty1/2	n	Left	Bilateral
wt	26	100%	0
b3 Met MO	27	96%	4%
772 sa MO	14	93%	7%
71 sa MO	11	91%	9%

C.

nkx	n	Left	Middle	Right	Bilateral
wt	59	90%	7%	3%	0
b3 Met MO	80	92.5%	4%	2.5%	1%
772 sa MO	56	78.5%	12.5%	9%	0
71 sa MO	56	70%	12.5%	12.5%	5%

Figure 43: *rgs3b* Morphant Phenotypes. Morphant phenotypes of (B) 15 hpf, (C) 20 hpf and (D) 30 hpf zebrafish embryos were characterized using the molecular markers (A) *pax2/krox20*, (B) *lefty1/2* and (C) and *nkx.*

CHAPTER 6

CONCLUSIONS AND FUTURE DIRECTIONS

Introduction

This thesis describes in detail the characterization of endogenous Ca^{2+} activity in zebrafish, identification and characterization of specific regulators of Wnt/Ca^{2+} activity, and the developmental consequences of altering RGS and Wnt family members which regulate Ca^{2+} dynamics. Together, these data highlight a previously unknown essential need for individual RGS proteins to tightly regulate key developmental pathways.

Summary

In chapter 1, I describe the Wnt signaling network, key players such as G proteins and the importance of precisely regulating the amplitude as well as duration of Wnt/Ca^{2+} signaling. In chapter 2, I describe endogenous Ca^{2+} dynamics from the very first cell divisions through early somitogenesis in zebrafish embryos. I find that each phase of zebrafish development has a distinct pattern of Ca^{2+} release, highlighting the complexity of Ca^{2+} ion and cellular physiology. Due to the fact that previous work in our lab and others had identified that G protein signaling is required for embryonic Ca^{2+} release activity, Chapter 3 investigated RGS proteins in zebrafish. Through this investigation I was able to identify *rgs3* as potential modulator of Ca^{2+} dynamics. I find that, r*gs*3 has an overlapping expression pattern with *wnt5b* in zebrafish. Additionally, I have identified that individual knockdown of either *rgs3* or *wnt5b* gene function produces similar somite patterning defects. In chapter 4, I expand on these observations by providing data supporting that Rgs3 function is necessary for appropriate frequency and amplitude of Ca^{2+} release during somitogenesis, and that Rgs3 functions downstream of Wnt5 activity. These results provide the first evidence for an essential developmental role of individual RGS proteins in modulating the duration of Wnt/Ca^{2+} signaling. These data support a model in which RGS functions at the level of activated G protein and when

combined with data from epistasis experiments supports the conclusion that G proteins function downstream of Fz and upstream of Dvl (Katanaev, Ponzielli et al. 2005), thereby indicating that Rgs3 functions downstream of Wnt and Fz and upstream of Dvl in the Wnt signaling network.

Having characterized Ca^{2+} release changes in Wnt5 overexpressing and wild-type embryos overexpressing Rgs3 and determined that the Wnt/Ca^{2+} signaling pathway is a target of Rgs3 is a substantial breakthrough in understanding how RGS proteins function with specific signaling pathways. Future experiments initiating characterization of how RGS function influences the polarized movement of blood vessels, cardiovascular function and cancer metastasis are necessary to unravel how RGS proteins influence normal development and how perturbation results in disease.

I hypothesize that other RGS genes may have a role in modulating Wnt/Ca^{2+} signaling in different tissues or at different stages. In chapter 5, I report the identification and characterization of Rgs3b, a paralogue to RGS3. The complementary expression patterns of *rgs3* and *rgs3b* support the conclusion that subfunctionalization has resulted in gene preservation of Rgs3 and Rgs3b. The strong expression of the *rgs3*b transcript in the developing brain supports the conclusion that *rgs3*b is poised to interact with Wnt11 which is also strongly expressed in the developing brain. These data support the inference that Wnt/Ca^{2+} signaling activity in the developing forebrain may be an in vivo target of Rgs3b, further indicating that individual RGS proteins function to regulate specific GPCR mediated signaling networks.

Conclusions

The output of G protein coupled signaling cascades is dependent upon a complex layering of different ligands, different GPCRs, multiple combinations of different $G\alpha\beta\gamma$ heterotrimeric proteins as well as different RGS proteins. Specific combinations of ligands, receptors, G proteins and regulators result in different signaling outputs. The

ability of RGS proteins to negatively regulate GPCR pathways raises two distinct possibilities: 1) Individual RGS proteins have the ability to globally inhibit all GPCR pathways or 2) Individual RGS proteins are able to selectively inhibit specific combinations of individual ligands, receptors and G proteins. Based on this thesis, I hypothesize that individual RGS proteins are able to selectively inhibit specific combinations of individual ligands, receptors and G proteins. I predict that, RGS with ubiquitous expression patterns such as *rgs*16 (Figure 17I-J) function in signaling cascades associated with cell maintenance (i.e. housekeeping) while, RGS proteins with dynamic expression patterns such as *rgs*3 (Figure 17C-D) and *rgs*5 (Figure 17G-H) function to selectively inhibit specific combinations of individual ligands, receptors and G proteins and translate the signal into distinct developmental outputs. To this end, evidence from this thesis support the conclusion that Rgs3 function is necessary for maintaining the appropriate frequency and amplitude of Ca^{2+} release during somitogenesis and is downstream of Wnt5 activity.

I believe that future experiments will highlight the essential roles that RGS proteins have in gene regulatory networks controlling developmental transitions. I predict that in ten years the RGS field will have substantial evidence supporting that RGS proteins are essential in limiting the range and output of key developmental signaling cascades. Thus the dynamic expression patterns of RGS proteins could allow cells in the same field receiving the ligand to translate the signal into different developmental outputs based on the presence or absence of an RGS protein. This allows cells with identical combinations of upstream components (i.e. Receptors, GPCRs and G proteins) to have strikingly different signaling duration.

Indeed data indicate that specific RGS proteins are involved in key developmental signaling cascades. RGS10-deficient mice have reduced osteoclast differentiation while ectopic expression of RGS10 increases osteoclast differentiation (Yang and Li 2007). Additionally, overexpression of PDZ-RGS3 with its receptor (Ephrin-b1) in the mouse

cerebral cortex blocks normal neural progenitor differentiation while overexpression of a dominant negative PDZ-RGS3 resulted in increased progenitor differentiation (Qiu, Wang et al. 2008). From these data the authors suggest a working model in which PDZ-RGS3 specifically interacts with Ephrin-B to promote neural progenitor maintenance while in the absence of PDZ-RGS3 activated G proteins signal to downstream effectors resulting in neural differentiation. Together these data from the mouse model system support the conclusion that the ability of RGS proteins to modulate G protein dependent developmental signaling cascades in specific tissues results in different developmental patterning events in the presence and absence of an RGS protein.

Future directions

The ability of RGS proteins to tightly regulate G protein signaling provides them with the opportunity to tightly regulate key developmental pathways involved in cardiovascular patterning as well as cancer metastasis. In support of an important role in cardiac development, experiments with specific antagonists of GPCR induce cardiac remodeling (Rockman, Koch et al. 2002). Ectopic expression of R4 subfamily members is sufficient to alter mouse cardiac function (Rogers, Tsirka et al. 2001). Additionally, R4 subfamily members, RGS1, 2, 3, 4 and 5 have been implicated in cardiovascular development. RGS1 is expressed in the human aorta and inhibits sphingosine 1-phosphate receptors ($S1P_1$, $S1P_2$, and $S1P_3$) (Cho, Harrison et al. 2003), RGS2 is expressed in the human aorta and selectively attenuates $S1P_2$, and $S1P_3$ signaling (Sinnarajah, Dessauer et al. 2001; Cho, Harrison et al. 2003), RGS3 is present in the human and rat heart and inhibits the action of α-adrenergic, endothelin and other agonists (Zhang, Watson et al. 1998), PDZ-RGS3 is present in the human atria and may have a role in angiogenesis (Cho, Harrison et al. 2003), RGS4 is involved in the regulation of Gi-subunit-gated potassium channels and is up-regulated in human heart failure (Zhang, Watson et al. 1998; Wieland and Mittmann 2003), while RGS5 is shown to be a signal

regulator in the vascular system (Wieland and Mittmann 2003). In addition to modulating cardiovascular developmental pathways, RGS proteins have been identified as possible tumor suppressors. In fact, repression of the R4 subfamily member RGS2 has been observed in thyroid cancers and in leukemic transformations (Tonjes, Miedlich et al. 2004; Schwable, Choudhary et al. 2005). Because RGS proteins are thought to tightly regulate G protein signaling in an environmentally dependent fashion, an *in vivo* analysis is essential in fully understanding the function of these RGS proteins. By highlighting the role of RGS proteins in development, this thesis identifies a need for future experiments investigating RGS function.

REFERENCES

Aanstad, P. and M. Whitaker (1999). "Predictability of dorso-ventral asymmetry in the cleavage stage zebrafish embryo: an analysis using lithium sensitivity as a dorso-ventral marker." Mech Dev **88**(1): 33-41.

Ahumada, A., D. C. Slusarski, et al. (2002). "Signaling of rat Frizzled-2 through phosphodiesterase and cyclic GMP." Science **298**(5600): 2006-10.

Albig, A. R. and W. P. Schiemann (2005). "Identification and characterization of regulator of G protein signaling 4 (RGS4) as a novel inhibitor of tubulogenesis: RGS4 inhibits mitogen-activated protein kinases and vascular endothelial growth factor signaling." Mol Biol Cell **16**(2): 609-25.

Angers, S., C. J. Thorpe, et al. (2006). "The KLHL12-Cullin-3 ubiquitin ligase negatively regulates the Wnt-beta-catenin pathway by targeting Dishevelled for degradation." Nat Cell Biol **8**(4): 348-57.

Axelrod, J. D., J. R. Miller, et al. (1998). "Differential recruitment of Dishevelled provides signaling specificity in the planar cell polarity and Wingless signaling pathways." Genes Dev **12**(16): 2610-22.

Becchetti, A. and M. Whitaker (1997). "Lithium blocks cell cycle transitions in the first cell cycles of sea urchin embryos, an effect rescued by myo-inositol." Development **124**(6): 1099-107.

Berridge, M. J. (1997). "The AM and FM of calcium signalling." Nature **386**(6627): 759-60.

Berridge, M. J., M. D. Bootman, et al. (2003). "Calcium signalling: dynamics, homeostasis and remodelling." Nat Rev Mol Cell Biol **4**(7): 517-29.

Berridge, M. J., C. P. Downes, et al. (1989). "Neural and developmental actions of lithium: a unifying hypothesis." Cell **59**(3): 411-9.

Blum, Y., H. G. Belting, et al. (2008). "Complex cell rearrangements during intersegmental vessel sprouting and vessel fusion in the zebrafish embryo." Dev Biol **316**(2): 312-22.

Boutros, M., N. Paricio, et al. (1998). "Dishevelled activates JNK and discriminates between JNK pathways in planar polarity and wingless signaling." Cell **94**(1): 109-18.

Cadigan, K. M. and Y. I. Liu (2006). "Wnt signaling: complexity at the surface." J Cell Sci **119**(Pt 3): 395-402.

Cadigan, K. M. and R. Nusse (1997). "Wnt signaling: a common theme in animal development." Genes Dev **11**(24): 3286-305.

Carreira-Barbosa, F., M. L. Concha, et al. (2003). "Prickle 1 regulates cell movements during gastrulation and neuronal migration in zebrafish." Development **130**(17): 4037-46.

Chang, D. C. and C. Meng (1995). "A localized elevation of cytosolic free calcium is associated with cytokinesis in the zebrafish embryo." J Cell Biol **131**(6 Pt 1): 1539-45.

Chang, D. C. and C. Meng (1995). "A Localized Elevation of Cytosolic Free Calcium is Associated with Cytokinesis in the Zebrafish Embryo." *The Journal of Cell Biology* **131**: 1539-1545.

Chen, C. K., M. E. Burns, et al. (2000). "Slowed recovery of rod photoresponse in mice lacking the GTPase accelerating protein RGS9-1." Nature **403**(6769): 557-60.

Cheng, C. W., J. C. Yeh, et al. (2008). "Wnt5a-mediated non-canonical Wnt signalling regulates human endothelial cell proliferation and migration." Biochem Biophys Res Commun **365**(2): 285-90.

Cheng, J. C., A. L. Miller, et al. (2004). "Organization and function of microfilaments during late epiboly in zebrafish embryos." Dev Dyn **231**(2): 313-23.

Cho, H., K. Harrison, et al. (2003). "The aorta and heart differentially express RGS (regulators of G-protein signalling) proteins that selectively regulate sphingosine 1-phosphate, angiotensin II and endothelin-1 signalling." Biochem J **371**(Pt 3): 973-80.

Christoffels, A., S. Brenner, et al. (2006). "Tetraodon genome analysis provides further evidence for whole-genome duplication in the ray-finned fish lineage." Comp Biochem Physiol Part D Genomics Proteomics **1**(1): 13-9.

Christoffels, A., E. G. Koh, et al. (2004). "Fugu genome analysis provides evidence for a whole-genome duplication early during the evolution of ray-finned fishes." Mol Biol Evol **21**(6): 1146-51.

Cirone, P., S. Lin, et al. (2008). "A role for planar cell polarity signaling in angiogenesis." Angiogenesis.

Creton, R., J. E. Speksnijder, et al. (1998). "Patterns of free calcium in zebrafish embryos." J Cell Sci **111 (Pt 12)**: 1613-22.

Dale, T. C. (1998). "Signal transduction by the Wnt family of ligands." Biochem J **329 (Pt 2)**: 209-23.

De Vries, L., B. Zheng, et al. (2000). "The regulator of G protein signaling family." Annu Rev Pharmacol Toxicol **40**: 235-71.

Dohlman, H. G., D. Apaniesk, et al. (1995). "Inhibition of G-protein signaling by dominant gain-of-function mutations in Sst2p, a pheromone desensitization factor in Saccharomyces cerevisiae." Mol Cell Biol **15**(7): 3635-43.

Dohlman, H. G., J. Song, et al. (1996). "Sst2, a negative regulator of pheromone signaling in the yeast Saccharomyces cerevisiae: expression, localization, and genetic interaction and physical association with Gpa1 (the G-protein alpha subunit)." Mol Cell Biol **16**(9): 5194-209.

Druey, K. M., K. J. Blumer, et al. (1996). "Inhibition of G-protein-mediated MAP kinase activation by a new mammalian gene family." Nature **379**(6567): 742-6.

Feigin, M. E. and C. C. Malbon (2007). "RGS19 regulates Wnt-beta-catenin signaling through inactivation of Galpha(o)." J Cell Sci **120**(Pt 19): 3404-14.

Force, T., K. Woulfe, et al. (2007). "Molecular scaffolds regulate bidirectional crosstalk between Wnt and classical seven-transmembrane-domain receptor signaling pathways." Sci STKE **2007**(397): pe41.

Fredriksson, R., M. C. Lagerstrom, et al. (2003). "The G-protein-coupled receptors in the human genome form five main families. Phylogenetic analysis, paralogon groups, and fingerprints." Mol Pharmacol **63**(6): 1256-72.

Freisinger, C. M., D. W. Houston, et al. (2008). "Image analysis of calcium release dynamics." Methods Mol Biol **468**: 145-56.

Freisinger, C. M., I. Schneider, et al. (2008). "Calcium dynamics integrated into signalling pathways that influence vertebrate axial patterning." Philos Trans R Soc Lond B Biol Sci **363**(1495): 1377-85.

Frohman, M. A. (1993). "Rapid amplification of complementary DNA ends for generation of full-length complementary DNAs: thermal RACE." Methods Enzymol **218**: 340-56.

Fujii, R., S. Yamashita, et al. (2000). "Asymmetric p38 activation in zebrafish: its possible role in symmetric and synchronous cleavage." J Cell Biol **150**(6): 1335-48.

Gao, C. and Y. G. Chen "Dishevelled: The hub of Wnt signaling." Cell Signal **22**(5): 717-27.

Gardner, C. A. and K. F. Barald (1992). "Expression patterns of engrailed-like proteins in the chick embryo." Dev Dyn **193**(4): 370-88.

Gilland, E., A. L. Miller, et al. (1999). "Imaging of multicellular large-scale rhythmic calcium waves during zebrafish gastrulation." Proc Natl Acad Sci U S A **96**(1): 157-61.

Gitler, A. D., M. M. Lu, et al. (2004). "PlexinD1 and semaphorin signaling are required in endothelial cells for cardiovascular development." Dev Cell **7**(1): 107-16.

Grillet, N., A. Pattyn, et al. (2005). "Generation and characterization of Rgs4 mutant mice." Mol Cell Biol **25**(10): 4221-8.

Grynkiewicz, G., M. Poenie, et al. (1985). "A new generation of Ca2+ indicators with greatly improved fluorescence properties." J Biol Chem **260**(6): 3440-50.

Hammerschmidt, M., F. Pelegri, et al. (1996). "Mutations affecting morphogenesis during gastrulation and tail formation in the zebrafish, Danio rerio." Development **123**: 143-51.

Hamzah, J., M. Jugold, et al. (2008). "Vascular normalization in Rgs5-deficient tumours promotes immune destruction." Nature **453**(7193): 410-4.

Heisenberg, C. P. and L. Solnica-Krezel (2008). "Back and forth between cell fate specification and movement during vertebrate gastrulation." Curr Opin Genet Dev **18**(4): 311-6.

Heisenberg, C. P., M. Tada, et al. (2000). "Silberblick/Wnt11 mediates convergent extension movements during zebrafish gastrulation." Nature **405**(6782): 76-81.

Heo, K., S. H. Ha, et al. (2006). "RGS2 promotes formation of neurites by stimulating microtubule polymerization." Cell Signal.

Hepler, J. R., D. M. Berman, et al. (1997). "RGS4 and GAIP are GTPase-activating proteins for Gq alpha and block activation of phospholipase C beta by gamma-thio-GTP-Gq alpha." Proc Natl Acad Sci U S A **94**(2): 428-32.

Hirose, K., S. Kadowaki, et al. (1999). "Spatiotemporal dynamics of inositol 1,4,5-trisphosphate that underlies complex Ca2+ mobilization patterns." Science **284**(5419): 1527-30.

Hollinger, S. and J. R. Hepler (2002). "Cellular regulation of RGS proteins: modulators and integrators of G protein signaling." Pharmacol Rev **54**(3): 527-59.

Holloway, B. A., S. Gomez de la Torre Canny, et al. (2009). "A novel role for MAPKAPK2 in morphogenesis during zebrafish development." PLoS Genet **5**(3): e1000413.

Jung, H., H. J. Kim, et al. (2009). "Negative feedback regulation of Wnt signaling by Gbetagamma-mediated reduction of Dishevelled." Exp Mol Med **41**(10): 695-706.

Kao, K. R. and R. P. Elinson (1988). "The entire mesodermal mantle behaves as Spemann's organizer in dorsoanterior enhanced Xenopus laevis embryos." Dev Biol **127**(1): 64-77.

Kao, K. R. and R. P. Elinson (1989). "Dorsalization of mesoderm induction by lithium." Dev Biol **132**(1): 81-90.

Kao, K. R. and R. P. Elinson (1998). "The legacy of lithium effects on development." Biol Cell **90**(8): 585-9.

Kao, K. R., Y. Masui, et al. (1986). "Lithium-induced respecification of pattern in Xenopus laevis embryos." Nature **322**(6077): 371-3.

Katanaev, V. L., R. Ponzielli, et al. (2005). "Trimeric G protein-dependent frizzled signaling in Drosophila." Cell **120**(1): 111-22.

Kawasaki, H., S. Nakayama, et al. (1998). "Classification and evolution of EF-hand proteins." Biometals **11**(4): 277-95.

Kehrl, J. H., D. Srikumar, et al. (2002). "Additional 5' exons in the RGS3 locus generate multiple mRNA transcripts, one of which accounts for the origin of human PDZ-RGS3." Genomics **79**(6): 860-8.

Keller, R. (2002). "Shaping the vertebrate body plan by polarized embryonic cell movements." Science **298**(5600): 1950-4.

Kimmel, C. B., W. W. Ballard, et al. (1995). "Stages of embryonic development of the zebrafish." Dev Dyn **203**(3): 253-310.

Kishida, S., H. Yamamoto, et al. (1999). "DIX domains of Dvl and axin are necessary for protein interactions and their ability to regulate beta-catenin stability." Mol Cell Biol **19**(6): 4414-22.

Klingensmith, J., R. Nusse, et al. (1994). "The Drosophila segment polarity gene dishevelled encodes a novel protein required for response to the wingless signal." Genes Dev **8**(1): 118-30.

Koelle, M. R. and H. R. Horvitz (1996). "EGL-10 regulates G protein signaling in the C. elegans nervous system and shares a conserved domain with many mammalian proteins." Cell **84**(1): 115-25.

Kohn, A. D. and R. T. Moon (2005). "Wnt and calcium signaling: beta-catenin-independent pathways." Cell Calcium **38**(3-4): 439-46.

Kozasa, T. (1998). "[Regulation of G protein-mediated signaling pathways by RGS proteins]." Seikagaku **70**(12): 1418-22.

Krumlauf, R. (1994). "Hox genes in vertebrate development." Cell **78**(2): 191-201.

Kudoh, T., M. Tsang, et al. (2001). "A gene expression screen in zebrafish embryogenesis." Genome Res **11**(12): 1979-87.

Kuhl, M., L. C. Sheldahl, et al. (2000). "The Wnt/Ca2+ pathway: a new vertebrate Wnt signaling pathway takes shape." Trends Genet **16**(7): 279-83.

Kume, S., T. Saneyoshi, et al. (2000). "Desensitization of IP3-induced Ca2+ release by overexpression of a constitutively active Gqalpha protein converts ventral to dorsal fate in Xenopus early embryos." Dev Growth Differ **42**(4): 327-35.

Lechleiter, J., S. Gira□d, et al. (1991). "Spiral Calcium Wave Propagation and Annihilation in *Xenopus laevi*s Oocytes." *Scienc*e **252**: 123-126.

Lechleiter, J., S. Girard, et al. (1991). "Spiral calcium wave propagation and annihilation in Xenopus laevis oocytes." Science **252**(5002): 123-6.

Lee, K. W., S. E. Webb, et al. (2003). "Ca2+ released via IP3 receptors is required for furrow deepening during cytokinesis in zebrafish embryos." Int J Dev Biol **47**(6): 411-21.

Lee, K. W., S. E. Webb, et al. (2006). "Requirement for a localized, IP3R-generated Ca2+ transient during the furrow positioning process in zebrafish zygotes." Zygote **14**(2): 143-55.

Lee, M. J., T. Tasaki, et al. (2005). "RGS4 and RGS5 are in vivo substrates of the N-end rule pathway." Proc Natl Acad Sci U S A **102**(42): 15030-5.

Leslie, J. D., L. Ariza-McNaughton, et al. (2007). "Endothelial signalling by the Notch ligand Delta-like 4 restricts angiogenesis." Development **134**(5): 839-44.

Levine, B. A., D. C. Dalgarno, et al. (1983). "The mobility of calcium-trigger proteins and its function." Ciba Found Symp **93**: 72-97.

Lin, F., S. Chen, et al. (2009). "Galpha12/13 regulate epiboly by inhibiting E-cadherin activity and modulating the actin cytoskeleton." J Cell Biol **184**(6): 909-21.

Liu, R. Z., Q. Sun, et al. (2005). "The cellular retinol-binding protein genes are duplicated and differentially transcribed in the developing and adult zebrafish (Danio rerio)." Mol Biol Evol **22**(3): 469-77.

Liu, T., A. J. DeCostanzo, et al. (2001). "G protein signaling from activated rat frizzled-1 to the beta-catenin-Lef-Tcf pathway." Science **292**(5522): 1718-22.

Liu, X., T. Liu, et al. (1999). "Activation of a frizzled-2/beta-adrenergic receptor chimera promotes Wnt signaling and differentiation of mouse F9 teratocarcinoma cells via Galphao and Galphat." Proc Natl Acad Sci U S A **96**(25): 14383-8.

Long, S. and M. Rebagliati (2002). "Sensitive two-color whole-mount in situ hybridizations using digoxygenin- and dinitrophenol-labeled RNA probes." Biotechniques **32**(3): 494, 496, 498 passim.

Luo, X., S. Popov, et al. (2001). "RGS proteins provide biochemical control of agonist-evoked [Ca2+]i oscillations." Mol Cell **7**(3): 651-60.

Lyman Gingerich, J., T. A. Westfall, et al. (2005). "hecate, a zebrafish maternal effect gene, affects dorsal organizer induction and intracellular calcium transient frequency." Dev Biol **286**(2): 427-39.

Lynch, M. and A. Force (2000). "The probability of duplicate gene preservation by subfunctionalization." Genetics **154**(1): 459-73.

Lynch, M., M. O'Hely, et al. (2001). "The probability of preservation of a newly arisen gene duplicate." Genetics **159**(4): 1789-804.

Makino, E. R., J. W. Handy, et al. (1999). "The GTPase activating factor for transducin in rod photoreceptors is the complex between RGS9 and type 5 G protein beta subunit." Proc Natl Acad Sci U S A **96**(5): 1947-52.

Mao, H., Q. Zhao, et al. (2004). "RGS17/RGSZ2, a novel regulator of Gi/o, Gz, and Gq signaling." J Biol Chem **279**(25): 26314-22.

Masckauchan, T. N., D. Agalliu, et al. (2006). "Wnt5a signaling induces proliferation and survival of endothelial cells in vitro and expression of MMP-1 and Tie-2." Mol Biol Cell **17**(12): 5163-72.

McCarron, J. G., D. MacMillan, et al. (2004). "Origin and mechanisms of Ca2+ waves in smooth muscle as revealed by localized photolysis of caged inositol 1,4,5-trisphosphate." J Biol Chem **279**(9): 8417-27.

Means, A. R. (2000). "Regulatory cascades involving calmodulin-dependent protein kinases." Mol Endocrinol **14**(1): 4-13.

Meyer, T. (1991). "Cell signaling by second messenger waves." Cell **64**(4): 675-8.

Moon, R. T., R. M. Campbell, et al. (1993). "Xwnt-5A: a maternal Wnt that affects morphogenetic movements after overexpression in embryos of Xenopus laevis." Development **119**(1): 97-111.

Moon, R. T., J. L. Christian, et al. (1993). "Dissecting Wnt signalling pathways and Wnt-sensitive developmental processes through transient misexpression analyses in embryos of Xenopus laevis." Dev Suppl: 85-94.

Morcos, P. A. (2000). "Gene switching: analyzing a broad range of mutations using steric block antisense oligonucleotides." Methods Enzymol **313**: 174-89.

Mukhopadhyay, S. and E. M. Ross (1999). "Rapid GTP binding and hydrolysis by G(q) promoted by receptor and GTPase-activating proteins." Proc Natl Acad Sci U S A **96**(17): 9539-44.

Muto, A., S. Kume, et al. (1996). "Calcium waves along the cleavage furrows in cleavage-stage Xenopus embryos and its inhibition by heparin." J Cell Biol **135**(1): 181-90.

Natochin, M., R. L. McEntaffer, et al. (1998). "Mutational analysis of the Asn residue essential for RGS protein binding to G-proteins." J Biol Chem **273**(12): 6731-5.

Nisancioglu, M. H., W. M. Mahoney, Jr., et al. (2008). "Generation and characterization of rgs5 mutant mice." Mol Cell Biol **28**(7): 2324-31.

Nomikos, M., L. M. Blayney, et al. (2005). "Role of phospholipase C-zeta domains in Ca2+-dependent phosphatidylinositol 4,5-bisphosphate hydrolysis and cytoplasmic Ca2+ oscillations." J Biol Chem **280**(35): 31011-8.

Ohno, S., U. Wolf, et al. (1968). "Evolution from fish to mammals by gene duplication." Hereditas **59**(1): 169-87.

Parekh, A. B. and J. W. Putney, Jr. (2005). "Store-operated calcium channels." Physiol Rev **85**(2): 757-810.

Park, T. J., R. S. Gray, et al. (2005). "Subcellular localization and signaling properties of dishevelled in developing vertebrate embryos." Curr Biol **15**(11): 1039-44.

Parmalee, N. L. and J. Kitajewski (2008). "Wnt signaling in angiogenesis." Curr Drug Targets **9**(7): 558-64.

Premont, R. T., J. Inglese, et al. (1995). "Protein kinases that phosphorylate activated G protein-coupled receptors." Faseb J **9**(2): 175-82.

Qiu, R., X. Wang, et al. (2008). "Regulation of neural progenitor cell state by ephrin-B." J Cell Biol **181**(6): 973-83.

Rauch, G. J., M. Hammerschmidt, et al. (1997). "Wnt5 is required for tail formation in the zebrafish embryo." Cold Spring Harb Symp Quant Biol **62**: 227-34.

Reinhard, E., H. Yokoe, et al. (1995). "Localized calcium signals in early zebrafish development." Dev Biol **170**(1): 50-61.

Rey, O., S. H. Young, et al. (2005). "Amino acid-stimulated Ca2+ oscillations produced by the Ca2+-sensing receptor are mediated by a phospholipase C/inositol 1,4,5-trisphosphate-independent pathway that requires G12, Rho, filamin-A, and the actin cytoskeleton." J Biol Chem **280**(24): 22875-82.

Rockman, H. A., W. J. Koch, et al. (2002). "Seven-transmembrane-spanning receptors and heart function." Nature **415**(6868): 206-12.

Roderick, H. L., M. J. Berridge, et al. (2003). "Calcium-induced calcium release." Curr Biol **13**(11): R425.

Rogers, J. H., A. Tsirka, et al. (2001). "RGS4 reduces contractile dysfunction and hypertrophic gene induction in Galpha q overexpressing mice." J Mol Cell Cardiol **33**(2): 209-18.

Ross, E. M. (2002). "Quantitative assays for GTPase-activating proteins." Methods Enzymol **344**: 601-17.

Ross, E. M. and T. M. Wilkie (2000). "GTPase-activating proteins for heterotrimeric G proteins: regulators of G protein signaling (RGS) and RGS-like proteins." Annu Rev Biochem **69**: 795-827.

Rozen, S. and H. Skaletsky (2000). "Primer3 on the WWW for general users and for biologist programmers." Methods Mol Biol **132**: 365-86.

Sambi, B. S., M. D. Hains, et al. (2006). "The effect of RGS12 on PDGFbeta receptor signalling to p42/p44 mitogen activated protein kinase in mammalian cells." Cell Signal **18**(7): 971-81.

Schneider, I., D. W. Houston, et al. (2008). "Calcium fluxes in dorsal forerunner cells antagonize beta-catenin and alter left-right patterning." Development **135**(1): 75-84.

Schoeber, J. P., C. N. Topala, et al. (2006). "RGS2 inhibits the epithelial Ca2+ channel TRPV6." J Biol Chem.

Schroder, B., C. Schlumbohm, et al. (1996). "Role of calbindin-D9k in buffering cytosolic free Ca2+ ions in pig duodenal enterocytes." J Physiol **492 (Pt 3)**: 715-22.

Schulte, G. and V. Bryja (2007). "The Frizzled family of unconventional G-protein-coupled receptors." Trends Pharmacol Sci **28**(10): 518-25.

Schwable, J., C. Choudhary, et al. (2005). "RGS2 is an important target gene of Flt3-ITD mutations in AML and functions in myeloid differentiation and leukemic transformation." Blood **105**(5): 2107-14.

Sepich, D. S., D. C. Myers, et al. (2000). "Role of the zebrafish trilobite locus in gastrulation movements of convergence and extension." Genesis **27**(4): 159-73.

Sharma, M. K., V. Saxena, et al. (2005). "Differential expression of the duplicated cellular retinoic acid-binding protein 2 genes (crabp2a and crabp2b) during zebrafish embryonic development." Gene Expr Patterns **5**(3): 371-9.

Shaw, K. M., D. A. Castranova, et al. (2006). "fused-somites-like mutants exhibit defects in trunk vessel patterning." Dev Dyn **235**(7): 1753-60.

Sheldahl, L. C., D. C. Slusarski, et al. (2003). "Dishevelled activates Ca2+ flux, PKC, and CamKII in vertebrate embryos." J Cell Biol **161**(4): 769-77.

Siderovski, D. P. and F. S. Willard (2005). "The GAPs, GEFs, and GDIs of heterotrimeric G-protein alpha subunits." Int J Biol Sci **1**(2): 51-66.

Sinnarajah, S., C. W. Dessauer, et al. (2001). "RGS2 regulates signal transduction in olfactory neurons by attenuating activation of adenylyl cyclase III." Nature **409**(6823): 1051-5.

Slusarski, D. C. and V. G. Corces (2000). "Calcium imaging in cell-cell signaling." Methods Mol Biol **135**: 253-61.

Slusarski, D. C., V. G. Corces, et al. (1997). "Interaction of Wnt and a Frizzled homologue triggers G-protein-linked phosphatidylinositol signalling." Nature **390**(6658): 410-3.

Slusarski, D. C. and F. Pelegri (2007). "Calcium signaling in vertebrate embryonic patterning and morphogenesis." Dev Biol **307**(1): 1-13.

Slusarski, D. C., J. Yang-Snyder, et al. (1997). "Modulation of embryonic intracellular Ca2+ signaling by Wnt-5A." Dev Biol **182**(1): 114-20.

Srinivasa, S. P., N. Watson, et al. (1998). "Mechanism of RGS4, a GTPase-activating protein for G protein alpha subunits." J Biol Chem **273**(3): 1529-33.

Stachel, S. E., D. J. Grunwald, et al. (1993). "Lithium perturbation and goosecoid expression identify a dorsal specification pathway in the pregastrula zebrafish." Development **117**(4): 1261-74.

Stoltzfus, A. (1999). "On the possibility of constructive neutral evolution." J Mol Evol **49**(2): 169-81.

Stricker, S. A. (1995). "Time-lapse confocal imaging of calcium dynamics in starfish embryos." Dev Biol **170**(2): 496-518.

Tada, M. and J. C. Smith (2000). "Xwnt11 is a target of Xenopus Brachyury: regulation of gastrulation movements via Dishevelled, but not through the canonical Wnt pathway." Development **127**(10): 2227-38.

Tesmer, J. J., D. M. Berman, et al. (1997). "Structure of RGS4 bound to AlF4--activated G(i alpha1): stabilization of the transition state for GTP hydrolysis." Cell **89**(2): 251-61.

Thisse, C., B. Thisse, et al. (1993). "Structure of the zebrafish snail1 gene and its expression in wild-type, spadetail and no tail mutant embryos." Development **119**(4): 1203-15.

Thore, S., O. Dyachok, et al. (2004). "Oscillations of phospholipase C activity triggered by depolarization and Ca2+ influx in insulin-secreting cells." J Biol Chem **279**(19): 19396-400.

Tonjes, A., S. Miedlich, et al. (2004). "Expression of regulators of g protein signaling mRNA is differentially regulated in hot and cold thyroid nodules." Thyroid **14**(11): 896-901.

Topol, L., X. Jiang, et al. (2003). "Wnt-5a inhibits the canonical Wnt pathway by promoting GSK-3-independent beta-catenin degradation." J Cell Biol **162**(5): 899-908.

Torres-Vazquez, J., A. D. Gitler, et al. (2004). "Semaphorin-plexin signaling guides patterning of the developing vasculature." Dev Cell **7**(1): 117-23.

Tosetti, P., N. Pathak, et al. (2003). "RGS3 mediates a calcium-dependent termination of G protein signaling in sensory neurons." Proc Natl Acad Sci U S A **100**(12): 7337-42.

Turner, D. L. and H. Weintraub (1994). "Expression of achaete-scute homolog 3 in Xenopus embryos converts ectodermal cells to a neural fate." Genes Dev **8**(12): 1434-47.

Ungar, A. R., G. M. Kelly, et al. (1995). "Wnt4 affects morphogenesis when misexpressed in the zebrafish embryo." Mech Dev **52**(2-3): 153-64.

van Eeden, F. J., M. Granato, et al. (1996). "Mutations affecting somite formation and patterning in the zebrafish, Danio rerio." Development **123**: 153-64.

Vandepoele, K., W. De Vos, et al. (2004). "Major events in the genome evolution of vertebrates: paranome age and size differ considerably between ray-finned fishes and land vertebrates." Proc Natl Acad Sci U S A **101**(6): 1638-43.

Vesque, C., M. Maconochie, et al. (1996). "Hoxb-2 transcriptional activation in rhombomeres 3 and 5 requires an evolutionarily conserved cis-acting element in addition to the Krox-20 binding site." Embo J **15**(19): 5383-96.

Wallingford, J. B., A. J. Ewald, et al. (2001). "Calcium signaling during convergent extension in Xenopus." Curr Biol **11**(9): 652-61.

Wallingford, J. B., K. M. Vogeli, et al. (2001). "Regulation of convergent extension in Xenopus by Wnt5a and Frizzled-8 is independent of the canonical Wnt pathway." Int J Dev Biol **45**(1): 225-7.

Watson, N., M. E. Linder, et al. (1996). "RGS family members: GTPase-activating proteins for heterotrimeric G-protein alpha-subunits." Nature **383**(6596): 172-5.

Webb, S. E., K. W. Lee, et al. (1997). "Localized calcium transients accompany furrow positioning, propagation, and deepening during the early cleavage period of zebrafish embryos." Dev Biol **192**(1): 78-92.

Webb, S. E. and A. L. Miller (2000). "Calcium signalling during zebrafish embryonic development." Bioessays **22**(2): 113-23.

Webb, S. E. and A. L. Miller (2003). "Imaging intercellular calcium waves during late epiboly in intact zebrafish embryos." Zygote **11**(2): 175-82.

Webb, S. E. and A. L. Miller (2006). "Ca2+ signaling during vertebrate somitogenesis." Acta Pharmacol Sin **27**(7): 781-90.

Webb, S. E. and A. L. Miller (2007). "Ca2+ signalling and early embryonic patterning during zebrafish development." Clin Exp Pharmacol Physiol **34**(9): 897-904.

Weinstein, B. (2002). "Vascular cell biology in vivo: a new piscine paradigm?" Trends Cell Biol **12**(9): 439-45.

Westerfield, M. (1995). The zebrafish book: a guide for the laboratory use of zebrafish (Danio rerio). Eugene, OR, M. Westerfield.

Westfall, T. A., R. Brimeyer, et al. (2003). "Wnt-5/pipetail functions in vertebrate axis formation as a negative regulator of Wnt/beta-catenin activity." J Cell Biol **162**(5): 889-98.

Westfall, T. A., B. Hjertos, et al. (2003). "Requirement for intracellular calcium modulation in zebrafish dorsal-ventral patterning." Dev Biol **259**(2): 380-91.

Wharton, K. A., Jr. (2003). "Runnin' with the Dvl: proteins that associate with Dsh/Dvl and their significance to Wnt signal transduction." Dev Biol **253**(1): 1-17.

Wieland, T. and C. Mittmann (2003). "Regulators of G-protein signalling: multifunctional proteins with impact on signalling in the cardiovascular system." Pharmacol Ther **97**(2): 95-115.

Wilding, M., K. Torok, et al. (1995). "Activation-dependent and activation-independent localisation of calmodulin to the mitotic apparatus during the first cell cycle of the Lytechinus pictus embryo." Zygote **3**(3): 219-24.

Willars, G. B. (2006). "Mammalian RGS proteins: Multifunctional regulators of cellular signalling." Semin Cell Dev Biol **17**(3): 363-76.

Willert, K. and R. Nusse (1998). "Beta-catenin: a key mediator of Wnt signaling." Curr Opin Genet Dev **8**(1): 95-102.

Wodarz, A. and R. Nusse (1998). "Mechanisms of Wnt signaling in development." Annu Rev Cell Dev Biol **14**: 59-88.

Wu, C., Q. Zeng, et al. (2000). "RGS proteins inhibit Xwnt-8 signaling in Xenopus embryonic development." Development **127**(13): 2773-84.

Yang, S. and Y. P. Li (2007). "RGS10-null mutation impairs osteoclast differentiation resulting from the loss of [Ca2+]i oscillation regulation." Genes Dev **21**(14): 1803-16.

Zerlin, M., M. A. Julius, et al. (2008). "Wnt/Frizzled signaling in angiogenesis." Angiogenesis **11**(1): 63-9.

Zhang, S., N. Watson, et al. (1998). "RGS3 and RGS4 are GTPase activating proteins in the heart." J Mol Cell Cardiol **30**(2): 269-76.